

Magmatism, migrating topography, and the onset of Basin and Range faulting

Jens-Erik Lund Sneek^{1,1} and Elizabeth Louise Miller^{1,1}

¹Stanford University

November 30, 2022

Abstract

The paleogeographic evolution of the western USA Great Basin from the Late Cretaceous to the Cenozoic is critical to understanding how the Cordillera at this latitude transitioned from Mesozoic shortening to Cenozoic extension. According to a widely applied model, Cenozoic extension was driven by collapse of elevated crust supported by crustal thicknesses that were potentially double the present ~30–35 km. This model is difficult to reconcile with more recent estimates of moderate regional extension ([?] 50%) and the discovery that most high-angle, basin–range faults slipped rapidly ca. 17 Ma, tens of millions of years after crustal thickening occurred. Here we integrate new and existing geochronology and geologic mapping in the Elko area of northeast Nevada, one of the few places in the Great Basin with substantial exposures of Paleogene strata. We improve age control for strata that have been targeted for studies of regional paleoelevation and paleoclimate across this critical time span. In addition, a regional compilation of the ages of material within a network of middle Cenozoic paleodrainages developed across the Great Basin shows that the age of basal paleovalley fill decreases southward roughly synchronously with voluminous ignimbrite flareup volcanism that swept south across the region ca. 45–20 Ma. Integrating these datasets with the regional record of faulting, sedimentation, erosion, and magmatism, we suggest that volcanism was accompanied by an elevation increase that disrupted drainage systems and shifted the continental divide east into central Nevada from its Late Cretaceous location along the Sierra Nevada arc. The north–south Eocene–Oligocene drainage divide defined by mapping of paleovalleys may thus have evolved as a dynamic feature that propagated southward with magmatism. Despite some local faulting, the northern Great Basin became a vast, elevated volcanic tableland that persisted until dissection by Basin and Range faulting that began ca. 21–17 Ma. Based on this more detailed geologic framework, it is unlikely that Basin and Range extension was driven by Cretaceous crustal overthickening; rather, pre-existing crustal structure was just one of several factors that led to Basin and Range faulting after ca. 17 Ma—in addition to thermal weakening of the crust associated with Cenozoic magmatism, thermally supported elevation, and changing boundary conditions. Because these causal factors evolved long after crustal thickening ended, during final removal and fragmentation of the shallowly subducting Farallon slab, they are compatible with normal (~45–50 km) thickness crust beneath the Great Basin prior to extension and do not require development of a strongly elevated, Altiplano-like region during Mesozoic shortening.

1 Magmatism, migrating topography, and the transition from
2 Sevier shortening to Basin and Range extension, western USA

3 Jens-Erik Lund Snee¹ and Elizabeth L. Miller²

4 ¹*U.S. Geological Survey Geosciences and Environmental Change Science Center, P.O. Box*
5 *25046, MS 980, Denver, CO 80225*

6 ²*Stanford University Department of Geological Sciences, 450 Serra Mall Bld. 320, Room 118,*
7 *Stanford, CA 94305*

8
9 **ABSTRACT**

10 The paleogeographic evolution of the western USA Great Basin from the Late Cretaceous
11 to the Cenozoic is critical to understanding how the Cordillera at this latitude transitioned from
12 Mesozoic shortening to Cenozoic extension. According to a widely applied model, Cenozoic
13 extension was driven by collapse of elevated crust supported by crustal thicknesses that were
14 potentially double the present ~30–35 km. This model is difficult to reconcile with more recent
15 estimates of moderate regional extension ($\leq 50\%$) and the discovery that most high-angle, basin–
16 range faults slipped rapidly ca. 17 Ma, tens of millions of years after crustal thickening occurred.
17 Here we integrate new and existing geochronology and geologic mapping in the Elko area of
18 northeast Nevada, one of the few places in the Great Basin with substantial exposures of
19 Paleogene strata. We improve age control for strata that have been targeted for studies of regional
20 paleoelevation and paleoclimate across this critical time span. In addition, a regional compilation
21 of the ages of material within a network of middle Cenozoic paleodrainages developed across the
22 Great Basin shows that the age of basal paleovalley fill decreases southward roughly
23 synchronous with voluminous ignimbrite flareup volcanism that swept south across the region
24 ca. 45–20 Ma. Integrating these datasets with the regional record of faulting, sedimentation,
25 erosion, and magmatism, we suggest that volcanism was accompanied by an elevation increase
26 that disrupted drainage systems and shifted the continental divide east into central Nevada from
27 its Late Cretaceous location along the Sierra Nevada arc. The north–south Eocene–Oligocene
28 drainage divide defined by mapping of paleovalleys may thus have evolved as a dynamic feature
29 that propagated southward with magmatism. Despite some local faulting, the northern Great
30 Basin became a vast, elevated volcanic tableland that persisted until dissection by Basin and

31 Range faulting that began ca. 21–17 Ma. Based on this more detailed geologic framework, it is
32 unlikely that Basin and Range extension was driven by Cretaceous crustal overthickening; rather,
33 pre-existing crustal structure was just one of several factors that that led to Basin and Range
34 faulting after ca. 17 Ma—in addition to thermal weakening of the crust associated with Cenozoic
35 magmatism, thermally supported elevation, and changing boundary conditions. Because these
36 causal factors evolved long after crustal thickening ended, during final removal and
37 fragmentation of the shallowly subducting Farallon slab, they are compatible with normal (~45–
38 50 km) thickness crust beneath the Great Basin prior to extension and do not require
39 development of a strongly elevated, Altiplano-like region during Mesozoic shortening.

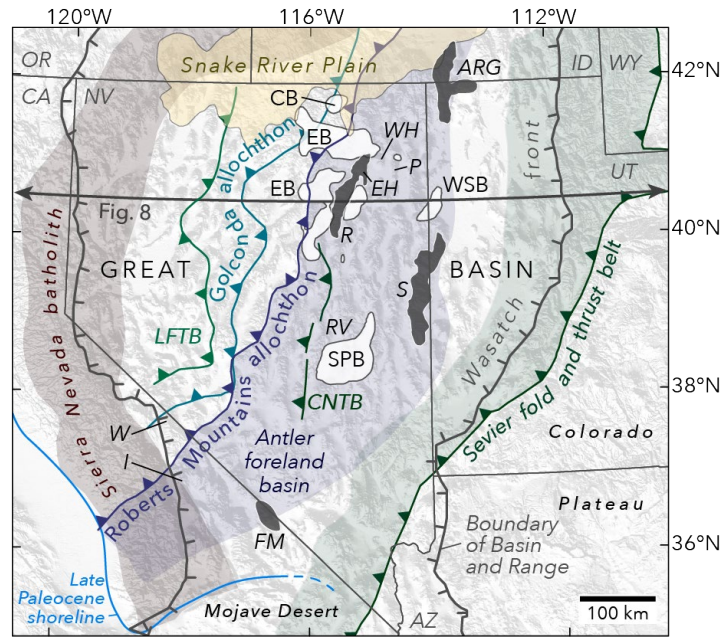
40

41 INTRODUCTION

42 The switch from Mesozoic shortening to Cenozoic extension in the western USA
43 Cordillera was a fundamental tectonic transition with implications for orogenic systems
44 worldwide, but its causes remain hotly debated and poorly understood. The many models
45 focusing on this time interval reveal disagreements regarding these basic questions: What was
46 the pre-extensional crustal structure, crustal thickness, and resulting topography across the west?
47 What was the causal mechanism for initiation of continental extension? What was the detailed
48 timing of important tectonic events across this time span and how do those events factor into our
49 understanding of causal mechanisms for the switch from shortening to extension?

50 The prevailing view argues that Mesozoic crustal thickening in the Sevier fold and thrust
51 belt produced a high plateau (the “*Nevadaplano*”) across the region of the present-day Great
52 Basin (Fig. 1) (DeCelles, 2004). Although the concept of the *Nevadaplano* is widely accepted,
53 there is little agreement regarding the timing and cause of plateau uplift (cf. Parsons et al., 1994;
54 Mix et al., 2011; Cassel et al., 2018), its peak elevation (cf. Chase et al., 1998; Wolfe et al., 1998;
55 Best et al., 2009; Cassel et al., 2012), whether or not “rugged topography” may have been
56 present on the plateau (cf. Chamberlain et al., 2007; Henry et al., 2012; Bahadori et al., 2018),
57 and the causes and timing of its inferred “collapse” (cf. Sonder et al., 1987; McQuarrie and
58 Chase, 2000; Colgan and Henry, 2009; Wells et al., 2012; Lee et al., 2017).

59



60

61 Figure 1. The Great Basin, including the northern and central Basin and Range province (BRP), western USA.
 62 The Mesozoic Sierra Nevada batholith is after Van Buer and Miller (2010). Paleogene basins are from Haynes
 63 (2003) and Smith et al. (2017). The approximate late Paleocene ocean shoreline is after Reid (1988) and
 64 Lechler and Niemi (2011). Luning-Fencemaker thrust belt (LFTB) locations are from Best et al. (2009).
 65 Locations of the Golconda and Roberts Mountains allochthons, Central Nevada thrust belt, and Sevier belt are
 66 from DeCelles (2004). The BRP boundary is from Dickinson (2013). ARG—Albion–Raft River–Grouse Creek
 67 Mountains; CB—Copper Basin; CNTB—Central Nevada thrust belt; EB—Elko Basin; EH—East Humboldt
 68 Range; FM—Funeral Mountains; I—Inyo Mountains; P—Pequop Mountains; R—Ruby Mountains; RV—
 69 Railroad Valley; S—Snake Range; SPB—Sheep Pass Basin, W—White Mountains; WH—Wood Hills;
 70 WSB—White Sage Basin.

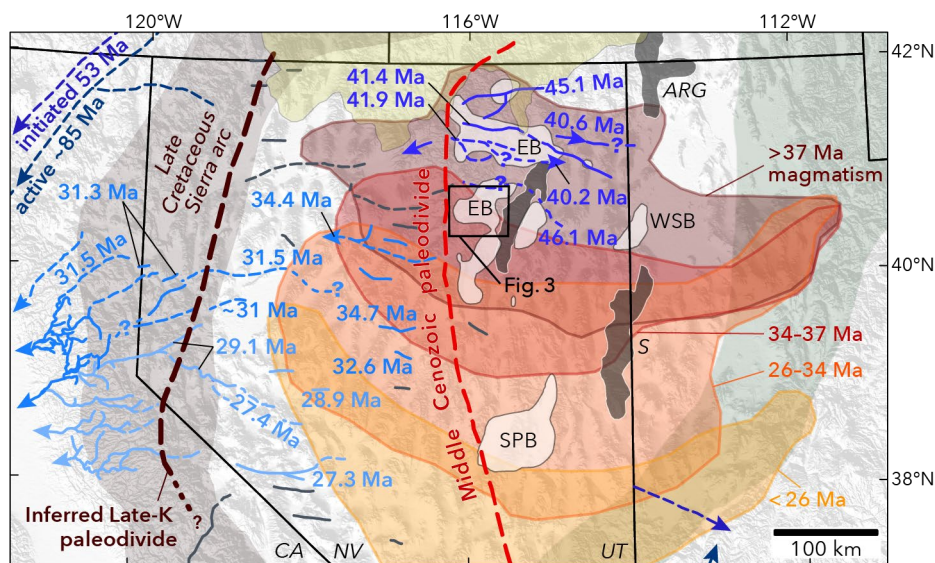
71

72 Related to these broader questions are more detailed questions about the resulting
 73 topography across this region. Studies based on the pattern of Cenozoic ash-flow tuffs that filled
 74 paleovalleys (e.g., Best et al., 2013; Henry and John, 2013) indicate a ~north–south-oriented
 75 divide that passed down the middle of central Nevada (Fig. 2), slightly west of the mostly older,
 76 Eocene Elko Basin (e.g., Haynes, 2003; Lund Snee et al., 2016; Camilleri et al., 2017) and the
 77 mostly Late Cretaceous and Eocene Sheep Pass Basin (e.g., Druschke et al., 2009a, 2009b).
 78 However, the divide has also been inferred to lie along the axis of the Mesozoic Sierra Nevada
 79 arc during the Late Cretaceous (Van Buer et al., 2009; Sharman et al., 2015). When, why and
 80 how did this eastward shift of the divide occur? Was the shift related to the south-sweeping
 81 middle Cenozoic volcanism of the ignimbrite flareup in the retroarc region (Fig. 2) (e.g.,

82 Armstrong and Ward, 1991; Christiansen and Yeats, 1992)? How did volcanism and the addition
83 of large volumes of magma and heat affect retroarc topography?

84 Here we integrate new and previously published geologic mapping and U-Pb detrital
85 zircon geochronology from Late Cretaceous(?)–Neogene sedimentary and volcanic rocks of the
86 Elko Basin of northeast Nevada, one of the only successions spanning large portions of the time
87 between Cretaceous crustal thickening and Neogene Basin and Range extension (Figs. 1 and 2).
88 We discuss the paleogeographic and tectonic significance of the stratigraphic succession and
89 published stable isotope records in the Elko area in the context of others from throughout the
90 region. We also compiled ages for the oldest volcanic or sedimentary material deposited in a
91 network of east- and west-draining paleovalleys active across the Great Basin in middle
92 Cenozoic time. Drawing upon all of this information, we present a revised view of the
93 paleogeographic and tectonic evolution of the northern Great Basin from Late Cretaceous to
94 Neogene time. Finally, we discuss the implications for estimates of crustal thickness and
95 topography prior to Cenozoic extension, including impacts for the *Nevadaplano* model.

96



97

98 Figure 2. Late Cretaceous and Cenozoic volcanism and topography in the Great Basin, showing paleodrainages
99 colored by the age of oldest reported material deposited within them, compiled from sources in the GSA Data
100 Repository. Lighter blues represent younger paleodrainages, and gray indicates no age information. The
101 approximate location of the Late Cretaceous paleodivide is inferred from Van Buer et al. (2009) and Sharman
102 et al. (2015). The Cenozoic paleodivide is from Henry and John (2013) and represents the conventional view
103 that the drainage divide was broadly static over Eocene–Oligocene time (and possibly earlier). Volcanic fields

104 are based on data from the North American Volcanic and Intrusive Rock Database (NAVDAT;
105 <http://ecp.iedadata.org>). Other references and acronyms as in Fig. 1.

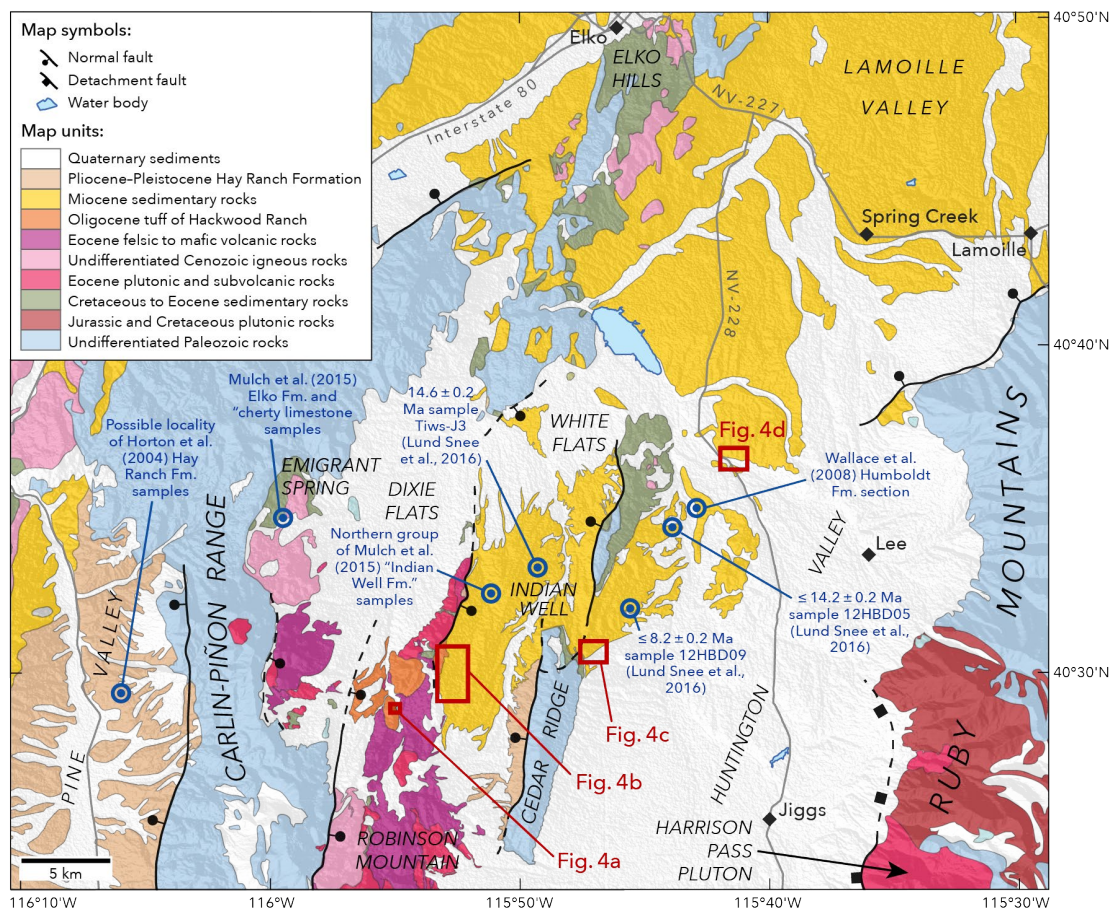
106

107 **GEOLOGIC SETTING**

108 Late Cretaceous and Cenozoic strata in northeast Nevada, in the area of the Eocene Elko
109 Basin (Figs. 1–3), unconformably overlie a thick (~10 km) Neoproterozoic to Triassic section
110 deposited along the passive margin of western North America (e.g., Willden and Kistler, 1979;
111 Colgan et al., 2010), formed after Neoproterozoic and early Paleozoic rifting of the Rodinia
112 supercontinent (e.g., Lund, 2008; Yonkee et al., 2014). West of the Elko area lie deep-marine
113 rocks of the Roberts Mountains and Golconda allochthons (Fig. 1) that were respectively thrust
114 across the continental margin in the earliest Mississippian and the Permian-Triassic (e.g.,
115 Stewart, 1980). These relations and the location of the initial $^{87}\text{Sr}/^{86}\text{Sr} = 0.706$ isopleth imply that
116 western Nevada was underlain by oceanic crust and that the thick passive margin succession at
117 the study area in northeast Nevada was underlain by thinned continental crust (Tosdal et al.,
118 2000). East-dipping subduction beneath the Cordilleran margin initiated as early as the Early
119 Triassic (e.g., Saleeby et al., 2008). The study area, which was in the retroarc region of the Sierra
120 Nevada arc, experienced two episodes of shortening and metamorphism during periods of
121 increased arc magmatism, one in the Middle to Late Jurassic ca. 170–155 Ma and the second in
122 the Late Cretaceous ca. 120–70 Ma (e.g., Dallmeyer et al., 1986; Miller and Gans, 1989;
123 Thorman et al., 1991; Smith et al., 1993; McGrew and Snee, 1994; Thorman and Peterson, 2003;
124 Du Bray, 2007; Zuza et al., 2020). Cretaceous thrust faulting at the latitudes of northern and
125 central Nevada was confined mostly to the Sevier fold and thrust belt to the east of the study
126 area, with significantly less shortening represented by the Central Nevada thrust belt in central
127 and southern Nevada (Fig. 1) (Taylor et al., 2000; Di Fiori et al., 2020).

128 Following Late Cretaceous subduction-related arc magmatism, volcanism initiated again
129 as part of the middle Cenozoic ignimbrite flareup, characterized by widespread caldera-forming
130 volcanism that migrated southward across the Great Basin, passing through northeast Nevada
131 (Fig. 2) ca. 42–36 Ma (Brooks et al., 1995; Ressel and Henry, 2006; Ryskamp et al., 2008; Henry
132 and John, 2013; Lund Snee et al., 2016). Although extension initiated locally as early as Eocene
133 time in certain areas (e.g., Henry et al., 2011; Miller et al., 2012; Wells et al., 2012), recognition
134 is growing that the primary extension that affected topography and supracrustal rocks across the

135 hinterland was an episode of rapid slip on high-angle normal faults that took place mostly during
 136 middle to late Miocene time and culminated in the present Basin and Range topography (Lund et
 137 al., 1993; Miller et al., 1999; Stockli et al., 2002; Henry, 2008; Colgan and Henry, 2009; Colgan
 138 et al., 2010; Colgan, 2013; Konstantinou and Miller, 2015; Lund Snee et al., 2016). This
 139 contribution presents new geochronologic and geological data obtained in the ancestral Elko
 140 Basin. We then examine the sedimentary record for the constraints it provides on the
 141 controversial and enigmatic history of the Late Cretaceous to the Miocene and, specifically, how
 142 the surface topography may have changed across this time span.
 143



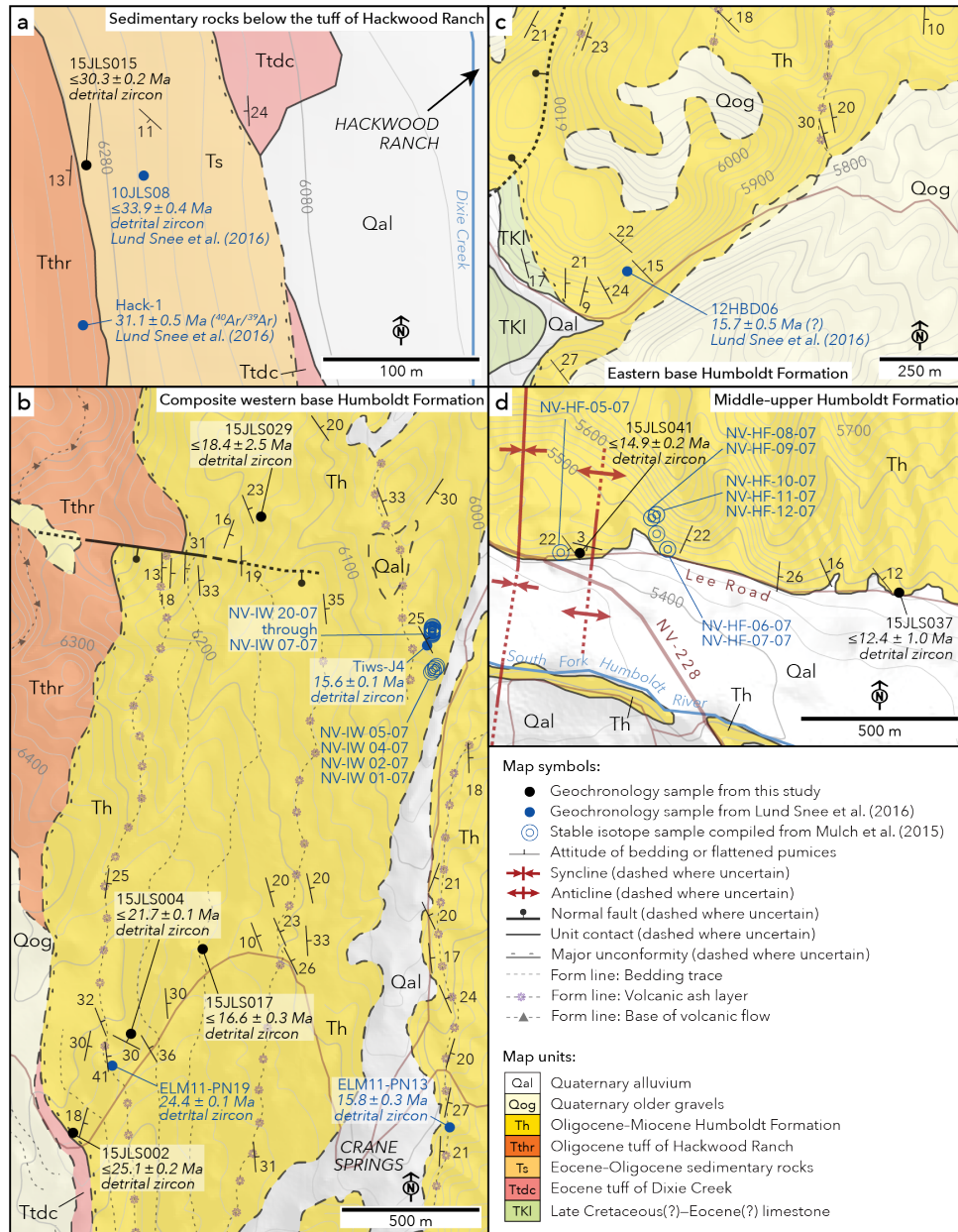
144
 145 Figure 3. Geologic map of the ancestral Elko Basin region, northeast Nevada (location shown in Fig. 2). Unit
 146 boundaries and faults are from Crafford (2007), Colgan et al. (2010), Lund Snee et al. (2016), and this study.
 147 The Ruby-East Humboldt detachment fault is presently a shallowly dipping fault system that experienced both
 148 ductile and brittle deformation (e.g., Dokka et al., 1986).
 149

150 **METHODS**

151 We mapped geologic units and tuffaceous beds, measured stratigraphic sections (Fig. 5),
152 and collected samples for U-Pb detrital zircon geochronology in Oligocene and Miocene
153 successions in Huntington Valley and the eastern Carlin-Piñon Range, northeast Nevada (Figs. 3
154 and 4), in and near the ancestral Elko Basin (Figs. 1 and 2). Our work refines geologic mapping
155 by Smith and Howard (1977), Smith and Ketner (1978), Lund Snee (2013), Lund Snee and
156 Miller (2015), and Lund Snee et al. (2016), who provided detailed descriptions of those rocks.
157 The GSA Data Repository contains detailed analytical methods and it presents the results of
158 seven additional U-Pb detrital zircon analyses to those by Lund Snee et al. (2016). Figure 5
159 shows the new and previous geochronology results within their *stratigraphic* framework.

160 Some of the same sections have previously been sampled for stable isotope analysis of
161 calcite cements, limestone, and paleosols (Horton et al., 2004; Mix et al., 2011) and our work
162 refines the age constraints and understanding of the depositional context for Neogene rocks
163 within those sections. Figure 6 shows stable isotope data from prior studies placed in their
164 revised *temporal* positions, with permissible depositional ages conservatively bounded by the
165 full 2σ uncertainty ranges for the depositional age constraints (e.g., including the 2σ uncertainties
166 for weighted mean ages). The Data Repository presents detailed methods for assigning age
167 constraints and preferred depositional ages, and it includes tables containing lithologic details,
168 sample localities, (maximum) depositional age information, and analytical data. Using these
169 same methods, we used published geochronologic data to improve depositional age constraints
170 for published stable isotope data that were obtained in older, Paleogene strata in the area
171 (locations in Fig. 3), for which a number of contradictory depositional ages have been reported
172 (cf. Horton et al., 2004; Mix et al., 2011; Chamberlain et al., 2012; Mulch et al., 2015; Smith et
173 al., 2017). In most cases, the permissible age bounds were not given in those studies, and sample
174 ages were reported as being absolute when in fact they were maximum depositional ages
175 (MDAs).

176



177

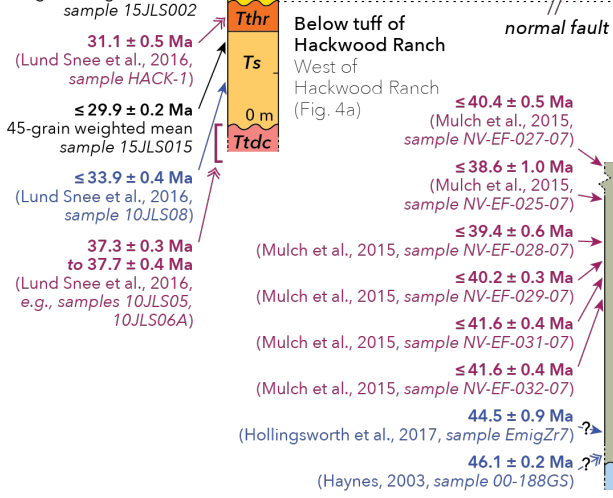
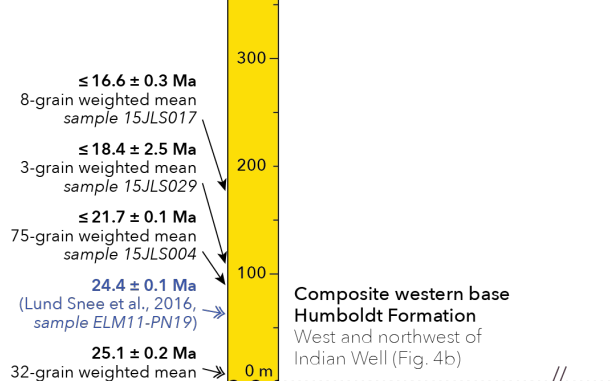
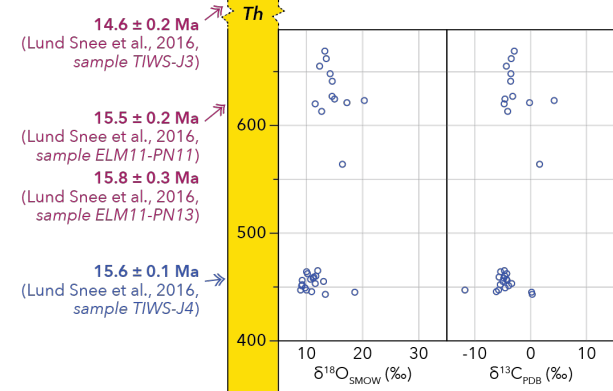
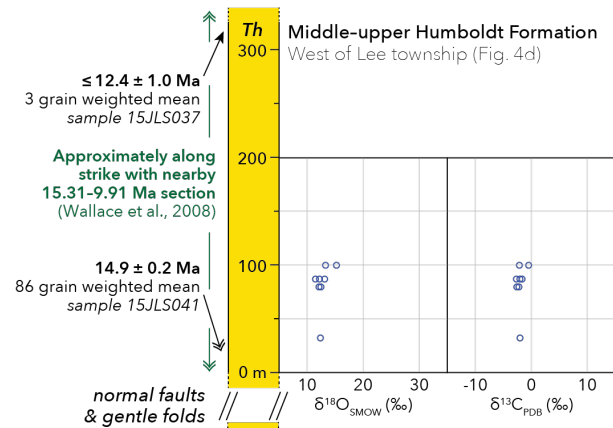
178 Figure 4. Geologic maps of areas sampled for this study. Unit boundaries and structures are from Smith and

179 Howard (1977), Crafford (2007), Lund Snee and Miller (2015), Lund Snee et al. (2016), and this study.

180 Maximum depositional ages are indicated with inequality symbols (“≤”), unlike for nearly absolute

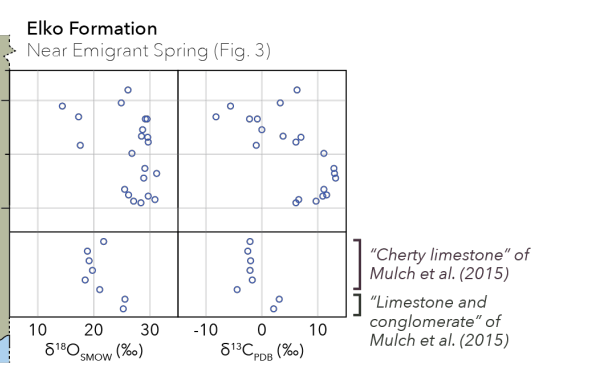
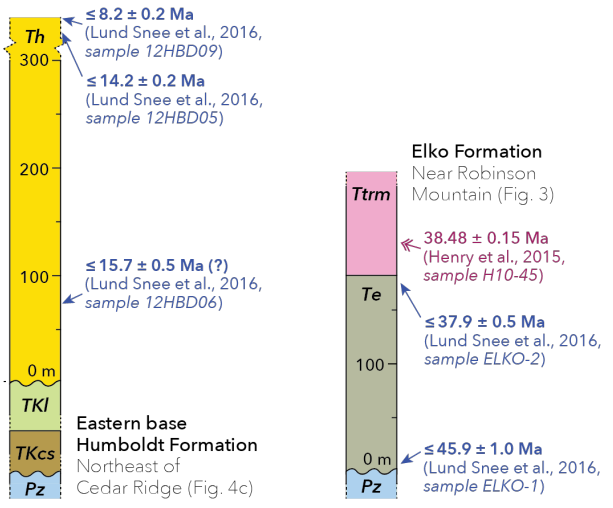
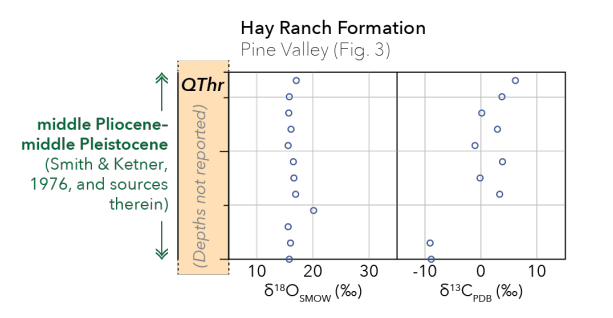
181 depositional ages from tuffaceous horizons.

182



~ Unconformity ○ Previous stable isotope measurement
 Geochronologic age from this study:
 → U-Pb detrital zircon *maximum* depositional age
 → U-Pb zircon depositional age from tuff
 Geochronologic age from previous work:
 → U-Pb detrital zircon *maximum* depositional age
 → U-Pb detrital zircon depositional age from tuff
 → Detrital $^{40}\text{Ar}/^{39}\text{Ar}$ *maximum* depositional age
 → $^{40}\text{Ar}/^{39}\text{Ar}$ depositional age from tuff
 → Fossil or other depositional age
 Map units:

QThr	Hay Ranch Formation	Ttrm	tuff of Robinson Mountain
Th	Humboldt Formation	Te	Elko Formation
Tthr	tuff of Hackwood Ranch	TKI	limestone
Ts	sedimentary rocks	TKcs	conglomerate, sandstone, siltstone
Ttdc	tuff of Dixie Creek	Pz	undifferentiated Paleozoic rocks



184 Figure 5. Isotopic analyses from Mulch et al. (2015) and sources therein plotted by stratigraphic section.
185 Section and sample locations are shown in Figs. 3 and 4. Maximum depositional ages are indicated with
186 inequality symbols (“≤”), unlike for nearly absolute depositional ages from interbedded tuffaceous horizons.
187 Plotted stable isotope measurements and age data are listed in the GSA Data Repository. Values of $\delta^{18}\text{O}$ are
188 reported relative to standard mean ocean water (SMOW) and values of $\delta^{13}\text{C}$ are reported relative to Peedee
189 belemnite (PDB) for consistency with prior studies in this region. These plots complement those in Fig. 6,
190 where isotopic measurements are plotted together by depositional age bounds.

191

192 **REVIEW OF THE SEDIMENTARY AND VOLCANIC RECORD**

193 **Elko area of northeast Nevada**

194 The Elko area is one of the only places in the Great Basin where well-preserved
195 sedimentary and volcanic rocks spanning the Late Cretaceous(?) to Neogene are exposed over
196 appreciable areas (e.g., Stewart, 1980). Because the term “Elko Basin,” *sensu stricto*, refers to
197 the part of northeast Nevada where the Elko Formation was deposited in Eocene time (see
198 Camilleri et al., 2017), we use the term “ancestral Elko Basin” to refer to this general area over a
199 wider time span.

200 As shown in Figure 6, little deposition is documented between the Cretaceous and early
201 Eocene in the ancestral Elko Basin region (Smith and Ketner, 1976; Fouch et al., 1979; Rahl et
202 al., 2002; Haynes, 2003; Crafford, 2007; Henry et al., 2011; Lund Snee and Miller, 2015),
203 reflecting the history of gradual erosion that prevailed throughout much of the hinterland from
204 the peak of Late Cretaceous deformation and magmatism until the middle Eocene (e.g., Van Buer
205 et al., 2009; Konstantinou et al., 2012). The first strata deposited during this time span within the
206 Elko area were Late Cretaceous(?) to early Eocene(?) redbeds and limestones (Figs. 3, 4c, 5, and
207 6), probably in isolated topographic lows, fault-bounded basins, or the bottoms of paleovalleys
208 (Armstrong, 1968, 1972; Smith and Ketner, 1976; Gans and Miller, 1983; Van Buer et al., 2009;
209 Konstantinou et al., 2012; Long, 2012; Lund Snee, 2013; Henry, 2018). These early deposits, as
210 well as the overlying Elko Formation (Fig. 5), contain clast compositions and detrital zircon age
211 distributions that reflect recycling from strata presently exposed beneath the Cenozoic
212 unconformity (Druschke et al., 2011; Ruksznis, 2015; Lund Snee et al., 2016; Canada et al.,
213 2020).

214 The more extensive middle to late Eocene Elko Formation (Figs. 5 and 6), which locally
215 reaches thicknesses of ~850 m (Henry, 2008), consists of a broadly upward-fining succession of

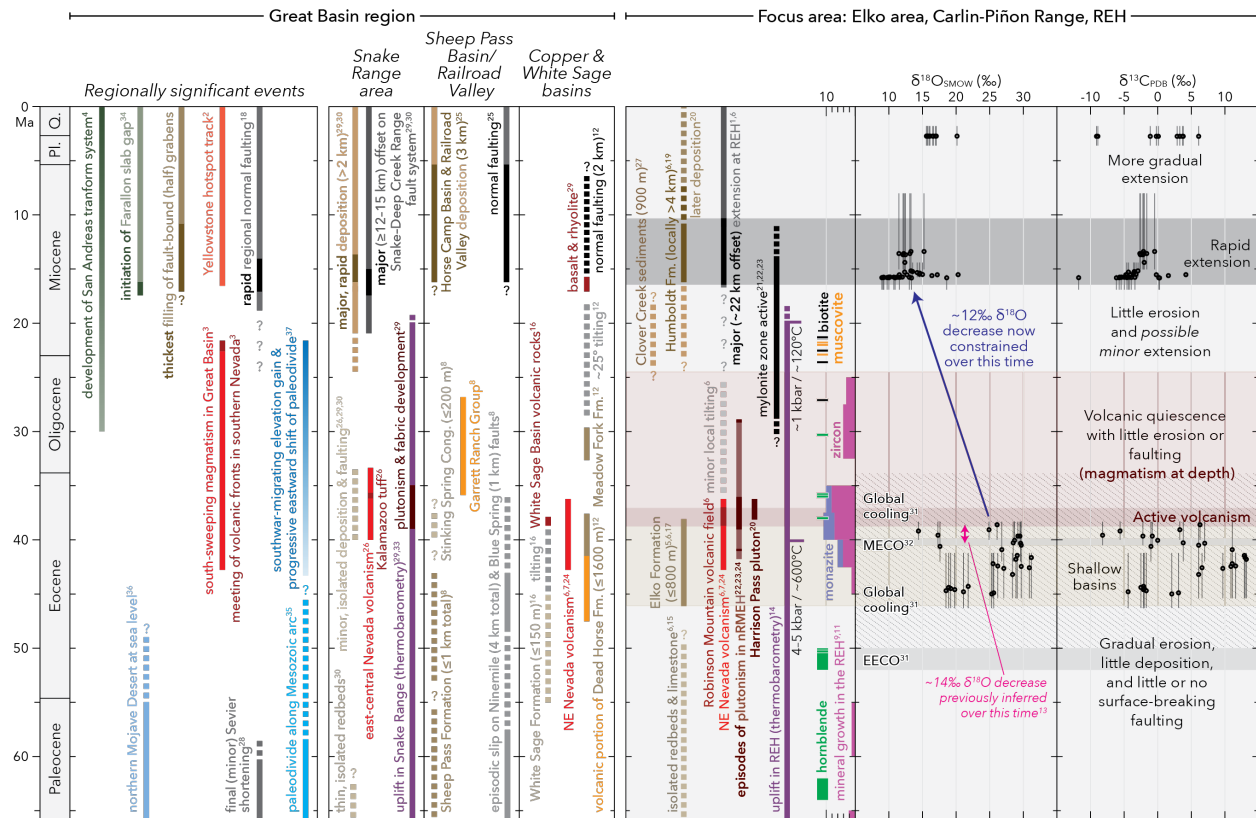
216 conglomerate, sandstone, siltstone, shale, clay, marl, and limestone (Smith and Ketner, 1976;
217 Solomon et al., 1979; Moore et al., 1983; Server and Solomon, 1983; Ketner and Alpha, 1992;
218 Haynes, 2003; Lund Snee and Miller, 2015; Smith et al., 2017). The presence of Cenozoic
219 tuffaceous material and other volcanic detritus is a key factor that distinguishes the Elko
220 Formation from older units (Smith and Ketner, 1976; Lund Snee et al., 2016). Deposition of the
221 Elko Formation began ca. 46.1 Ma (Fig. 5), based on a U-Pb zircon age of an ash-fall tuff
222 deposited near its base (Haynes, 2003). The end of Elko Formation deposition is tightly
223 constrained at ca. 38.4 Ma, based on a U-Pb detrital zircon maximum depositional age (MDA) of
224 37.9 ± 0.5 Ma from its upper stratigraphic levels within the eastern Carlin-Piñon Range, south of
225 Robinson Mountain (Fig. 3; sample ELKO-2 of Lund Snee et al., 2016) and a minimum
226 depositional age of 38.47 ± 0.15 Ma from $^{40}\text{Ar}/^{39}\text{Ar}$ plagioclase analysis on an overlying ash-
227 flow tuff nearby (sample H10-45 of Henry et al., 2015) (Fig. 5). These dates revise an estimate of
228 40.4 Ma for the end of Elko Formation deposition by Smith et al. (2017) and they are compatible
229 with estimates of ca. 39–38 Ma by Haynes (2003) and Mulch et al. (2015). The initiation of
230 shallow basin development recorded by the onset of Elko Formation deposition ca. 46–44 Ma,
231 shortly before arrival of volcanism (see below), indicates that volcanism occurring to the north in
232 southern Idaho may have been responsible for a change in topography and regional stress state.
233 The development of accommodation for deposition at this time, following tens of millions of
234 years with little or no sedimentation, suggests initiation of a mechanism such as normal faulting,
235 development of sags or uplifts, and/or establishment of broad paleodrainages (e.g., Howard,
236 2003; Smith et al., 2017; Henry, 2018; this study). Lithofacies characterization and $\delta^{13}\text{C}_{\text{carbonate}}$,
237 $\delta^{18}\text{O}_{\text{carbonate}}$, and $\delta\text{D}_{\text{glass}}$ measurements suggest that the Elko Basin experienced a profound
238 transition in depositional setting between the lower and upper Elko Formation ca. 40 Ma, as
239 volcanism became more proximal (Fig. 2), although published interpretations are contradictory.
240 Mulch et al. (2015) suggested that elevations increased and lake waters freshened within the
241 Elko Basin around this time, whereas Smith et al. (2017) proposed an upward transition from
242 freshwater fluvial-lacustrine to saline and anoxic profundal settings, with substantial uplift only
243 after the end of Elko Formation deposition.

244 The ca. 38.5–36.8 Ma Robinson Mountain volcanic field (Ressel and Henry, 2006; Henry
245 et al., 2015; Lund Snee et al., 2016) is a thick succession (>1 km) of rocks associated with the
246 ignimbrite flareup on the eastern flanks of the Carlin-Piñon Range (Fig. 3), and it conformably

247 overlies the Elko Formation (Smith and Ketner, 1976, 1978; Ressel and Henry, 2006; Ryskamp
248 et al., 2008; Lund Snee and Miller, 2015). Following volcanism, sedimentation and faulting
249 effectively ceased in this area (Fig. 6), with few exceptions, until Basin and Range faulting began
250 in the middle Miocene (Henry et al., 2011; Lund Snee et al., 2016; this study). Any faulting that
251 accompanied magmatism and crustal flow at depth might have been limited to the immediate
252 areas above the metamorphic core complexes (MCCs), where the surface record is incomplete
253 due to younger faulting and erosion (Miller et al., 1999; Colgan et al., 2010; Konstantinou et al.,
254 2013a; Lee et al., 2017). Lund Snee et al. (2016) documented 10–15° tilting events following
255 volcanism, between ca. 36.8–33.9 Ma and between ca. 31.1–24.4 Ma (better constrained by this
256 study to between ca. 31.1–25.1 Ma as shown in Figs. 4b, 5, and 6), which they interpreted to
257 represent local deformation associated with deeper crustal flow leading to surface adjustments by
258 either faulting and/or doming adjacent to the developing Ruby Mountains–East Humboldt Range
259 (REH) MCC. Best and Christiansen (1991) made a similar interpretation for the limited and
260 localized faulting that occurred during the ~10 Myr following volcanism throughout the Great
261 Basin.

262 An early phase of gradual extension within this generally quiescent interval may be
263 represented by deposition of ca. 25 Ma and progressively younger fluvial-lacustrine material
264 near the base of the Humboldt Formation (Figs. 3, 4a, and 6; Lund Snee et al., 2016; this study),
265 as well as the possibly correlative late Oligocene and/or early Miocene sedimentary sequence of
266 Clover Creek (McGrew and Snoke, 2015) near the East Humboldt Range (Fig. 1). Subsequently,
267 rapid slip initiated on basin-bounding faults at 17–16 Ma (e.g., Colgan et al., 2010), represented
268 in northeast Nevada by thick middle to late Miocene deposits of the Humboldt Formation. Near
269 the REH (Figs. 3, 4b–d, and 5), the Humboldt Formation locally exceeds 4 km thickness
270 (Satarugsa and Johnson, 2000), by far dwarfing the thicknesses of older Cenozoic units.

271



272
 273 Figure 6. Regional Cenozoic tectonic events and measured isotopic values in the Elko area, northeast Nevada.
 274 Stable isotope data are from Mulch et al. (2015) and sources therein. Vertical bars indicate the full permissible
 275 age range for each analysis, conservatively including the 2σ uncertainties of the bounding age constraints.
 276 Values of $\delta^{18}\text{O}$ are reported relative to standard mean ocean water (SMOW) and values of $\delta^{13}\text{C}$ are reported
 277 relative to Peedee belemnite (PDB) for consistency with prior studies in this region. Cong.—Conglomerate;
 278 EECO—Early Eocene Climatic Optimum; Fm.—Formation; MECO—Middle Eocene Climatic Optimum;
 279 REH—Ruby Mountains–East Humboldt Range. References: 1—Colgan and Henry (2009); 2—Coble and
 280 Mahood (2012); 3—Armstrong and Ward (1991); 4—Atwater (1989); 5—Haynes (2003); 6—Lund Snee et al.
 281 (2016); 7—Brooks et al. (1995); 8—Druschke et al. (2009a, 2009b); 9—Howard et al. (2011); 10—Henry et
 282 al. (2011); 11—McGrew and Snee (1994); 12—Rahl et al. (2002) and McGrew et al. (2007); 13—Mulch et al.
 283 (2015); 14—McGrew et al. (2000); 15—Smith and Ketner (1976); 16—Potter et al. (1995) and Dubiel et al.
 284 (1996); 17—Henry (2008); 18—Stockli (2005); 19—Satarugsa and Johnson (2000); 20—Colgan et al. (2010);
 285 21—Haines and Van Der Pluijm (2010); 22—Wright and Snoke (1993); 23—MacCready et al. (1997); 24—
 286 Ryskamp et al. (2008); 25—Horton and Schmitt (1998); 26—Gans et al. (1989); 27—McGrew and Snoke
 287 (2015); 28—DeCelles and Coogan (2006); 29—Miller et al. (1999); 30—Rukshnis (2015); 31—Zachos et al.
 288 (2001); 32—Sluijs et al. (2013); 33—Cooper et al. (2010); 34—Liu and Stegman (2012); 35—Van Buer et al.
 289 (2009); 36—Lechler and Niemi (2011); 37—this study.
 290

291 **Great Basin region**

292 Here we expand the above discussion to include rocks of Late Cretaceous to Neogene age
293 deposited elsewhere in the Great Basin, primarily in the Copper, White Sage, and Sheep Pass
294 basins (Fig. 1). As can be seen in Figure 6, the histories of deposition and tectonism in these
295 areas are broadly similar, characterized by limited and localized Late Cretaceous to Paleogene
296 sedimentation and faulting (e.g., Gans and Miller, 1983; Best and Christiansen, 1991; Burchfiel
297 et al., 1992; Van Buer et al., 2009; Henry et al., 2011; Konstantinou et al., 2012; Long, 2012;
298 Henry and John, 2013) followed by volcanism, a subsequent hiatus in sedimentation, and then
299 rapid sedimentation and tilting in the middle Miocene.

300 Regionally, the most significant deposition in the Late Cretaceous to Paleogene interval
301 was in the greater Sheep Pass Basin of east-central Nevada (Fig. 1), where deposition of up to
302 ~1200 m of Late Cretaceous–middle Eocene Sheep Pass Formation and late Eocene Stinking
303 Spring Conglomerate (Fig. 6) was associated with potentially 3 km of normal slip on the
304 northwest-dipping Ninemile fault system (Druschke et al., 2009a, 2009b). Sedimentation and
305 tilting occurred elsewhere in east-central Nevada (Gans et al., 1989), including near the Snake
306 Range MCC (Figs. 1 and 6), but deposition was localized (Best and Christiansen, 1991).

307 As in the case of the Elko area described above, the limited pre-Miocene deposition that
308 did take place elsewhere in the Great Basin occurred several millions of years before ignimbrite
309 flareup volcanism (Fig. 6), suggesting that early magmatic processes could have prompted
310 changes in topography. In the Copper Basin of northeast Nevada (Fig. 1), localized late Eocene–
311 Oligocene deposition may have occurred due to basin development associated with normal fault
312 slip shortly before and during nearby volcanism (Axelrod, 1966; Rahl et al., 2002). Alternatively,
313 these units (and the nearby Elko Formation) may have been deposited into paleochannels, some
314 of which could have been partially dammed by faulting (Henry, 2008, 2018). In the White Sage
315 Basin of western Utah, ~150 m of early Eocene deposits experienced modest tilting in the middle
316 Eocene before being blanketed ca. 40–39 Ma by ignimbrite flareup volcanic rocks (Potter et al.,
317 1995; Dubiel et al., 1996). These datasets appear to preclude significant activity and offset along
318 Late Cretaceous to Oligocene faults, consistent with prior compilations for the Great Basin (Best
319 and Christiansen, 1991; Colgan and Henry, 2009; Henry et al., 2011; Henry and John, 2013).

320 In most places, sedimentation effectively ceased following volcanism, lasting at least
321 through most of the Oligocene. Similar to the REH MCC, gradual sedimentation near the Snake

322 Range MCC re-initiated as early as the late Oligocene or earliest Miocene (Miller et al., 1999;
323 Ruksznis, 2015). Nevertheless, by far the most significant episode of sedimentation, tilting, and
324 uplift in the Great Basin occurred during middle Miocene time, ca. 17–16 Ma, resulting in
325 region-wide development of deep (often >2 km) half-graben basins that filled rapidly with
326 sediments (Noble, 1972; Stockli et al., 2002; Colgan, 2013).

327

328 **REVIEW OF STABLE ISOTOPE MEASUREMENTS**

329 Numerous studies have targeted strata in the ancestral Elko Basin for stable isotope
330 analysis in efforts to understand regional paleoelevation and paleoclimate histories (Fig. 3).
331 Stable isotope measurements from Elko area carbonates have served as key constraints in
332 regional studies arguing that large and rapid negative shifts in $\delta^{18}\text{O}$, which proceeded southward
333 across the western USA approximately synchronous with migrating middle Cenozoic volcanism,
334 indicate simultaneous south-migrating topographic uplift (Horton et al., 2004; Davis et al., 2006;
335 Mix et al., 2011; Chamberlain et al., 2012), supporting a model initially proposed by Gans
336 (1990). Specifically, these conclusions were based on a proposed ~7–10‰ decrease in $\delta^{18}\text{O}$
337 values at ca. 50–47 Ma in southwestern Montana and eastern Idaho (Kent-Corson et al., 2006),
338 followed by a decrease of up to ~15‰ in the Elko Basin, proposed to have occurred between ca.
339 40.2–39.4 Ma (Mulch et al., 2015), and finally a ~4‰ decrease after ca. 23 Ma in southern
340 Nevada (Chamberlain et al., 2012). This timing is generally corroborated by comparable negative
341 shifts of $\delta^{18}\text{O}$ values ca. 44–40 Ma in foreland basin deposits east of the Sevier fold and thrust
342 belt at the latitude of northeast Nevada (Fig. 1), which have been attributed to high-elevation
343 catchment areas in the Sevier hinterland (e.g., Carroll et al., 2008; Davis et al., 2009). In the
344 ancestral Elko Basin, the decrease in $\delta^{18}\text{O}$ values was interpreted to suggest 2.5 km of uplift
345 occurring over <2 Myr (Chamberlain et al., 2012). Mulch et al. (2015) subsequently suggested
346 that a component of the up to 15‰ decrease in $\delta^{18}\text{O}$ values in the Elko Basin should be
347 attributed to climatic and diagenetic factors, including late Eocene global cooling.

348 More recently, however, the sedimentary age constraints, mean $\delta^{18}\text{O}$ values, and
349 interpretations of depositional environment underpinning some of these studies have changed,
350 both for the ancestral Elko Basin (Lund Snee et al., 2016; Smith et al., 2017) and the Sage Creek
351 Basin of southwest Montana (Kent-Corson et al., 2010; Schwartz et al., 2019). In southwest
352 Montana, Kent-Corson et al. (2010) revised the magnitude of the negative shift in $\delta^{18}\text{O}$ values

353 from 7‰ to only 4–5‰ (all $\delta^{18}\text{O}$ values are relative to standard mean ocean water, SMOW). The
354 4–5‰ shift was corroborated by Schwartz et al. (2019), who also established that it occurred
355 rapidly at ca. 47 Ma, across a conformable stratigraphic boundary. The ~1 Myr time interval for
356 this shift in $\delta^{18}\text{O}$ values may be too rapid to be explained by topographic changes associated with
357 Challis and Absaroka volcanism, which reached southwest Montana ~5 Myr earlier.

358 In the Elko area, Lund Snee et al. (2016) found that the rocks previously mapped as part
359 of the Oligocene Indian Well Formation (Fig. 3) are mostly middle Miocene and younger in age
360 and hence part of the Miocene Humboldt Formation. As a result, that study recommended
361 abandoning the Indian Well Formation name. Because much of the marked decrease in $\delta^{18}\text{O}$
362 values (an interpreted ~14–15‰ decrease from ~+29.1 to +14.4‰) occurred across this angular
363 unconformity, the age revisions imply that the timing of the shift could have occurred anytime
364 within a large window of time between 40–15.5 Ma. Our new geochronologic data and more
365 conservative approach to constraining temporal bounds (Fig. 6) do not significantly narrow the
366 time interval over which the $\delta^{18}\text{O}$ shift occurred, but they do constrain the ages more rigorously
367 and in greater detail than prior studies (e.g., Mix et al., 2011; Mulch et al., 2015; Lund Snee et
368 al., 2016; Smith et al., 2017). The record of $\delta^{18}\text{O}$ values with improved age constraints shown in
369 Fig. 6 indicates considerable scatter in $\delta^{18}\text{O}$ values both in the upper part of the Eocene Elko
370 Formation and in lower levels of the Humboldt Formation for which stable isotope values have
371 been measured. This scatter leads us to interpret a slightly different shift of ~–12‰, from ~+25
372 (but ranging between ~+14–+30‰) in upper Elko Formation strata with preferred ages spanning
373 ca. 40.9–38.6 Ma to ~+13‰ (ranging between ~+9–+20‰) in strata within the lower Humboldt
374 Formation with preferred ages spanning ca. 15.8–15.5 Ma. Although prior workers (e.g., Mulch
375 et al., 2015) argued that the decrease in $\delta^{18}\text{O}$ values occurred within the upper Elko Formation
376 because of a ~14–15‰ decrease that is observed within that succession, we point out that this
377 interpretation was made on the basis of three nonsequential data points and that $\delta^{18}\text{O}$ values
378 increase again by ~10‰ (from +14.4–+17.6‰ to +24.9–+26.1‰) immediately above and still
379 within the Elko Formation (Fig. 6). Such rapid oscillation of $\delta^{18}\text{O}$ values within a narrow part of
380 the succession are unlikely to reflect changes in topography. Hence, we conclude that the ~12‰
381 (or possibly less) decrease in $\delta^{18}\text{O}$ values observed in the Elko Basin occurred at an unknown
382 rate sometime between ca. 38.6–15.8 Ma. Moreover, our new age constraints and stratigraphic
383 thickness measurements show that >400 m of stratigraphic section are present below the lowest

384 measured Humboldt Formation $\delta^{18}\text{O}$ values, with a depositional age of 25.1 ± 0.2 Ma now
385 established for a tuffaceous bed near the base of that unit (Figs. 4 and 5). A consequence of the
386 improved age constraints is that we do not know when the decrease in Elko Basin $\delta^{18}\text{O}$ values
387 occurred relative to the onset of volcanism (Figs. 2 and 3) ca. 39–38 Ma (Ressel and Henry,
388 2006; Henry et al., 2015; Lund Snee et al., 2016). The sign and magnitude of the decrease in
389 $\delta^{18}\text{O}$ values is clearly consistent with an elevation increase, although it is also not definitive of
390 that because of the potential for climatic and diagenetic influences over this interval.

391 Stable isotopic studies focused instead on volcanic rocks erupted across the Great Basin
392 (including the Elko region) and westward to the Sierra Nevada flank have argued that a high
393 plateau persisted across the former Sevier hinterland between 41–23 Ma on the basis of relatively
394 low δD values in altered volcanic glass that span this age spectrum (Cassel et al., 2009, 2014,
395 2018). These results were interpreted to suggest that the inferred high plateau developed in
396 Cretaceous time (Henry et al., 2012). However, the δD values vary with sample age and location.
397 This led Cassel et al. (2018) to propose that elevations across the hinterland were ~ 2.25 – 3.0 km
398 during late Eocene time and then fell by ~ 0.5 – 1 km by early Oligocene time, followed by ~ 1.5
399 km uplift between the early and late Oligocene (to as high as 3.5 km in central Nevada), before
400 eventually falling to present-day mean elevations around 1.75 km. Although the presence of an
401 elevated plateau following the arrival of volcanism is consistent with the other geologic and
402 stable isotopic evidence discussed here, these proposed oscillatory elevation changes are difficult
403 to reconcile with geologic evidence as they imply multiple episodes of faulting and
404 sedimentation that are not corroborated by the geologic record (see above and summaries by Best
405 and Christiansen, 1991; Henry et al., 2011; Henry and John, 2013). Moreover, the age brackets of
406 $\delta^{18}\text{O}$ values from Elko Basin carbonates (Fig. 6; Horton et al., 2004; Mix et al., 2011;
407 Chamberlain et al., 2012; Mulch et al., 2015) are not consistent with models that require
408 elevations to have *decreased* between ca. 42–13 Ma (e.g., Coney and Harms, 1984; Sonder et al.,
409 1987; Bahadori et al., 2018; Cassel et al., 2018) because $\delta^{18}\text{O}$ and $\delta^{13}\text{C}$ values were generally
410 low from ca. 16 Ma onward and prior to ca. 42 Ma were substantially higher (Fig. 6).

411 In summary, recent work to improve age constraints and better define depositional
412 settings in both northeast Nevada and southwest Montana (Kent-Corson et al., 2010; Lund Snee
413 et al., 2016; Schwartz et al., 2019; this study) indicates that the stable isotope record does not
414 alone provide clear evidence for south-migrating topography across the region. On the basis of

415 more rigorous age constraints, the negative shift in $\delta^{18}\text{O}$ values within the ancestral Elko Basin
416 cannot be decisively linked to the age of south-migrating volcanism, although it is consistent
417 with uplift occurring at that time or later and is inconsistent with models requiring a decrease in
418 elevation anytime between ca. 42–13 Ma (Fig. 6). Far stronger evidence for south-migrating
419 topography is demonstrated by the other datasets discussed here: the record of sedimentation,
420 faulting, erosion, and reorganization of drainage networks. Stable isotope studies based on δD
421 values in altered volcanic glass present a more complex pattern with space and time. Published
422 interpretations of those results cannot presently be reconciled with the existing record of
423 sedimentation and faulting.

424

425 **RE-EVALUATING THE EVOLUTION OF PRE-BASIN AND RANGE DRAINAGE** 426 **SYSTEMS**

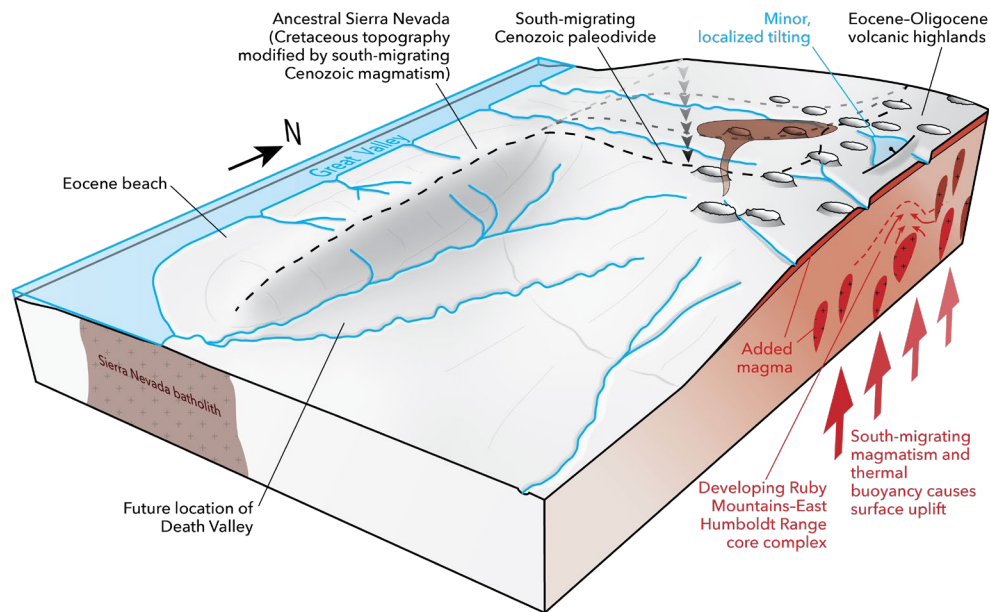
427 Rocks preserved within a mapped network of Eocene–Oligocene paleovalleys (Fig. 2)
428 provide additional insights for the region’s topographic evolution that can be interpreted in
429 concert with the sedimentary record. The paleovalleys are defined and mapped by their thicker
430 sequences of volcanic fill and can be traced generally east–west from range to range across
431 Nevada (Henry, 2008). The rocks filling the paleovalleys are precisely dated and consist of well
432 correlated middle Cenozoic ignimbrites that flowed hundreds of kilometers east and west along
433 these channels from their source calderas (e.g., Henry and John, 2013). The flow directions
434 defined by these relations outline a north–south-trending paleodivide through central Nevada
435 (Henry, 2008; Best et al., 2013), which has been widely displayed in subsequent publications
436 portraying the paleotopography of the west. The paleodivide is viewed as a static feature at least
437 through the early Cenozoic if not as far back as the Cretaceous (e.g., Henry et al., 2012).

438 Figure 2 shows the Cenozoic temporal evolution of volcanism together with the ages of
439 oldest material dated within each paleodrainage (compiled from MacGinitie, 1941; Yeend, 1974;
440 Goldstrand, 1992, 1994; Garside et al., 2005; Henry, 2008; Henry et al., 2012; Henry and John,
441 2013; Dumitru et al., 2015, 2016). The age of the oldest dated material in each paleovalley
442 decreases systematically southward, broadly accompanied by the southward progression of
443 volcanism. We consider it unusual that no basal paleovalley deposits have known ages
444 significantly older than nearby magmatism. This is especially remarkable considering that the
445 ignimbrites were capable of traveling hundreds of kilometers north and south of their eruptive

446 centers (Henry and John, 2013). For each stage of migrating volcanism, the earliest deposits are
447 preserved near the source calderas, filling paleovalleys to the west, east, and sometimes north.
448 Yet—critically—the record of fill preserved at the *bottoms* of paleovalleys (Fig. 2) shows few to
449 no examples of eruptive products that would have had to travel significantly south (e.g., ≥ 100
450 km).

451 The likeliest explanation is that most or all of these drainages did not exist more than a
452 few million years before magmatism began at a given latitude and paleovalleys were filled with
453 volcanic material. We propose that the paleovalleys could have developed diachronously in
454 response to dynamic topographic uplift that likely occurred during south-migrating ignimbrite
455 flareup volcanism, when large amounts of magmatic material and thermal energy were added to
456 the crust. In this context, fluvial paleovalleys with valley-margin relief approaching 1.2 km (e.g.,
457 Henry et al., 2012) were incised into the rising hinterland, similar to the paleovalleys that formed
458 during the Paleocene–Eocene to the north of the study area (e.g., Schwartz and Schwartz, 2013;
459 Schwartz et al., 2019). Migrating eruptions would have progressively filled any newly developed
460 valleys with resistant volcanic rocks that eventually (because they blanketed the landscape)
461 constructed an elevated, relatively flat plateau such as described by Best et al. (2009), with
462 surface elevations substantially increased by magmatic and thermal input into the crust.

463



464

465 Figure 7. Schematic illustration of southward-migrating topographic uplift in the Great Basin related to the
466 ignimbrite flareup. This figure depicts a late Eocene (ca. 36 Ma) snapshot of thermally and magmatically

467 supported volcanic highlands (to the north). At the latitude of the highlands, the drainage divide has shifted
468 east from its Late Cretaceous to Paleocene position along the axis of the ancestral Sierra Nevada range (Van
469 Buer et al., 2009) toward the center of the highlands. Latitudes farther south have not yet experienced surface
470 uplift, and the divide remains along the ancestral Sierra Nevada range. Drainage networks have been
471 reorganized near and north of the uplifted region, which remains elevated after cessation of volcanism due to
472 input of substantial heat (as indicated by ongoing partial melting in the Ruby Mountains–East Humboldt
473 Range metamorphic core complex; Fig. 6) and voluminous volcanic and plutonic material to the crust.

474

475 Figure 7 presents a schematic diagram of the proposed paleotopographic evolution ca. 36
476 Ma, immediately following the end of volcanism in the Elko area. As magmatism swept south
477 across the Sevier hinterland in Eocene and Oligocene time, it prompted the growth of topography
478 due to the voluminous addition of magma to the crust together with accompanying thermal
479 uplift. We suggest that highlands developed near the main eruptive centers at any given time and
480 that the ~north–south-trending paleodivide proposed by Henry (2008), Henry et al. (2012), and
481 Best et al. (2013) was a southward-propagating dynamic feature, with the highest topography
482 located above the region of the most active caldera centers. Prior to volcanism, drainages likely
483 flowed east and west away from the axis of the Cretaceous arc (Figs. 2 and 6), as defined by the
484 locus of intrusion of the youngest plutonic complexes (Van Buer et al., 2009; Van Buer and
485 Miller, 2010; Sharman et al., 2015). This inference is based on the significantly higher calculated
486 magnitudes of erosion (~5–7 km) in the arc compared to 1–3 km across the back-arc region west
487 of the Sevier fold and thrust belt (Van Buer et al., 2009). The detrital zircon signatures of Late
488 Cretaceous–Eocene sediments deposited in the California forearc basin, west of the arc axis, also
489 indicate derivation from the Sierra Nevada magmatic arc (Figs. 1 and 2) and do not indicate
490 detectable sediment derivation from farther east (Sharman et al., 2015). Some drainages may also
491 have flowed southward toward the Mojave region (Fig. 1), much of which was a marine
492 environment during Paleocene time (e.g., Lofgren et al., 2008; Lechler and Niemi, 2011).
493 Evolving southward-moving uplift would have tended to reorganize pre-existing topography and
494 drainages that were holdovers from the Late Cretaceous, resulting in paleodrainages that
495 emanated to the west, east, and south from the new paleodivide in Nevada (e.g., Best et al., 2013;
496 Henry and John, 2013; Lechler and Niemi, 2011; Miller et al., this volume). Notably, exposures
497 of the Eocene Titus Canyon Formation in the Funeral Range, southeast California (Fig. 1), herald
498 the onset of volcanism in north central Nevada and include clast compositions and detrital zircon

499 age components that suggest that sediment traveled through this region in south-flowing river
500 systems from higher elevations located at least 300 km to the north-northeast (Miller et al., 2019;
501 Miller et al., this volume). At the same time, paleodrainages were unlikely to flow northward
502 from active calderas due to the presence of predecessor high topography (Fig. 7).

503 Removal of the Farallon slab during middle Cenozoic time is thought to have caused the
504 asthenospheric upwelling and subsequent ignimbrite flareup magmatism that would have also
505 thinned the lithosphere below the Great Basin (Humphreys, 1995). Thermally driven uplift is an
506 established consequence of both lithospheric thinning and addition of magmatic material (e.g.,
507 Lachenbruch and Morgan, 1990). The precise magnitude of elevation increase due to ignimbrite
508 flareup volcanism is uncertain, but analogy with other regions suggests that it was 1 km or more
509 (see Crough, 1978; Pierce and Morgan, 1992; Larimer et al., 2019; Schwartz et al., 2019). Along
510 and adjacent to the Yellowstone hotspot track (approximately the Snake River Plain on Fig. 1),
511 localized volcanism between middle Miocene time and the present was accompanied by an east-
512 migrating zone of pronounced uplift, faulting, reorganization of drainage systems, and shifts of
513 the continental divide (Anders and Sleep, 1992; Pierce et al., 1992; Beranek et al., 2006; Coble
514 and Mahood, 2016; Camilleri et al., 2017; Larimer et al., 2019). Detrital zircon records indicate
515 that northeastward migration of Yellowstone hotspot magmatism profoundly disrupted drainage
516 networks, causing streams to emanate away from the associated topographic bulge as it
517 progressed, producing a northeast-oriented paleodivide that was centered either on or at the
518 southern margin of the hotspot track, which later evolved into a crescent-shaped divide around
519 the northwest, east, and southeast sides of Yellowstone (Beranek et al., 2006; Camilleri et al.,
520 2017). The uplift near Yellowstone has led to 1 km deep river incision since 3.6 Ma, an incision
521 rate of nearly 300 m/Myr (Pierce and Morgan, 2009). If the middle Cenozoic Great Basin
522 paleovalleys shown in Fig. 2 developed as a result of magmatism as we propose, then the up to
523 1.2 km of mapped paleovalley relief (Henry, 2008; Henry et al., 2012) provides a minimum
524 estimate for the amount of syn-volcanic uplift, comparable to recent incision near Yellowstone.
525 The lack of evidence for paleorivers that incised into this elevated volcanic tableland following
526 the decline of volcanism (Figs. 6 and 7) might have been a consequence of post-volcanic areas
527 being slightly lower than areas to the south that were still experiencing active volcanism, and/or
528 due to the erosional resistivity of the volcanic rocks. The uplift rates along the Yellowstone
529 hotspot track not only demonstrate the significance of thermally driven topographic changes but

530 also underscore that hundreds of meters of paleovalley erosion/incision may occur relatively
531 rapidly, such as on the order of 1 to 10 Myr, rather than over long periods of geologic time, such
532 as from the Late Cretaceous to middle Eocene (see, e.g., Colgan and Henry, 2017). We propose
533 that the same processes that are active today near Yellowstone were active in the Great Basin, but
534 at a grander scale, during the much more voluminous middle Cenozoic ignimbrite flareup.

535

536 **PALEOGEOGRAPHIC EVOLUTION OF NORTHEAST NEVADA AND THE GREAT** 537 **BASIN**

538 Based on the evidence presented above from the sedimentary, structural, and magmatic
539 records of the Elko area, integrated with data from surrounding areas, we present a summary
540 view of the evolution of the Late Cretaceous to Cenozoic paleogeography of the northern Great
541 Basin, as illustrated in Fig. 8. The timeline applies to northeast Nevada (right-hand panels of Fig.
542 6), but we suggest that it is also applicable to much of the Great Basin, especially where
543 pertaining to regional tectonic events (left-hand panels of Fig. 6). This paleogeographic and
544 tectonic history is based upon the well-preserved and less controversial surface geologic record,
545 but it is also intended to reconcile some of the contradictory models for the tectonic evolution of
546 the region.

547

548 **Late Cretaceous to middle Eocene (until ca. 46 Ma): Gradual erosion**

549 Surface-breaking thrust faults were active along the Sevier belt (Fig. 1) in the Late
550 Cretaceous (Fig. 8a), and they created topography as the thrust belt finalized its development and
551 shed its erosional debris into the foreland basin (e.g., Malone et al., this volume). In addition to
552 voluminous foreland basin deposits, erosion of the Sevier belt is reflected by the basal Cenozoic
553 unconformity map that shows erosion carved much deeper into the miogeoclinal section within
554 the thrust belt (e.g., Armstrong, 1968, 1972; Van Buer et al., 2009; Konstantinou et al., 2012).
555 The Sevier thrust faults ceased most of their motion by Paleocene time (Fig. 6) as deformation
556 moved east to the Rocky Mountains during the middle Late Cretaceous to Eocene Laramide
557 orogeny (e.g., DeCelles and Coogan, 2006; Copeland et al., 2017), but motion along the Paris
558 thrust of the Sevier belt in southeast Idaho and northeast Utah may have continued into the
559 Oligocene (Malone et al., this volume). The switch to Laramide-style deformation is thought to
560 be linked to the onset of shallow slab subduction of part of the Farallon plate (Fig. 8a), as

561 documented by both the cessation of magmatism in the Sierra Nevada arc and the eastward shift
562 of deformation (e.g., Dickinson and Snyder, 1978).

563 Throughout the Late Cretaceous and early Cenozoic (Fig. 6), northeast Nevada and much
564 of the Great Basin region to the west of the Sevier thrust belt (its hinterland) appears to have
565 experienced only modest erosion (less than 3 km in most areas) with evidence for faulting and
566 tectonism in the surficial record only located around a handful of previously identified structures
567 (e.g., Van Buer et al., 2009; Konstantinou et al., 2012; Long, 2012). These inferences are farther
568 supported by reconstructions of the middle Cenozoic unconformity and paleogeologic maps of
569 units beneath that unconformity. The observation of generally low conodont alteration index
570 values across much of the Great Basin (Harris et al., 1980; Gans and Miller, 1983; Gans et al.,
571 1990; Crafford and Harris, 2005) likewise indicates burial only to stratigraphic depths and is
572 consistent with erosion mostly limited to the upper part of the Paleozoic-Mesozoic shelf
573 stratigraphic section. During the Late Cretaceous and early Cenozoic, multiple lines of evidence
574 discussed above suggest that the regional topographic divide was located near the axis of the
575 Cretaceous magmatic arc (Figs. 2, 6, and 8a; Van Buer et al., 2009; Sharman et al., 2015). To the
576 east of the Sevier fold and thrust belt, parts of the foreland basin system in Utah were near sea
577 level (Fig. 8a) in the Late Cretaceous (DeCelles and Coogan, 2006). The southern margin of the
578 Great Basin also lay near sea level in Paleocene and possibly early Eocene time (Figs. 1 and 6),
579 as indicated by the Paleogene marine fossils near the southeastern part of the Sierra Nevada, on
580 the northern margin of the Mojave Desert (Lofgren et al., 2008; Lechler and Niemi, 2011).
581 Consequently, elevations most likely decreased both to the east (Fig. 8a) and south from the
582 Cretaceous Sierra Nevada arc and the Sevier hinterland.

583

584 **Middle Eocene (ca. 46–38 Ma): Shallow basins and early volcanism in northeast Nevada**

585 The Elko and Copper basins developed during middle Eocene time as shallow basins in
586 northeast Nevada (Figs. 1 and 2), initiating by ca. 46 Ma and perhaps locally as early as ca. 49
587 Ma (Haynes, 2003; Lund Snee et al., 2016; Smith et al., 2017). At about this time, the Farallon
588 shallow slab is inferred to have started to steepen (Fig. 8b), triggering upwelling of hot
589 asthenosphere that contributed to an influx of magma and heat to the crust (e.g., Armstrong and
590 Ward, 1991; Humphreys, 1995; Konstantinou et al., 2012; Konstantinou and Miller, 2015). The
591 Elko and Copper basins (Fig. 1) provide the first indications of an eastward shift of the

592 topographic divide (Fig. 8b) in middle Eocene time. Deposits preserved in paleovalleys indicate
593 both eastward and westward flow of ignimbrites away from an area west and north of the Elko
594 Basin (Fig. 2) in northern Nevada (Henry, 2008). As suggested above, the mapped
595 paleodrainages developed approximately during magmatism (Fig. 6), changing an earlier
596 landscape through topographic growth and reorganizing and replacing pre-existing drainage
597 networks (Fig. 7).

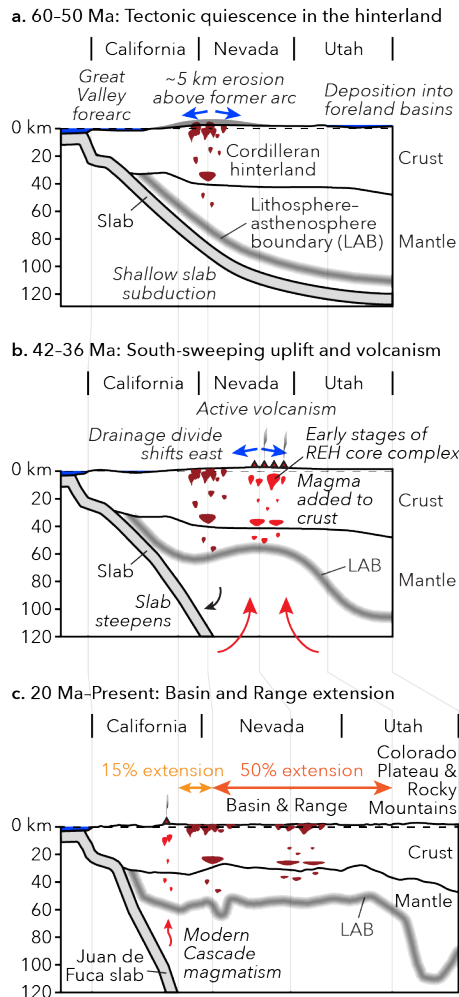
598 Basin development may have been a result of normal faulting (Vandervoort and Schmitt,
599 1990; Rahl et al., 2002; Haynes, 2003; Howard, 2003) and/or isostatic adjustments associated
600 with steepening of the Farallon slab and associated asthenospheric upwelling (Smith et al., 2017)
601 and/or the onset of magma chamber formation and volcanism. Faulting before and during
602 ignimbrite flareup volcanism “was minor and/or exceedingly local” throughout the Great Basin
603 (e.g., Henry and John, 2013, p. 954), but such faulting shortly before—and in rare cases during—
604 volcanism is observed in several areas, including northeast Nevada (e.g., Henry et al., 2011) and
605 central Nevada (e.g., Gans et al., 1989; Best and Christiansen, 1991; Miller et al., 1999;
606 Druschke et al., 2009a; Ruksznis, 2015). Localized faulting may have occurred due to rapid but
607 differential emplacement of voluminous magma bodies and heat transfer to the upper crust,
608 and/or to localized thermal weakening of crust experiencing far-field extensional strain, as has
609 been suggested for the vicinity of all three Great Basin MCCs (Miller et al., 1999; Konstantinou
610 et al., 2012, 2013a; Konstantinou and Miller, 2015; Lund Snee et al., 2016; Lee et al., 2017).
611 Arrival of volcanism was accompanied by a marked increase of heat input to the crust as
612 indicated by increased high-T mineral (zircon and monazite) growth ca. 42 Ma at deeper levels
613 of the crust now exposed in the REH MCC (Fig. 6; Howard et al., 2011).

614

615 **Late Eocene (ca. 38–36 Ma): Active magmatism with volcanism**

616 Sedimentation effectively ceased with the inception of volcanism (see above and Fig. 6),
617 which blanketed the focus area with volcanic flows and ignimbrites beginning ca. 38 Ma
618 (Haynes, 2003; Ressel and Henry, 2006; Lund Snee et al., 2016). These volcanic rocks formed a
619 flat regional tableland (Best et al., 2009) that persisted in northeast Nevada with little erosion
620 until the onset of Neogene Basin and Range faulting. Similar relationships are likely across the
621 entire northern Great Basin (Fig. 6), as documented by the widespread preservation of volcanic
622 rocks above the regional lower Cenozoic unconformity (e.g., Gans and Miller, 1983; Van Buer et

623 al., 2009; Konstantinou et al., 2012). Following the last eruption within the study area ca. 36.8
 624 Ma (Lund Snee et al., 2016), magmatism continued southward (e.g., Ryskamp et al., 2008),
 625 likely in tandem with elevation gain, as proposed in this paper (Fig. 7).
 626



627
 628 Figure 8. Cross sections along 40.5°N latitude (line of section shown in Fig. 1) from Late Cretaceous time to
 629 the present. Present-day crustal thickness is from Shen and Ritzwoller (2016), the lithosphere–asthenosphere
 630 boundary is after the combined Sp–Ps interpretation of Levander and Miller (2012), and the Juan de Fuca slab
 631 position is after McCrory et al. (2012) and Tian and Zhao (2012). Extension magnitudes are based loosely on
 632 those estimated by Colgan et al. (2004) and Colgan and Henry (2009).
 633

634 **Late Eocene to latest Oligocene (ca. 36–25 Ma): Volcanic quiescence with little erosion or**
 635 **faulting at the Earth’s surface (but continuing magmatism and crustal melting at depth)**

636 Partial melting and magmatism continued in the deeper crust within the developing REH
637 MCC and the Albion–Raft River–Grouse Creek (ARG) MCC to the north (Figs. 1, 2, and 6),
638 long after the cessation of surface volcanism, and concomitant with relative rise of metamorphic
639 rocks (McGrew and Snee, 1994; McGrew et al., 2000; Howard et al., 2011; Konstantinou et al.,
640 2013a). The persistence of elevated temperatures, combined with ongoing and prior magmatic
641 addition to the crust from the mantle, likely ensured that topography remained thermally elevated
642 to some degree (Fig. 7), at least through much of the Oligocene. The near absence of sedimentary
643 deposits between ca. 38–25 Ma in the study area (Fig. 6) and following volcanism throughout the
644 northern Great Basin in general (Henry et al., 2011) confirm that whatever surface-breaking
645 faulting that occurred during the 10 Myr or more time span following volcanism was very
646 limited in extent and magnitude.

647

648 **Latest Oligocene to middle Miocene (ca. 25–16.5 Ma): Little erosion and limited faulting**

649 The sedimentary record in northeast Nevada indicates that tectonic quiescence and
650 gradual erosion occurred between latest Oligocene and middle Miocene time (Fig. 6). Locally,
651 however, lacustrine sedimentation (indicating the formation of basin accommodation) may have
652 initiated (Figs. 4b, 5, and 6), based on ages of the earliest fluvial-lacustrine sediments deposited
653 above Eocene and Oligocene volcanic rocks in Huntington Valley (Figs. 4b and 5) and near the
654 East Humboldt Range (Fig. 1) (Frerichs and Pekarek, 1994; McGrew and Snoke, 2015; Lund
655 Snee et al., 2016). Minor deposition in the latest Oligocene or early Miocene has also been
656 recorded near the Snake Range MCC (Gans et al., 1989; Miller et al., 1999; Ruksznis, 2015) and
657 elsewhere (Fig. 6).

658

659 **Middle Miocene (17–16 Ma) to present: Rapid and then more gradual extension**

660 As discussed above, rapid slip on Basin and Range normal faults with formation of
661 ensuing topography similar to that of today occurred across most of the central part of the
662 northern BRP (Figs. 1, 2, 6, and 8c) ca. 17–16 Ma (e.g., Noble, 1972; Lund et al., 1993; Miller et
663 al., 1999; Stockli, 2005; Colgan et al., 2010). Across this region, fault slip rates decreased
664 beginning ca. 12–10 Ma (Fig. 6), based on thermochronologic data and sedimentation rates (e.g.,
665 Colgan et al., 2008; Colgan and Henry, 2009). Extension that began in these central areas
666 subsequently propagated west, east, and north (Surpless et al., 2002; Stockli, 2005; Colgan et al.,

667 2006; Lerch et al., 2008). Extension continues at a slow rate today as active slip takes place
668 primarily on faults now close to the boundaries of the province (Thatcher et al., 1999; Kreemer et
669 al., 2010). The timing of rapid extension coincides closely with a number of notable tectonic
670 events (Figs. 6 and 8c), including final removal of the Farallon slab ca. 20 Ma (Humphreys,
671 1995), development of a gap in the Farallon slab ca. 17 Ma and subsequent impingement of the
672 Yellowstone hotspot (Liu and Stegman, 2012), and the progressive development of the San
673 Andreas transform boundary with northward migration of the Mendocino triple junction over
674 Neogene time (Atwater and Stock, 1998).

675

676 **IMPLICATIONS FOR PALEOTOPOGRAPHY AND CRUSTAL THICKNESS**

677 The paleogeographic and crustal history outlined in the above synthesis (Figs. 6, 7, and 8)
678 has direct implications for the topographic and crustal evolution of the hinterland region between
679 the Cretaceous arc and Sevier thrust belt (Figs. 1 and 2). Multiple lines of evidence suggest that
680 appreciable elevation gain (probably 1 km or more, as suggested above) may have taken place
681 much later than Mesozoic time (Fig. 8a), roughly synchronous with and persisting to some
682 degree after Cenozoic volcanism swept across the region (Figs. 2 and 8b), before subsiding to its
683 present ~1.5–2.0 km average elevations and sawtooth topography during and/or after Basin and
684 Range extension (Fig. 8c). The growing database discussed here indicates an important time lag
685 between crustal thickening and extension that is inconsistent with suggestions that a high plateau
686 was supported by gravitationally unstable crust overthickened during the Mesozoic (e.g., Sonder
687 et al., 1987; Chase et al., 1998; Druschke et al., 2009b; Wells et al., 2012; Wells and Hoisch,
688 2012; Affinati et al., this volume). In addition, an important consideration is that the heat budget
689 represented by ultimately mantle-derived Cenozoic magmatism by far exceeded that related to
690 thermal equilibration of crust thickened by thrust faulting (Gottlieb, 2018; Gottlieb et al., this
691 volume).

692 The thermal effects from voluminous and widespread ignimbrite flareup magmatism are
693 rarely considered in topographic and tectonic models of the Great Basin. Studies that estimate
694 pre-extensional crustal thicknesses by restoring Cenozoic extension (e.g., Bahadori et al., 2018;
695 Long, 2018) do not account for the substantial thicknesses of middle Cenozoic volcanic material
696 added to the surface in many areas nor the potentially much greater volumes of associated
697 plutonic material; thus, their inferred post-thickening and pre-extensional crustal thicknesses are

698 likely overestimates. A (map view) restoration of topography across the northern Great Basin by
699 Bahadori et al. (2018) proposed a narrow, tall (crest ≥ 4 km and peaks >6 km) mountain range
700 atop a ~ 55 – 60 km thick welt of crust in the Eocene. That study restored pre-extensional crustal
701 thicknesses based on the kinematic model by McQuarrie and Wernicke (2005), combined with an
702 isostatic compensation model. The geometry of the resulting crustal welt is broadly similar to
703 that shown by Long (2018), which was based largely on the Sevier thrust belt reconstruction of
704 DeCelles and Coogan (2006). The modeled mountain chain by Bahadori et al. (2018) lies ~ 200
705 km east of the middle Cenozoic paleodivide that was inferred by Henry et al. (2012) and Best et
706 al. (2013) using the paleoflow directions of channelized ignimbrites. The suggestion of a rugged,
707 ≥ 4 km-tall mountain chain along the Utah-Nevada border, supported by relatively thick crust, is
708 at odds with evidence that pre-volcanic erosion magnitudes were modest and smoothly
709 distributed throughout the area of the inferred crustal welt (Gans and Miller, 1983; Miller and
710 Gans, 1989; Konstantinou et al., 2012; Long, 2012). It would also be unusual for such steep
711 topography to develop just to the west of the active fold and thrust belt. This disagreement
712 between these estimates of crustal thickness and topography and the geologic data described in
713 this paper suggests the need for (1) Retrodeformation studies that consider the limited crustal
714 thicknesses that lay beneath the passive margin sequence west of its depositional hingeline; (2)
715 Tighter constraints on the magnitude of westward crustal underthrusting (see Craddock et al., this
716 volume; Gottlieb et al., this volume); (3) Incorporation of updated models of Cenozoic extension
717 and possible magmatic additions to the crust during the ignimbrite flareup; and (4) Consideration
718 of the thermal state of the crust and the likelihood of regional-scale lower crustal flow that might
719 flatten the Moho before and during extension (Gans, 1987).

720 The assortment of geologic data presented here is incompatible with suggestions that
721 crustal thicknesses became so great during Mesozoic shortening that they led to gravitationally
722 driven extensional collapse (e.g., Wells et al., 2012). There is also little in the record of
723 sedimentation, stable isotope values, and deformation such as surface faulting to suggest
724 significant changes in elevation between the Late Cretaceous and shortly before the arrival of
725 middle Cenozoic volcanism. What little deposition occurred was mostly within the Sheep Pass
726 Basin, where up to ~ 1 km of Sheep Pass Formation sediments was deposited throughout Late
727 Cretaceous to middle Eocene time (Figs. 1, 2, and 6; Druschke et al., 2009a, 2009b). We point
728 out that the gradual, localized occurrence of normal faulting thought to have provided

729 accommodation for these deposits need not signify wholesale gravitational collapse of
730 overthickened crust across the immense region envisaged as encompassing the *Nevadaplano*.
731 Moreover, topographic relief (which would result from widespread surface-breaking faulting)
732 likely was low across most of the Sevier hinterland before middle Cenozoic time (Fig. 8a), based
733 on the depositional patterns of far-traveled Cenozoic ash-flow tuffs (e.g., Best et al., 2009) and
734 the modest magnitudes of pre-Eocene erosion and tilting documented in the Elko region (Brooks
735 et al., 1995; Henry et al., 2011; Lund Snee et al., 2016; Canada et al., 2019; this study) and
736 across the hinterland in general (Gans and Miller, 1983; Gans et al., 1990; Crafford and Harris,
737 2005; Van Buer et al., 2009; Long, 2012; Konstantinou et al., 2013b). Suggestions that the
738 hinterland was early on characterized by rugged, mountainous topography (Druschke et al.,
739 2011; Bahadori et al., 2018; Bahadori and Holt, 2019) are clearly at odds with the above set of
740 observations.

741 Few constraints are available for absolute elevations of the Sevier hinterland prior to
742 extension, during the Late Cretaceous and early Cenozoic. Measurements from Eocene fossil
743 leaves in Copper Basin (Figs. 1 and 2), representing the time at the onset of volcanism, provide
744 widely distributed elevation estimates ranging from 0.6–1.2 km (Christiansen and Yeats, 1992)
745 and 1.6 ± 1.6 km (Chase et al., 1998), to 2.0 ± 0.2 km (Wolfe et al., 1998) and 2.8 ± 1.8 km
746 (Chase et al., 1998). This broad range complicates efforts to employ such estimates
747 quantitatively. A definitive minimum hinterland elevation bound of 1.2 km was provided by
748 Henry et al. (2012), based on measured middle Cenozoic paleovalley depths, which we suggest
749 developed only after uplift related to ignimbrite flareup volcanism. Probably the most reliable
750 estimates of absolute elevation are provided by two clumped isotope studies. Snell et al. (2014)
751 estimated that absolute elevations in the Sheep Pass Basin (Fig. 1) of east-central Nevada ranged
752 between 2.0–3.1 km in latest Cretaceous to early Paleocene time. Also using clumped isotope
753 thermometry, Lechler et al. (2013) estimated only ≤ 2 km paleoelevation for the Sheep Pass
754 Basin, integrated over the younger but overlapping latest Cretaceous–early Eocene interval.
755 Although different, these two elevation estimates overlap at ~ 2 km, suggesting that this may be a
756 reasonable elevation value for east-central Nevada in latest Cretaceous–early Eocene time.
757 Additional lines of evidence support suggestions of only modest elevations across the Sevier
758 hinterland prior to volcanism. As noted, marine fossils, stable isotope data, and detrital
759 populations show that the southern Sierra Nevada and areas slightly to the east ($\sim 35.5^\circ\text{N}$

760 latitude), which have a similar geologic history to the Great Basin, were *at or near sea level* in
761 the Paleocene (Figs. 1 and 6) and may have remained very low (<1 km) into Eocene time
762 (Lofgren et al., 2008; Lechler and Niemi, 2011). If a significantly elevated plateau was present
763 across the Great Basin in Late Cretaceous and Paleogene time, then it must have been limited to
764 areas north of ~37–38°N and bounded on the south by slopes leading nearly to sea level.

765 It is challenging to reconcile the above narrative of Great Basin surface evolution with
766 implications for 10–20 km of relative uplift implied by quantitative geobarometry on Cretaceous
767 metamorphic assemblages in MCCs (Hodges et al., 1992; Lewis et al., 1999; McGrew et al.,
768 2000; Cooper et al., 2010; Hallett and Spear, 2013). These analyses represent the primary
769 evidence supporting suggestions of large crustal thicknesses that drove gravitational collapse of
770 the hinterland prior to Miocene time. A more complete discussion of these questions is provided
771 by Hoiland et al. (this volume), but two hypotheses are relevant: 1.) In recent years, it
772 was recognized that the assumptions underpinning these geobarometric methods may in some
773 cases be invalid, particularly the expectations that mineral assemblages were in equilibrium
774 during formation (Spear et al., 2014) and that the pressure measurements can be interpreted
775 as representing steady-state overburden pressures (proportional to burial depth) rather than
776 transient and/or non-isostatic (tectonic) stresses (Schmalholz et al., 2014; Gerya, 2015). This
777 leaves open a number of other possibilities to explain high pressure estimates in Great Basin
778 MCCs, including tectonic “overpressure” (Henry et al., 2018; Thorman et al., 2020; Zuza et al.,
779 2020; Hoiland et al., this volume). 2.) If some or all of the proposed uplift in developing MCCs
780 was Cenozoic in age, then uplift could have occurred with little surface-breaking extension
781 provided that lower crustal rocks were locally decoupled from surface deformation due to
782 strongly elevated heat flow during mid-crustal melting (MacCready et al., 1997; Miller et al.,
783 1999; Konstantinou et al., 2012; Lund Snee et al., 2016; Lee et al., 2017). This mechanism
784 would explain the difference in timing of subsurface uplift versus surface-breaking extension, as
785 elegantly demonstrated for the ARG (Fig. 1) MCC (Konstantinou et al., 2013a).

786

787 **CONCLUSIONS**

788 We have presented an updated view of the enigmatic transition from Mesozoic shortening
789 to Cenozoic extension in the Great Basin (Figs. 1 and 2), focusing primarily on the supracrustal
790 records of sedimentation, erosion, faulting, volcanism, and stable isotope values, and how those

791 relate to topography development. This integrated record shows that gradual erosion, limited
792 deposition, and general tectonic quiescence prevailed between Late Cretaceous and middle
793 Cenozoic time (Fig. 6). Although surface-breaking faults are documented across this time
794 interval, they were local in scale and significance, involving relatively low magnitudes of slip
795 (e.g., Best and Christiansen, 1991; Henry et al., 2011). The arrival of south-migrating ignimbrite
796 flareup volcanism in the middle Cenozoic profoundly affected topography, disrupting hinterland
797 drainage networks. This is most clearly shown by the systematic southward-younging ages of the
798 oldest material recorded at the base of west- and east-flowing Eocene–Oligocene paleovalleys
799 (Fig. 2), suggesting that new drainages formed progressively southward, roughly synchronous
800 with volcanism. In some areas, volcanism was also preceded by development of shallow basins,
801 relatively minor offset along normal faults, and limited sedimentation. We suggest that volcanism
802 caused pronounced uplift, perhaps of the order of 1.2 km based on the measured height of
803 paleovalleys active during this time (Henry et al., 2012). Given the massive influx (see, e.g., Best
804 et al., 2009) of heat associated with the addition of volcanic and plutonic material to the
805 lithosphere, uplift is an expected result (e.g., Lachenbruch and Morgan, 1990), as exemplified
806 today by the >1 km uplift around Yellowstone (e.g., Pierce et al., 1992). However, while the
807 records of sedimentation, erosion, faulting, drainage development, and magmatism all support an
808 elevation increase associated with the ignimbrite flareup, this is no longer clearly supported by
809 the available stable isotope information from carbonates in basins across the western USA. A
810 consequence of the improved age control and characterization of those sections near Elko (Lund
811 Snee et al., 2016; Smith et al., 2017; this study) and in southwest Montana (Schwartz et al.,
812 2019) is that prominent decreases in $\delta^{18}\text{O}$ values during the early and middle Cenozoic (e.g.,
813 Horton et al., 2004; Davis et al., 2006; Kent-Corson et al., 2006; Mix et al., 2011; Chamberlain et
814 al., 2012) can no longer be tied directly to the onset of volcanism in these areas.

815 We propose that dynamic uplift accompanying ignimbrite flareup magmatism shifted the
816 continental divide eastward into central Nevada from its prior position along the crest of the
817 Cretaceous magmatic arc (Van Buer et al., 2009) and that this shift occurred in a southward-
818 propagating fashion (Figs. 7 and 8). The middle Cenozoic highlands that supported this
819 developing paleodivide were not static but instead responded dynamically as eruptions occurred
820 and calderas formed. Volcanism left behind a plateau, with little documented erosion, tectonism,
821 or sedimentation occurring until ca. 17 Ma (Figs. 6–8), although minor deposition initiated as

822 early as latest Oligocene time in certain areas (Fig. 6), dominantly near developing metamorphic
823 core complexes (Gans et al., 1989; Frerichs and Pekarek, 1994; Miller et al., 1999; Lund Snee et
824 al., 2016; McGrew and Snoke, 2015; Ruksznis, 2015; this study). Elevations likely remained
825 high following volcanism (perhaps with some component of gradual subsidence) due to the
826 largely irreversible addition of magma to the crust and evidence that rocks currently exposed in
827 MCCs experienced partial melting tens of millions of years later than the onset of Cenozoic
828 magmatism (Howard et al., 2011; Strickland et al., 2011; Konstantinou et al., 2012, 2013a;
829 Konstantinou and Miller, 2015). Rapid regional extension by Basin and Range faulting initiated
830 ca. 17 Ma (Stockli, 2005; Colgan and Henry, 2009; Colgan, 2013), probably in response to
831 changing boundary conditions, and driven by crust that remained elevated and thermally
832 weakened.

833 The tectonic and topographic history and its temporal framework discussed here
834 challenge suggestions that Mesozoic shortening produced a greatly thickened and elevated crust
835 that drove gravitational collapse across the Sevier hinterland either during shortening or soon
836 after (see also Konstantinou, this volume). Evidence for rapidly evolving topography, drainage
837 divides, and highlands related to and during Cenozoic magmatism also challenges the traditional
838 notion of a long-lived, strongly elevated *Nevadaplano* (Cassel et al., 2012; Wells et al., 2012;
839 Best et al., 2013) with a fixed (Late Cretaceous to) Cenozoic drainage divide (Henry et al.,
840 2012). These suggestions pose implications for our understanding of orogenic and magmatic
841 systems worldwide, underscoring the short time scales over which major changes in elevation
842 and catchment can occur, particularly when the influence of magmatism on topography is
843 considered.

844

845 **ACKNOWLEDGEMENTS**

846 We thank Trevor A. Dumitru for guidance with detrital zircon geochronology, Mark E.
847 Raftrey for analyzing four detrital zircon samples, and Stephen Pearcey and Virginia Isava for
848 assisting with sampling. The manuscript benefitted from discussions with Simon L. Klemperer,
849 George A. Thompson, Joseph P. Colgan, Karen I. Lund, Norm H. Sleep, and Theresa M.
850 Schwartz. We are grateful to John P. Craddock for thoughtful editorial work and to Kathryn E.
851 Snell, Theresa M. Schwartz, and David H. Malone for detailed comments that considerably

852 improved the manuscript. This research was funded by NSF grant EAR-1322084 to Miller and a
853 Stanford University G.J. Lieberman Fellowship to Lund Snee.

854

855 REFERENCES

856 Affinati, S.C., Hoisch, T.D., Wells, M.L., and Wright, S., 2021, Timing of Jurassic burial and
857 exhumation in the hinterland of the Sevier orogen in Barrovian metamorphic rocks dated by
858 monazite petrochronology, Funeral Mountains, California, in Craddock, J.P., Malone, D.H.,
859 Foreman, B.Z., and Konstantinou, A. eds., *Tectonic Evolution of the Sevier-Laramide*
860 *Hinterland, Thrust Belt, Foreland and Post-Orogenic Slab Rollback (150-20 Ma)*, Boulder,
861 Colorado, Geological Society of America.

862 Anders, M.H., and Sleep, N.H., 1992, Magmatism and extension—The thermal and mechanical
863 effects of the Yellowstone hotspot: *Journal of Geophysical Research*, v. 97, p. 15,379-
864 15,393, doi:10.1029/92JB01376.

865 Armstrong, R.L., 1972, Low-angle (denudation) faults, hinterland of the sevier orogenic belt,
866 eastern Nevada and western Utah: *Bulletin of the Geological Society of America*, v. 83, p.
867 1729–1754, doi:10.1130/0016-7606(1972)83[1729:LDFHOT]2.0.CO;2.

868 Armstrong, R.L., 1968, Sevier orogenic belt in Nevada and Utah: *Bulletin of the Geological*
869 *Society of America*, v. 79, p. 429–458, doi:10.1130/0016-
870 7606(1968)79[429:SOBINA]2.0.CO;2.

871 Armstrong, R.L., and Ward, P., 1991, Evolving geographic patterns of Cenozoic magmatism in
872 the North American Cordillera: The temporal and spatial association of magmatism and
873 metamorphic core complexes: *Journal of Geophysical Research*, v. 96, p. 13,201–13,224,
874 doi:10.1029/91JB00412.

875 Atwater, T., 1989, Plate tectonic history of the northeast Pacific and western North America, *in*
876 Winterer, E.L., Hussong, D.M., and Decker, R.W. eds., *The Geology of North America: The*
877 *Eastern Pacific Ocean and Hawaii*, v. N, p. 499–522.

878 Atwater, T., and Stock, J.M., 1998, Pacific-North America plate tectonics of the Neogene
879 southwestern United States: An update: *International Geology Review*, v. 40, p. 375–402,
880 doi:10.1080/00206819809465216.

881 Axelrod, D.I., 1966, *The Eocene Copper Basin flora of northeastern Nevada*: Berkeley,
882 University of California Press, v. 59, 83 p.

883 Bahadori, A., and Holt, W.E., 2019, Geodynamic evolution of southwestern North America since
884 the late Eocene: *Nature Communications*, v. 10, p. 1–18, doi:10.1038/s41467-019-12950-8.

885 Bahadori, A., Holt, W.E., and Rasbury, E.T., 2018, Reconstruction modeling of crustal thickness
886 and paleotopography of western North America since 36 Ma: *Geosphere*, v. 14, p. 1207–
887 1231, doi:10.1130/GES01604.1.

888 Beranek, L.P., Link, P.K., and Fanning, C.M., 2006, Miocene to Holocene landscape evolution of
889 the western Snake River Plain region, Idaho: Using the SHRIMP detrital zircon provenance
890 record to track eastward migration of the Yellowstone hotspot: *Bulletin of the Geological
891 Society of America*, v. 118, p. 1027–1050, doi:10.1130/B25896.1.

892 Best, M.G., Barr, D.L., Christiansen, E.H., Gromme, S., Deino, A.L., and Tingey, D.G., 2009,
893 The Great Basin Altiplano during the middle Cenozoic ignimbrite flareup: insights from
894 volcanic rocks: *International Geology Review*, v. 51, p. 589–633,
895 doi:10.1080/00206810902867690.

896 Best, M.G., and Christiansen, E.H., 1991, Limited extension during peak Tertiary volcanism,
897 Great Basin of Nevada and Utah: *Journal of Geophysical Research*, v. 96, p. 13509,
898 doi:10.1029/91JB00244.

899 Best, M.G., Christiansen, E.H., and Gromme, S., 2013, Introduction: The 36-18 Ma southern
900 Great Basin, USA, ignimbrite province and flareup: Swarms of subduction-related
901 supervolcanoes: *Geosphere*, v. 9, p. 260–274, doi:10.1130/GES00870.1.

902 Du Bray, E.A., 2007, Time, space, and composition relations among northern Nevada intrusive
903 rocks and their metallogenic implications: *Geosphere*, v. 3, p. 381–405,
904 doi:10.1130/GES00109.1.

905 Brooks, W.E., Thorman, C.H., Snee, L.W., and Al, B.E.T., 1995, Ar ages and tectonic setting of
906 the middle Eocene northeast Nevada volcanic field: *Journal of Geophysical Research*, v.
907 100, p. 10403–10416, doi:10.1029/94JB03389.

908 Van Buer, N.J., and Miller, E.L., 2010, Sawtooth batholith, NW Nevada: Cretaceous arc flareup
909 in a basinal terrane: *Lithosphere*, v. 2, p. 423–446, doi:10.1130/L105.1.

910 Van Buer, N.J., Miller, E.L., and Dumitru, T.A., 2009, Early Tertiary paleogeologic map of the
911 northern Sierra Nevada batholith and the northwestern Basin and Range: *Geology*, v. 37, p.
912 371–374, doi:10.1130/G25448A.1.

913 Burchfiel, C., Cowan, D.S., and Davis, G.A., 1992, Tectonic overview of the Cordilleran orogen

914 in the western United States, *in* Burchfiel, B.C., Lipman, P.W., and Zoback, M.L. eds., *The*
915 *Geology of North America*, v. G-3, p. 407–479.

916 Camilleri, P.A., Deibert, J., and Perkins, M.E., 2017, Middle Miocene to Holocene tectonics,
917 basin evolution, and paleogeography along the southern margin of the Snake River Plain in
918 the Knoll Mountain-Ruby-East Humboldt Range region, northeastern Nevada and south-
919 central Idaho: *Geosphere*, v. 13, p. 1901–1948, doi:10.1130/GES01318.1.

920 Canada, A.S., Cassel, E.J., Stockli, D.F., Smith, M.E., Jicha, B.R., and Singer, B.S., 2020,
921 Accelerating exhumation in the Eocene North American Cordilleran hinterland:
922 Implications from detrital zircon (U-Th)/(He-Pb) double dating: *GSA Bulletin*, v. 132, p.
923 198–214, doi:10.1130/B35160.1.

924 Carroll, A.R., Doebbert, A.C., Booth, A.L., Chamberlain, C.P., Rhodes-Carson, M.K., Smith,
925 M.E., Johnson, C.M., and Beard, B.L., 2008, Capture of high-altitude precipitation by a
926 low-altitude Eocene lake, western U.S: *Geology*, v. 36, p. 791–794,
927 doi:10.1130/G24783A.1.

928 Cassel, E.J., Breecker, D.O., Henry, C.D., Larson, T.E., and Stockli, D.F., 2014, Profile of a
929 paleo-orogen: High topography across the present-day Basin and Range from 40 to 23 Ma:
930 *Geology*, v. 42, p. 1007–1010, doi:10.1130/G35924.1.

931 Cassel, E.J., Graham, S.A., and Chamberlain, C.P., 2009, Cenozoic tectonic and topographic
932 evolution of the northern Sierra Nevada, California, through stable isotope paleoaltimetry in
933 volcanic glass: *Geology*, v. 37, p. 547–550, doi:10.1130/G25572A.1.

934 Cassel, E.J., Graham, S.A., Chamberlain, C.P., and Henry, C.D., 2012, Early Cenozoic
935 topography, morphology, and tectonics of the northern Sierra Nevada and western Basin and
936 Range: *Geosphere*, v. 8, p. 229–249, doi:10.1130/GES00671.1.

937 Cassel, E.J., Smith, M.E., and Jicha, B.R., 2018, The impact of slab rollback on Earth’s surface:
938 Uplift and extension in the hinterland of the North American Cordillera: *Geophysical*
939 *Research Letters*, p. 1–9, doi:10.1029/2018GL079887.

940 Chamberlain, C.P., Mix, H.T., Mulch, A., Hren, M.T., Kent-Corson, M.L., Davis, S.J., Horton,
941 T.W., and Graham, S.A., 2012, The Cenozoic climatic and topographic evolution of the
942 western North American Cordillera: *American Journal of Science*, v. 312, p. 213–262,
943 doi:10.2475/02.2012.05.

944 Chamberlain, C.P., Mulch, A., Kent-Corson, M.L., Davis, S.J., Carroll, A.R., and Graham, S.A.,

945 2007, Cenozoic topographic evolution of the Western North America Cordillera:
946 *Geochimica Et Cosmochimica Acta*, v. 71, p. A157–A157.

947 Chase, C.G., Gregory-Wodzicki, K., Parrish, J.T., and DeCelles, P.G., 1998, Topographic history
948 of the Western Cordillera of North America and controls on climate, *in* Crowley, T.J. and
949 Burke, K. eds., *Tectonic boundary conditions for climate reconstructions*, Oxford University
950 Press, v. 39, p. 73–99,
951 [https://books.google.ch/books?hl=en&lr=&id=HbamVUkDTLMC&oi=fnd&pg=PA73&dq=chase+1998+western+cordillera&ots=qen7llUxn_&sig=WUIfZKMs-](https://books.google.ch/books?hl=en&lr=&id=HbamVUkDTLMC&oi=fnd&pg=PA73&dq=chase+1998+western+cordillera&ots=qen7llUxn_&sig=WUIfZKMs-ftiRgSKQKshUJ8wYUk#v=onepage&q=chase+1998+western+cordillera&f=false)
952 [ftiRgSKQKshUJ8wYUk#v=onepage&q=chase 1998 western cordillera&f=false](https://books.google.ch/books?hl=en&lr=&id=HbamVUkDTLMC&oi=fnd&pg=PA73&dq=chase+1998+western+cordillera&ots=qen7llUxn_&sig=WUIfZKMs-ftiRgSKQKshUJ8wYUk#v=onepage&q=chase+1998+western+cordillera&f=false).

954 Christiansen, R.L., and Yeats, R.S., 1992, Post-Laramide geology of the US Cordilleran region,
955 *in* Burchfiel, B.C., Lipman, P.W., and Zoback, M.L. eds., *The Geology of North America*, v.
956 3, p. 261–406.

957 Coble, M.A., and Mahood, G.A., 2012, Initial impingement of the Yellowstone plume located by
958 widespread silicic volcanism contemporaneous with Columbia River flood basalts:
959 *Geology*, v. 40, p. 655–658, doi:10.1130/G32692.1.

960 Coble, M.A., and Mahood, G.A., 2016, Geology of the High Rock caldera complex, northwest
961 Nevada, and implications for intense rhyolitic volcanism associated with flood basalt
962 magmatism and the initiation of the Snake River Plain- Yellowstone trend: *Geosphere*, v.
963 12, p. 58–113, doi:10.1130/GES01162.1.

964 Colgan, J.P., 2013, Reappraisal of the relationship between the northern Nevada rift and Miocene
965 extension in the northern Basin and Range Province: *Geology*, v. 41, p. 211–214,
966 doi:10.1130/G33512.1.

967 Colgan, J.P., Dumitru, T.A., McWilliams, M.O., and Miller, E.L., 2006, Timing of Cenozoic
968 volcanism and Basin and Range extension in northwestern Nevada: New constraints from
969 the northern Pine Forest Range: *Bulletin of the Geological Society of America*, v. 118, p.
970 126–139, doi:10.1130/B25681.1.

971 Colgan, J.P., Dumitru, T.A., and Miller, E.L., 2004, Diachroneity of Basin and Range extension
972 and Yellowstone hotspot volcanism in northwestern Nevada: *Geology*, v. 32, p. 121,
973 doi:10.1130/G20037.1.

974 Colgan, J.P., and Henry, C.D., 2009, Rapid middle Miocene collapse of the Mesozoic orogenic
975 plateau in north-central Nevada: *International Geology Review*, v. 51, p. 920–961,

976 doi:10.1080/00206810903056731.

977 Colgan, J.P., and Henry, C.D., 2017, Eruptive history, geochronology, and post-eruption
978 structural evolution of the late Eocene Hall Creek caldera, Toiyabe Range, Nevada: U.S.
979 Geological Survey Professional Paper 1832, 44 p., doi:10.1130/abs/2016am-285314.

980 Colgan, J.P., Howard, K.A., Fleck, R.J., and Wooden, J.L.P., 2010, Rapid middle Miocene
981 extension and unroofing of the southern Ruby Mountains, Nevada: *Tectonics*, v. 29, p. 417,
982 doi:10.1029/2009TC002655.

983 Colgan, J.P., John, D.A., Henry, C.D., and Fleck, R.J., 2008, Large-magnitude Miocene
984 extension of the Eocene Caetano caldera, Shoshone and Toiyabe Ranges, Nevada:
985 *Geosphere*, v. 4, p. 107–130, doi:10.1130/GES00115.1.

986 Coney, P.J., and Harms, T.A., 1984, Cordilleran metamorphic core complexes: Cenozoic
987 extensional relics of Mesozoic compression: *Geology*, v. 12, p. 550–554, doi:10.1130/0091-
988 7613(1984)12<550:CMCCCE>2.0.CO;2.

989 Cooper, F.J., Platt, J.P., Anczkiewicz, R., and Whitehouse, M.J., 2010, Footwall dip of a core
990 complex detachment fault: Thermobarometric constraints from the northern Snake Range
991 (Basin and Range, USA): *Journal of Metamorphic Geology*, v. 28, p. 997–1020,
992 doi:10.1111/j.1525-1314.2010.00907.x.

993 Copeland, P., Currie, C.A., Lawton, T.F., and Murphy, M.A., 2017, Location, location, location:
994 The variable lifespan of the Laramide orogeny: *Geology*, v. 45, p. 223–226,
995 doi:10.1130/G38810.1.

996 Craddock, J.P., Malone, D.H., Konstantinou, A., Spruell, J., and Porter, R., 2021, Calcite
997 twinning strains associated with Laramide uplifts, Wyoming Province, in Craddock, J.P.,
998 Malone, D.H., Foreman, B.Z., and Konstantinou, A. eds., *Tectonic Evolution of the Sevier-
999 Laramide Hinterland, Thrust Belt, Foreland and Post-Orogenic Slab Rollback (150-20 Ma)*,
1000 Boulder, Colorado, Geological Society of America.

1001 Crafford, A.E.J., 2007, Geologic Map of Nevada: U.S. Geological Survey Data Series 249: U.S.
1002 Geological Survey Data Series 249, p. 46.

1003 Crafford, A.E.J., and Harris, A.G., 2005, New digital conodont color alteration index (CAI) maps
1004 of Nevada, *in Geological Society of America Abstracts with Programs*, Salt Lake City,
1005 Utah, v. 37, p. 379, https://gsa.confex.com/gsa/2005AM/finalprogram/abstract_94308.htm.

1006 Crough, S.T., 1978, Thermal origin of mid-plate hot-spot swells: *Geophysical Journal of the*

1007 Royal Astronomical Society, v. 55, p. 451–469, doi:10.1111/j.1365-246X.1978.tb04282.x.
1008 Dallmeyer, R.D., Snoke, A.W., and McKee, E.H., 1986, The Mesozoic-Cenozoic tectonothermal
1009 evolution of the Ruby Mountains, East Humboldt Range, Nevada: A Cordilleran
1010 metamorphic core complex: *Tectonics*, v. 5, p. 931, doi:10.1029/TC005i006p00931.
1011 Davis, S.J., Mix, H.T., Wiegand, B.A., Carroll, A.R., and Chamberlain, C.P., 2009, Synorogenic
1012 evolution of large-scale drainage patterns: Isotope paleohydrology of sequential laramide
1013 basins: *American Journal of Science*, v. 309, p. 549–602, doi:10.2475/07.2009.02.
1014 Davis, S.J., Mulch, A., Carroll, A.R., Horton, T.W., and Chamberlain, C.P., 2006, Paleogene
1015 landscape evolution of the central North American Cordillera: Developing topography and
1016 hydrology in the Laramide foreland: *Geological Society of America Bulletin*, v. preprint, p.
1017 1, doi:10.1130/B26308.1.
1018 DeCelles, P.G., 2004, Late Jurassic to Eocene evolution of the Cordilleran thrust belt and
1019 foreland basin system, western U.S.A.: *American Journal of Science*, v. 304, p. 105–168,
1020 doi:10.2475/ajs.304.2.105.
1021 DeCelles, P.G., and Coogan, J.C., 2006, Regional structure and kinematic history of the Sevier
1022 fold-and-thrust belt, central Utah: *Bulletin of the Geological Society of America*, v. 118, p.
1023 841–864, doi:10.1130/B25759.1.
1024 Di Fiori, R.V., Long, S.P., Fetrow, A.C., Snell, K.E., Bonde, J.W., and Vervoort, J., 2020,
1025 Syncontractional deposition of the Cretaceous Newark Canyon Formation, Diamond
1026 Mountains, Nevada: Implications for strain partitioning within the U.S. Cordillera:
1027 *Geosphere*, v. 16, p. 546–566, doi:10.1130/GES02168.1.
1028 Dickinson, W.R., 2013, Phanerozoic palinspastic reconstructions of Great Basin geotectonics
1029 (Nevada-Utah, USA): *Geosphere*, v. 9, p. 1384–1396, doi:10.1130/GES00888.1.
1030 Dickinson, W.R., and Snyder, W.S., 1978, Plate tectonics of the Laramide orogeny, *in* *Geological*
1031 *Society of America Memoir*, v. 151, p. 355–366, doi:10.1130/MEM151-p355.
1032 Dokka, R.K., Mahaffie, M.J., and Snoke, A.W., 1986, Thermochronologic evidence of major
1033 tectonic denudation associated with detachment faulting, Northern Ruby Mountains-East
1034 Humboldt Range, Nevada: *Tectonics*, v. 5, p. 995, doi:10.1029/TC005i007p00995.
1035 Druschke, P., Hanson, A.D., and Wells, M.L., 2009a, Structural, stratigraphic, and
1036 geochronologic evidence for extension predating Palaeogene volcanism in the Sevier
1037 hinterland, east-central Nevada: *International Geology Review*, v. 51, p. 743–775,

1038 doi:10.1080/00206810902917941.

1039 Druschke, P., Hanson, A.D., Wells, M.L., Gehrels, G.E., and Stockli, D.F., 2011,
1040 Paleogeographic isolation of the Cretaceous to Eocene Sevier hinterland, east-central
1041 Nevada: Insights from U-Pb and (U-Th)/He detrital zircon ages of hinterland strata: *Bulletin*
1042 *of the Geological Society of America*, v. 123, p. 1141–1160, doi:10.1130/B30029.1.

1043 Druschke, P., Hanson, A.D., Wells, M.L., Rasbury, T., Stockli, D.F., and Gehrels, G.E., 2009b,
1044 Synconvergent surface-breaking normal faults of Late Cretaceous age within the Sevier
1045 hinterland, east-central Nevada: *Geology*, v. 37, p. 447–450, doi:10.1130/G25546A.1.

1046 Dubiel, R.F., Potter, C.J., Good, S.C., and Snee, L.W., 1996, Reconstructing an Eocene
1047 extensional basin: The White Sage Formation, eastern Great Basin: *GSA Special Paper 303*,
1048 p. 14, doi:10.1130/0-8137-2303-5.1.

1049 Dumitru, T.A., Elder, W.P., Hourigan, J.K., Chapman, A.D., Graham, S.A., and Wakabayashi, J.,
1050 2016, Four Cordilleran paleorivers that connected Sevier thrust zones in Idaho to
1051 depocenters in California, Washington, Wyoming, and, indirectly, Alaska: *Geology*, v. 44, p.
1052 75–78, doi:10.1130/G37286.1.

1053 Dumitru, T.A., Ernst, W.G., Hourigan, J.K., and McLaughlin, R.J., 2015, Detrital zircon U–Pb
1054 reconnaissance of the Franciscan subduction complex in northwestern California:
1055 *International Geology Review*, v. 57, p. 767–800, doi:10.1080/00206814.2015.1008060.

1056 Fouch, T.D., Hanley, J.H., and Forester, R.M., 1979, Preliminary correlation of Cretaceous and
1057 Paleogene lacustrine and related nonmarine sedimentary and volcanic rocks in parts of the
1058 eastern Great Basin of Nevada and Utah, *in* 1979 Basin and Range Symposium, Rocky
1059 Mountain Association of Geologists, v. 69, p. 305–312.

1060 Frerichs, W.E., and Pekarek, A.H., 1994, Lower Miocene petroleum potential of northeast Elko
1061 County, *in* Schalla, R.A. and Johnson, E.H. eds., *Oil fields of the Great Basin: Special*
1062 *Publication of the Nevada Petroleum Society*, p. 151–159.

1063 Gans, P.B., 1987, An open-system, two-layer crustal stretching model for the eastern Great
1064 Basin: *Tectonics*, v. 6, p. 1–12, doi:10.1029/TC006i001p00001.

1065 Gans, P.B., 1990, Space-time patterns of Cenozoic N–S extension, N–S shortening, E–W
1066 extension, and magmatism in the Basin and Range Province: Evidence for active rifting, *in*
1067 *Geological Society of America Abstracts with Programs*, v. 22, p. 24.

1068 Gans, P.B., Mahood, G.A., and Schermer, E., 1989, Synextensional magmatism in the Basin and

1069 Range Province; a case study from the eastern Great Basin: GSA Special Paper 233, p. 1–
1070 53, doi:10.1130/SPE233-p1.

1071 Gans, P.B., and Miller, E.L., 1983, Style of mid-Tertiary extension in east-central Nevada:
1072 Special Studies of the Utah Geological and Mineral Survey, v. 59, p. 107–160.

1073 Gans, P.B., Repetski, J.E., Harris, A.G., and Clark, D.H., 1990, Conodont geothermometry of
1074 Paleozoic supracrustal rocks in the eastern Great Basin, *in* Geological Society of Nevada
1075 Symposium, p. 103.

1076 Garside, L.J., Henry, C.D., Faulds, J.E., and Hinz, N.H., 2005, The upper reaches of the Sierra
1077 Nevada auriferous gold channels, California and Nevada: Geological Society of Nevada
1078 Symposium, p. 209–235.

1079 Gerya, T., 2015, Tectonic overpressure and underpressure in lithospheric tectonics and
1080 metamorphism: *Journal of Metamorphic Geology*, v. 33, p. 785–800,
1081 doi:10.1111/jmg.12144.

1082 Goldstrand, P.M., 1992, Evolution of Late Cretaceous and early Tertiary Basins of southwest
1083 Utah based on clastic petrology: *Journal of Sedimentary Research*, v. 62, p. 495–507,
1084 doi:10.1306/D4267933-2B26-11D7-8648000102C1865D.

1085 Goldstrand, P.M., 1994, Tectonic development of Upper Cretaceous to Eocene strata of
1086 southwestern Utah: *Bulletin of the Geological Society of America*, v. 106, p. 145–154,
1087 doi:10.1130/0016-7606(1994)106<0145.

1088 Gottlieb, E.S., 2018, *Geologic insights from zircon inheritance*: Stanford University, 354 p.

1089 Gottlieb, E.S., Miller, E.L., Valley, J.W., Premo, W.R., Fisher, C.M., Vervoort, J.D., and
1090 Kitajima, K., 2021, Zircon petrochronology of Cretaceous Cordilleran Interior granites in
1091 the Sevier hinterland, Nevada, Utah, USA, *in* Craddock, J.P., Malone, D.H., Foreman, B.Z.,
1092 and Konstantinou, A. eds., *Tectonic Evolution of the Sevier-Laramide Hinterland, Thrust
1093 Belt, Foreland and Post-Orogenic Slab Rollback (150-20 Ma)*, Boulder, Colorado,
1094 Geological Society of America.

1095 Haines, S.H., and Van Der Pluijm, B.A., 2010, Dating the detachment fault system of the Ruby
1096 Mountains, Nevada: Significance for the kinematics of low-angle normal faults: *Tectonics*,
1097 v. 29, p. TC4028, doi:10.1029/2009TC002552.

1098 Hallett, B.W., and Spear, F.S., 2013, The P-T history of anatexitic pelites of the northern East
1099 Humboldt Range, Nevada: Evidence for tectonic loading, decompression, and anatexis:

1100 Journal of Petrology, v. 55, p. 3–36, doi:10.1093/petrology/egt057.

1101 Harris, A.G., Wardlaw, B.R., Rust, C.C., and Merrill, G.K., 1980, Maps for assessing thermal
1102 maturity (conodont color alteration index maps) in Ordovician through Triassic rocks in
1103 Nevada and Utah and adjacent parts of Idaho and California: U.S. Geological Survey
1104 Miscellaneous Investigations Series Map I-1249, 1:2,500,000 scale.

1105 Haynes, S.R., 2003, Development of the Eocene Elko Basin, northeastern Nevada: Implications
1106 for paleogeography and regional tectonism: The University of British Columbia,
1107 https://circle.ubc.ca/bitstream/id/34598/ubc_2003-0240.pdf.

1108 Henry, C.D., 2008, Ash-flow tuffs and paleovalleys in northeastern Nevada: Implications for
1109 Eocene paleogeography and extension in the Sevier hinterland, northern Great Basin:
1110 Geosphere, v. 4, p. 1–35, doi:10.1130/GES00122.1.

1111 Henry, C.D., 2018, The Eocene Elko Basin and Elko Formation, NE Nevada: Paleotopographic
1112 controls on area, thickness, facies distribution, and petroleum potential: AAPG Annual
1113 Convention, v. May 20-23, p. 2857031.

1114 Henry, C.D., Hinz, N.H., Faulds, J.E., Colgan, J.P., John, D.A., Brooks, E.R., Cassel, E.J.,
1115 Garside, L.J., Davis, D.A., and Castor, S.B., 2012, Eocene-early Miocene paleotopography
1116 of the Sierra Nevada-Great Basin-Nevadaplano based on widespread ash-flow tuffs and
1117 paleovalleys: Geosphere, v. 8, p. 1–27, doi:10.1130/GES00727.1.

1118 Henry, C.D., Jackson, M.R., Mathewson, D.C., Koehler, S.R., and Moore, S.C., 2015, Eocene
1119 igneous geology and relation to mineralization: Railroad District, southern Carlin Trend,
1120 Nevada, *in* Pennell, W.M. and Garside, L.J. eds., Geological Society of Nevada, New
1121 Concepts and Discoveries, p. 939–965.

1122 Henry, C.D., and John, D.A., 2013, Magmatism, ash-flow tuffs, and calderas of the ignimbrite
1123 flareup in the western Nevada volcanic field, Great Basin, USA: Geosphere, v. 9, p. 951,
1124 doi:10.1130/GES00867.1.

1125 Henry, C.D., McGrew, A.J., Colgan, J.P., Snoke, A.W., and Brueseke, M.E., 2011, Timing,
1126 distribution, amount, and style of Cenozoic extension in the northern Great Basin, *in* Evans,
1127 J.P. and Lee, J. eds., Geological Society of America Field Guide 21, p. 27–66,
1128 doi:10.1130/2011.0021(02).

1129 Henry, C.D., Zuza, A. V., Thorman, C.H., Ressel, M.W., and Dee, S., 2018, Geologic mapping of
1130 the Pequop Mountains, NE Nevada: Exploring basic and applied topics in the easternmost

1131 Ruby Mountains-East Humboldt Range metamorphic core complex, *in* AGU Fall Meeting
1132 Abstracts,.

1133 Hodges, K. V., Snoke, A.W., and Hurlow, H.A., 1992, Thermal evolution of a portion of the
1134 Sevier Hinterland: The Northern Ruby Mountains-East Humboldt Range and Wood Hills,
1135 northeastern Nevada: *Tectonics*, v. 11, p. 154, doi:10.1029/91TC01879.

1136 Hoiland, C.W., Hourigan, J.K., and Miller, E.L., 2021, Evidence for large departures from
1137 lithostatic pressure during Late Cretaceous metamorphism in the northern Snake Range
1138 metamorphic core complex, Nevada, *in* Craddock, J.P., Malone, D.H., Foreman, B.Z., and
1139 Konstantinou, A. eds., *Tectonic Evolution of the Sevier-Laramide Hinterland, Thrust Belt,*
1140 *Foreland and Post-Orogenic Slab Rollback (150-20 Ma)*, Boulder, Colorado, Geological
1141 Society of America.

1142 Hollingsworth, E.R., Ressel, M.W., and Henry, C.D., 2017, Age and depth of Carlin-type gold
1143 deposits in the southern Carlin trend: Eocene mountain lakes, big volcanoes, and
1144 widespread, shallow hydrothermal circulation, *in* Bedell, R.L. and Ressel, M.W. eds.,
1145 *Geological Society of Nevada field trip guidebook: Shallow expressions of Carlin-type gold*
1146 *deposits: Alligator Ridge and Emigrant mines, Nevada, Reno, NV*, p. 149–173.

1147 Horton, B.K., and Schmitt, J.G., 1998, Development and exhumation of a Neogene sedimentary
1148 basin during extension, east-central Nevada: *Bulletin of the Geological Society of America*,
1149 v. 110, p. 163–172, doi:10.1130/0016-7606(1998)110<0163:DAEOAN>2.3.CO;2.

1150 Horton, T.W., Sjostrom, D.J., Abruzzese, M.J., Poage, M.A., Waldbauer, J.R., Hren, M.T.,
1151 Wooden, J.L.P., and Chamberlain, C.P., 2004, Spatial and temporal variation of Cenozoic
1152 surface elevation in the Great Basin and Sierra Nevada: *American Journal of Science*, v.
1153 304, p. 862–888, doi:10.2475/ajs.304.10.862.

1154 Howard, K.A., 2003, Crustal structure in the Elko-Carlin Region, Nevada, during Eocene gold
1155 mineralization: Ruby-East Humboldt metamorphic core complex as a guide to the deep
1156 crust: *Economic Geology*, v. 98, p. 249–268, doi:10.2113/gsecongeo.98.2.249.

1157 Howard, K.A., Wooden, J.L., Barnes, C.G., Premo, W.R., Snoke, A.W., and Lee, S., 2011,
1158 Episodic growth of a Late Cretaceous and Paleogene intrusive complex of pegmatitic
1159 leucogranite, Ruby Mountains core complex, Nevada, USA: *Geosphere*, v. 7, p. 1220,
1160 doi:10.1130/GES00668.1.

1161 Humphreys, E.D., 1995, Post-Laramide removal of the Farallon slab, western United States:

1162 Geology, v. 23, p. 987, doi:10.1130/0091-7613(1995)023<0987:PLROTF>2.3.CO;2.

1163 Kent-Corson, M.L., Mulch, A., Graham, S.A., Carroll, A.R., Ritts, B.D., and Chamberlain, C.P.,
1164 2010, Diachronous isotopic and sedimentary responses to topographic change as indicators
1165 of mid-Eocene hydrologic reorganization in the western United States: Basin Research, v.
1166 22, p. 829–845, doi:10.1111/j.1365-2117.2009.00456.x.

1167 Kent-Corson, M.L., Sherman, L.S., Mulch, A., and Chamberlain, C.P., 2006, Cenozoic
1168 topographic and climatic response to changing tectonic boundary conditions in western
1169 North America: Earth and Planetary Science Letters, v. 252, p. 453–466,
1170 doi:10.1016/j.epsl.2006.09.049.

1171 Ketner, K.B., and Alpha, A.G., 1992, Mesozoic and Tertiary rocks near Elko, Nevada: Evidence
1172 for Jurassic to Eocene folding and low-angle faulting: Evolution of sedimentary basins—
1173 Eastern Great Basin: U.S. Geological Survey Bulletin 1988-C, p. 13.

1174 Konstantinou, A., 2021, The “death” of the Sevier-Laramide orogen: Gravitational collapse of
1175 the crust or something else?, *in* Craddock, J.P., Malone, D.H., Foreman, B.Z., and
1176 Konstantinou, A. eds., Tectonic Evolution of the Sevier-Laramide Hinterland, Thrust Belt,
1177 Foreland and Post-Orogenic Slab Rollback (150-20 Ma), Boulder, Colorado, Geological
1178 Society of America.

1179 Konstantinou, A., and Miller, E.L., 2015, Evidence for a long-lived accommodation/transfer zone
1180 beneath the Snake River Plain: A possible influence on Neogene magmatism? Tectonics, v.
1181 34, p. 2387–2398, doi:10.1002/2015TC003863.

1182 Konstantinou, A., Strickland, A., Miller, E.L., Vervoort, J.D., Fisher, C.M., Wooden, J.L.P., and
1183 Valley, J.W., 2013a, Synextensional magmatism leading to crustal flow in the Albion-Raft
1184 River-Grouse Creek metamorphic core complex, northeastern Basin and Range: Tectonics,
1185 v. 32, p. 1384–1403, doi:10.1002/tect.20085.

1186 Konstantinou, A., Strickland, A., Miller, E.L., and Wooden, J.P., 2012, Multistage Cenozoic
1187 extension of the Albion–Raft River–Grouse Creek metamorphic core complex:
1188 Geochronologic and stratigraphic constraints: Geosphere, v. 8, p. 1429–1466,
1189 doi:10.1130/GES00778.1.

1190 Konstantinou, A., Valley, J.W., Strickland, A., Miller, E.L., Fisher, C.M., Vervoort, J.D., and
1191 Wooden, J.L.P., 2013b, Geochemistry and geochronology of the Jim Sage volcanic suite,
1192 southern Idaho: Implications for Snake River Plain magmatism and its role in the history of

1193 Basin and Range extension: *Geosphere*, v. 9, p. 1681–1703, doi:10.1130/GES00948.1.

1194 Kreemer, C., Blewitt, G., and Hammond, W.C., 2010, Evidence for an active shear zone in
1195 southern Nevada linking the Wasatch fault to the Eastern California shear zone: *Geology*, v.
1196 38, p. 475–478, doi:10.1130/G30477.1.

1197 Lachenbruch, A.H., and Morgan, P., 1990, Continental extension, magmatism and elevation;
1198 formal relations and rules of thumb: *Tectonophysics*, v. 174, p. 39–62.

1199 Larimer, J.E., Yanites, B.J., Phillips, W., and Mittelstaedt, E., 2019, Late Miocene rejuvenation of
1200 central Idaho landscape evolution: A case for surface processes driven by plume-lithosphere
1201 interaction: *Lithosphere*, v. 11, p. 59–72, doi:10.1130/L746.1.

1202 Lechler, A.R., and Niemi, N.A., 2011, Sedimentologic and isotopic constraints on the Paleogene
1203 paleogeography and paleotopography of the southern Sierra Nevada, California: *Geology*, v.
1204 39, p. 379–382, doi:10.1130/G31535.1.

1205 Lechler, A.R., Niemi, N.A., Hren, M.T., and Lohmann, K.C., 2013, Paleoelevation estimates for
1206 the northern and central proto-Basin and Range from carbonate clumped isotope
1207 thermometry: *Tectonics*, v. 32, p. 295–316, doi:10.1002/tect.20016.

1208 Lee, J., Blackburn, T., and Johnston, S., 2017, Timing of mid-crustal ductile extension in the
1209 northern Snake Range metamorphic core complex, Nevada: Evidence from U/Pb zircon
1210 ages: *Geosphere*, v. 13, p. 439–459, doi:10.1130/GES01429.1.

1211 Lerch, D.W., Miller, E.L., McWilliams, M.O., and Colgan, J.P., 2008, Tectonic and magmatic
1212 evolution of the northwestern Basin and Range and its transition to unextended volcanic
1213 plateaus: Black Rock Range, Nevada: *Bulletin of the Geological Society of America*, v. 120,
1214 p. 300–311, doi:10.1130/B26151.1.

1215 Levander, A., and Miller, M.S., 2012, Evolutionary aspects of lithosphere discontinuity structure
1216 in the western U.S.: *Geochemistry, Geophysics, Geosystems*, v. 13, p. n/a-n/a,
1217 doi:10.1029/2012GC004056.

1218 Lewis, C.J., Wernicke, B.P., Selverstone, J., and Bartley, J.M., 1999, Deep burial of the footwall
1219 of the northern Snake Range decollement, Nevada: *Bulletin of the Geological Society of*
1220 *America*, v. 111, p. 39–51, doi:10.1130/0016-7606(1999)111<0039:DBOTFO>2.3.CO;2.

1221 Liu, L., and Stegman, D.R., 2012, Origin of Columbia River flood basalt controlled by
1222 propagating rupture of the Farallon slab: *Nature*, v. 482, p. 386–389,
1223 doi:10.1038/nature10749.

- 1224 Lofgren, D.L., Honey, J.G., McKenna, M.C., Zondervan, R.L., and Smith, E.E., 2008, Paleocene
1225 primates from the Goler Formation of the Mojave Desert in California, *in* Wang, X. and
1226 Barnes, L.G. eds., Science Series 41: Geology and Vertebrate Paleontology of Western and
1227 Southern North America, Natural History Museum of Los Angeles County, p. 11–28.
- 1228 Long, S.P., 2018, Geometry and extension magnitude of the Basin and Range Province (39°N),
1229 Utah, Nevada, and California, USA: Constraints from a province-scale cross section:
1230 Geological Society of America Bulletin, doi:10.1130/B31974.
- 1231 Long, S.P., 2012, Magnitudes and spatial patterns of erosional exhumation in the Sevier
1232 hinterland, eastern Nevada and western Utah, USA: Insights from a Paleogene
1233 paleogeologic map: *Geosphere*, v. 8, p. 881, doi:10.1130/GES00783.1.
- 1234 Lund, K., 2008, Geometry of the Neoproterozoic and Paleozoic rift margin of western Laurentia:
1235 Implications for mineral deposit settings: *Geosphere*, v. 4, p. 429, doi:10.1130/GES00121.1.
- 1236 Lund, K., Beard, L.S., and Perry, W.J., 1993, Relation between extensional geometry of the
1237 northern Grant Range and oil occurrences in Railroad Valley, east-central Nevada: *AAPG*
1238 *Bulletin*, v. 77, p. 945–962.
- 1239 Lund Snee, J.-E., 2013, Geology and geochronology of Cenozoic units in the Piñon Range and
1240 Huntington Valley, Nevada: Stanford University, 263 p.,
1241 <http://purl.stanford.edu/hx388mg6634>.
- 1242 Lund Snee, J.-E., and Miller, E.L., 2015, Preliminary geologic map of Cenozoic units of the
1243 central Robinson Mountain volcanic field and northwestern Huntington Valley: Nevada
1244 Bureau of Mines and Geology Open File, v. 15–2, p. 42, 1:24,000 scale,
1245 <http://pubs.nbmgs.unr.edu/product-p/of2015-02.htm>.
- 1246 Lund Snee, J.-E., Miller, E.L., Grove, M., Hourigan, J.K.J.K., and Konstantinou, A., 2016,
1247 Cenozoic paleogeographic evolution of the Elko Basin and surrounding region, northeast
1248 Nevada: *Geosphere*, v. 12, p. 464–500, doi:10.1130/GES01198.1.
- 1249 MacCready, T., Snoke, A.W., Wright, J.E., and Howard, K. a., 1997, Mid-crustal flow during
1250 Tertiary extension in the Ruby Mountains core complex, Nevada: *Bulletin of the Geological*
1251 *Society of America*, v. 109, p. 1576–1594, doi:10.1130/0016-
1252 7606(1997)109<1576:MCFDTE>2.3.CO;2.
- 1253 MacGinitie, H.D., 1941, Contributions to Paleontology: Middle Eocene flora from the central
1254 Sierra Nevada: Washington, D.C., Carnegie Institution of Washington Publication 534.

1255 McCrory, P.A., Blair, J.L., Waldhauser, F., and Oppenheimer, D.H., 2012, Juan de Fuca slab
1256 geometry and its relation to Wadati-Benioff zone seismicity: *Journal of Geophysical*
1257 *Research: Solid Earth*, v. 117, doi:10.1029/2012JB009407.

1258 McGrew, A.J., Foland, K.A., and Stockli, D.F., 2007, Evolution of Cenozoic volcanism and
1259 extension in the Copper Mountains, northeastern Nevada, *in* *Abstracts with Programs -*
1260 *Geological Society of America*, v. 39, p. 226,
1261 [http://search.proquest.com/docview/50467319?accountid=14503%5Cnhttp://libraries.colora](http://search.proquest.com/docview/50467319?accountid=14503%5Cnhttp://libraries.colorado.edu:4550/resserv?genre=article&issn=00167592&title=Abstracts+with+Programs+-+Geological+Society+of+America&volume=39&issue=6&date=2007-10-01&atitle=Evolution+of+Cenoz.)
1262 [do.edu:4550/resserv?genre=article&issn=00167592&title=Abstracts+with+Programs+-](http://search.proquest.com/docview/50467319?accountid=14503%5Cnhttp://libraries.colorado.edu:4550/resserv?genre=article&issn=00167592&title=Abstracts+with+Programs+-+Geological+Society+of+America&volume=39&issue=6&date=2007-10-01&atitle=Evolution+of+Cenoz.)
1263 [+Geological+Society+of+America&volume=39&issue=6&date=2007-10-](http://search.proquest.com/docview/50467319?accountid=14503%5Cnhttp://libraries.colorado.edu:4550/resserv?genre=article&issn=00167592&title=Abstracts+with+Programs+-+Geological+Society+of+America&volume=39&issue=6&date=2007-10-01&atitle=Evolution+of+Cenoz.)
1264 [01&atitle=Evolution+of+Cenoz.](http://search.proquest.com/docview/50467319?accountid=14503%5Cnhttp://libraries.colorado.edu:4550/resserv?genre=article&issn=00167592&title=Abstracts+with+Programs+-+Geological+Society+of+America&volume=39&issue=6&date=2007-10-01&atitle=Evolution+of+Cenoz.)

1265 McGrew, A.J., Peters, M.T., and Wright, J.E., 2000, Thermobarometric constraints on the
1266 tectonothermal evolution of the East Humboldt Range metamorphic core complex, Nevada:
1267 *Bulletin of the Geological Society of America*, v. 112, p. 45–60, doi:10.1130/0016-
1268 7606(2000)112<45:TCOTTE>2.0.CO;2.

1269 McGrew, A.J., and Snee, L.W., 1994, $^{40}\text{Ar}/^{39}\text{Ar}$ thermochronologic constraints on the
1270 tectonothermal evolution of the northern East Humboldt Range metamorphic core complex,
1271 Nevada: *Tectonophysics*, v. 238, p. 425–450, doi:10.1016/0040-1951(94)90067-1.

1272 McGrew, A.J., and Snoke, A.W., 2015, *Geology of the Welcome Quadrangle and adjacent part of*
1273 *the Wells Quadrangle, Elko County, Nevada: Nevada Bureau of Mines and Geology Map*
1274 *184, 1:24,000 scale, 40 p., 2 sheets.*

1275 McQuarrie, N., and Chase, C.G., 2000, *Raising the Colorado Plateau: Geology*, v. 28, p. 91,
1276 doi:10.1130/0091-7613(2000)028<0091:RTCP>2.0.CO;2.

1277 McQuarrie, N., and Wernicke, B.P., 2005, An animated tectonic reconstruction of southwestern
1278 North America since 36 Ma: *Geosphere*, v. 1, p. 147–172, doi:10.1130/GES00016.1.

1279 Malone, D.H., Craddock, J.P., and Konstantinou, A., 2021, Timing and structural evolution of the
1280 Sevier thrust belt, *in* Craddock, J.P., Malone, D.H., Foreman, B.Z., and Konstantinou, A.
1281 eds., *Tectonic Evolution of the Sevier-Laramide Hinterland, Thrust Belt, Foreland and Post-*
1282 *Orogenic Slab Rollback (150-20 Ma)*, Boulder, Colorado, Geological Society of America.

1283 Miller, E.L., Dumitru, T.A., Brown, R.W., and Gans, P.B., 1999, Rapid Miocene slip on the
1284 Snake Range–Deep Creek Range fault system, east-central Nevada: *Geological Society of*
1285 *America Bulletin*, v. 111, p. 886–905, doi:10.1130/0016-

1286 7606(1999)111<0886:RMSOTS>2.3.CO;2.

1287 Miller, E.L., and Gans, P.B., 1989, Cretaceous crustal structure and metamorphism in the
1288 hinterland of the Sevier thrust belt, western U.S. Cordillera: *Geology*, v. 17, p. 59–62,
1289 doi:10.1130/0091-7613(1989)017<0059.

1290 Miller, E.L., Konstantinou, A., and Strickland, A., 2012, Comment on “Geodynamics of
1291 synconvergent extension and tectonic mode switching: Constraints from the Sevier-
1292 Laramide orogen” by Michael L. Wells et al.: *Tectonics*, v. 31, p. n/a-n/a,
1293 doi:10.1029/2012TC003103.

1294 Miller, E.L., Raftrey, M.E., and Lund Snee, J.-E., 2021, Downhill from Austin and Ely to Las
1295 Vegas: U-Pb detrital zircon suites from the Eocene-Oligocene Titus Canyon Formation and
1296 associated strata, Death Valley, CA, *in* Craddock, J.P., Malone, D.H., Foreman, B.Z., and
1297 Konstantinou, A. eds., *Tectonic Evolution of the Sevier-Laramide Hinterland, Thrust Belt,*
1298 *Foreland and Post-Orogenic Slab Rollback (150-20 Ma)*, Boulder, Colorado, Geological
1299 Society of America.

1300 Miller, E.L., Raftrey, M.E., Perez-Lopez, S.A., and Harbaugh, D.W., 2019, Preliminary detrital
1301 zircon study of the Oligocene Titus Canyon Formation, Death Valley, suggests central
1302 Nevada sources, *in* Geological Society of America Abstracts with Programs. Vol. 51, No. 4,
1303 doi:10.1130/abs/2019CD-329243.

1304 Mix, H.T., Mulch, A., Kent-Corson, M.L., and Chamberlain, C.P., 2011, Cenozoic migration of
1305 topography in the North American Cordillera: *Geology*, v. 39, p. 87–90,
1306 doi:10.1130/G31450.1.

1307 Moore, S.W., Madrid, H.B., and Server, G.T., 1983, Results of oil-shale investigations in
1308 northeastern Nevada: U.S. Geological Survey Open File Report 83-586, p. C1–C18.

1309 Mulch, A., Chamberlain, C.P., Cosca, M.A., Teyssier, C., Methner, K., Hren, M.T., and Graham,
1310 S.A., 2015, Rapid change in high-elevation precipitation patterns of western North America
1311 during the Middle Eocene Climatic Optimum (MECO): *American Journal of Science*, v.
1312 315, p. 317–336, doi:10.2475/04.2015.02.

1313 Noble, D.C., 1972, Some observations on the Cenozoic volcano-tectonic evolution of the Great
1314 Basin, western United States: *Earth and Planetary Science Letters*, v. 17, p. 142–150,
1315 doi:10.1016/0012-821X(72)90269-5.

1316 Parsons, T., Thompson, G.A., and Sleep, N.H., 1994, Mantle plume influence on the Neogene

1317 uplift and extension of the US western Cordillera? *Geology*, v. 22, p. 83–86,
1318 doi:10.1130/0091-7613(1994)022<0083:MPIOTN>2.3.CO;2.

1319 Pierce, K.L., and Morgan, L.A., 2009, Is the track of the Yellowstone hotspot driven by a deep
1320 mantle plume? --- Review of volcanism, faulting, and uplift in light of new data: *Journal of*
1321 *Volcanology and Geothermal Research*, v. 188, p. 1–25,
1322 doi:10.1016/j.jvolgeores.2009.07.009.

1323 Pierce, K.L., Morgan, L.A., and Link, P.K., 1992, The track of the Yellowstone hot spot:
1324 Volcanism, faulting, and uplift: Regional geology of eastern Idaho and western Wyoming:
1325 Geological Society of America Memoir, v. 179, p. 1–53.

1326 Potter, C.J., Dubiel, R.F., Snee, L.W., and Good, S.C., 1995, Eocene extension of early Eocene
1327 lacustrine strata in a complex deformed Sevier-Laramide hinterland, northwest Utah and
1328 northeast Nevada: *Geology*, v. 23, p. 181–184, doi:10.1130/0091-
1329 7613(1995)023<0181:EEOEEL>2.3.CO;2.

1330 Rahl, J.M., McGrew, A.J., and Foland, K.A., 2002, Transition from Contraction to Extension in
1331 the Northeastern Basin and Range: New Evidence from the Copper Mountains, Nevada:
1332 *The Journal of Geology*, v. 110, p. 179–194, doi:10.1086/338413.

1333 Reid, S.A., 1988, Late Cretaceous and Paleogene sedimentation along east side of San Joaquin
1334 Basin, California, *in* Graham, S.A. ed., *Studies of the Geology of the San Joaquin Valley,*
1335 *Pacific Section, SEPM (Society for Sedimentary Geology)*, v. 60, p. 157–171,
1336 doi:10.1306/94885890-1704-11D7-8645000102C1865D.

1337 Ressel, M.W., and Henry, C.D., 2006, Igneous geology of the Carlin trend, Nevada:
1338 Development of the Eocene plutonic complex and significance for Carlin-type gold
1339 deposits: *Economic Geology*, v. 101, p. 347–383, doi:10.2113/gsecongeo.101.2.347.

1340 Ruksznis, A., 2015, *Geology and geochronology of Cenozoic sedimentary basins, east-central*
1341 *Nevada: Stanford University*, 219 p.

1342 Ryskamp, E.B., Abbott, J.T., Christiansen, E.H., Keith, J.D., Vervoort, J.D., and Tingey, D.G.,
1343 2008, Age and petrogenesis of volcanic and intrusive rocks in the Sulphur Spring Range,
1344 central Nevada: Comparisons with ore-associated Eocene magma systems in the Great
1345 Basin: *Geosphere*, v. 4, p. 496, doi:10.1130/GES00113.1.

1346 Saleeby, J.B., Ducea, M.N., Busby, C.J., Nadin, E.S., and Wetmore, P.H., 2008, Chronology of
1347 pluton emplacement and regional deformation in the southern Sierra Nevada batholith,

1348 California: Special Paper of the Geological Society of America, v. 438, p. 397–427,
1349 doi:10.1130/2008.2438(14).

1350 Satarugsa, P., and Johnson, R.A., 2000, Cenozoic tectonic evolution of the Ruby Mountains
1351 metamorphic core complex and adjacent valleys, northeastern Nevada: *Rocky Mountain*
1352 *Geology*, v. 35, p. 205–230, doi:10.2113/35.2.205.

1353 Schmalholz, S.M., Medvedev, S., Lechmann, S.M., and Podladchikov, Y.Y., 2014, Relationship
1354 between tectonic overpressure, deviatoric stress, driving force, isostasy and gravitational
1355 potential energy: *Geophysical Journal International*, p. 680–696, doi:10.1093/gji/ggu040.

1356 Schwartz, T.M., Methner, K., Mulch, A., Graham, S.A., and Chamberlain, C.P., 2019, Paleogene
1357 topographic and climatic evolution of the Northern Rocky Mountains from integrated
1358 sedimentary and isotopic data: *Bulletin of the Geological Society of America*, v. 131, p.
1359 1203–1223, doi:10.1130/B32068.1.

1360 Schwartz, T.M., and Schwartz, R.K., 2013, Paleogene postcompressional intermontane basin
1361 evolution along the frontal Cordilleran fold-and-thrust belt of southwestern Montana:
1362 *Bulletin of the Geological Society of America*, v. 125, p. 961–984, doi:10.1130/B30766.1.

1363 Server, G.T., and Solomon, B.J., 1983, *Geology and oil shale deposits of the Elko Formation,*
1364 *Pinon Range, Elko County, Nevada: U.S. Geological Survey Miscellaneous Field Studies*
1365 *Map MF-1546, 1:24,000 scale.*

1366 Sharman, G.R., Graham, S.A., Grove, M., Kimbrough, D.L., and Wright, J.E., 2015, Detrital
1367 zircon provenance of the Late Cretaceous-Eocene California forearc: Influence of Laramide
1368 low-angle subduction on sediment dispersal and paleogeography: *Bulletin of the Geological*
1369 *Society of America*, v. 127, p. 38–60, doi:10.1130/B31065.1.

1370 Shen, W., and Ritzwoller, M.H., 2016, Crustal and uppermost mantle structure beneath the
1371 United States: *Journal of Geophysical Research: Solid Earth*, v. 121, p. 4306–4342,
1372 doi:10.1002/2016JB012887.

1373 Sluijs, A., Zeebe, R.E., Bijl, P.K., and Bohaty, S.M., 2013, A middle Eocene carbon cycle
1374 conundrum: *Nature Geoscience*, v. 6, p. 429–434, doi:10.1038/ngeo1807.

1375 Smith, M.E., Cassel, E.J., Jicha, B.R., Singer, B.S., and Canada, A.S., 2017, Hinterland drainage
1376 closure and lake formation in response to middle Eocene Farallon slab removal, Nevada,
1377 U.S.A.: *Earth and Planetary Science Letters*, v. 479, p. 156–169,
1378 doi:10.1016/j.epsl.2017.09.023.

1379 Smith, J.F., and Howard, K.A., 1977, Geologic map of the Lee Quadrangle: U.S. Geological
1380 Survey Map GQ-1393, 1:62,500 scale.

1381 Smith, J.F., and Ketner, K.B., 1978, Geologic map of the Carlin-Pinon Range area, Elko and
1382 Eureka Counties, Nevada: U.S. Geological Survey Miscellaneous Investigations Series I-
1383 1028, 1:62,500 scale.

1384 Smith, J.F., and Ketner, K.B., 1976, Stratigraphy of post-Paleozoic rocks and summary of
1385 resources in the Carlin-Pinon Range area, Nevada: U.S. Geological Survey Professional
1386 Paper 867-B, p. 1–48.

1387 Smith, D.L., Miller, E.L., Wyld, S.J., and Wright, J.E., 1993, Progression and timing of Mesozoic
1388 crustal shortening in the northern Great Basin, western U.S.A, *in* Mesozoic Paleogeography
1389 of the Western United States-II, v. 71, p. 389–406,
1390 [http://archives.datapages.com.stanford.idm.oclc.org/data/pac_sep/088/088001/pdfs/389.p](http://archives.datapages.com.stanford.idm.oclc.org/data/pac_sep/088/088001/pdfs/389.pdf)
1391 [df](http://archives.datapages.com.stanford.idm.oclc.org/data/pac_sep/088/088001/pdfs/389.pdf).

1392 Snell, K.E., Koch, P.L., Druschke, P., Foreman, B.Z., and Eiler, J.M., 2014, High elevation of the
1393 ‘Nevadaplano’ during the Late Cretaceous: *Earth and Planetary Science Letters*, v. 386, p.
1394 52–63, doi:10.1016/j.epsl.2013.10.046.

1395 Solomon, B.J., McKee, E.H., and Andersen, D.W., 1979, Stratigraphy and depositional
1396 environments of Paleogene rocks near Elko, Nevada, *in* Pacific Coast Paleogeography
1397 Symposium 3: Cenozoic Paleogeography of the Western United States, Pacific Section,
1398 SEPM (Society for Sedimentary Geology), p. 75–88.

1399 Sonder, L.J., England, P.C., Wernicke, B.P., and Christiansen, R.L., 1987, A physical model for
1400 Cenozoic extension of western North America: Geological Society, London, Special
1401 Publications, v. 28, p. 187–201, doi:10.1144/GSL.SP.1987.028.01.14.

1402 Spear, F.S., Thomas, J.B., and Hallett, B.W., 2014, Overstepping the garnet isograd: A
1403 comparison of QuiG barometry and thermodynamic modeling: *Contributions to Mineralogy*
1404 *and Petrology*, v. 168, doi:10.1007/s00410-014-1059-6.

1405 Stewart, J.H., 1980, Geology of Nevada: Nevada Bureau of Mines and Geology, Special
1406 Publication, v. 4, p. 136.

1407 Stockli, D.F., 2005, Application of low-temperature thermochronometry to extensional tectonic
1408 settings: *Reviews in Mineralogy and Geochemistry*, v. 58, p. 411–448,
1409 doi:10.2138/rmg.2005.58.16.

1410 Stockli, D.F., Surpless, B., Dumitru, T.A., and Farley, K. a., 2002, Thermochronological
1411 constraints on the timing and magnitude of Miocene and Pliocene extension in the central
1412 Wassuk Range, western Nevada: *Tectonics*, v. 21, p. 10–19, doi:10.1029/2001TC001295.

1413 Strickland, A., Miller, E.L., Wooden, J.L., Kozdon, R., and Valley, J.W., 2011, Syn-extensional
1414 plutonism and peak metamorphism in the Albion-Raft River-Grouse Creek metamorphic
1415 core complex: *American Journal of Science*, v. 311, p. 261–314, doi:10.2475/04.2011.01.

1416 Surpless, B., Stockli, D.F., Dumitru, T.A., and Miller, E.L., 2002, Two-phase westward
1417 encroachment of Basin and Range extension into the northern Sierra Nevada: *Tectonics*, v.
1418 21, p. 2-1-2–13, doi:10.1029/2000TC001257.

1419 Taylor, W.J., Bartley, J.M., Martin, M.W., Geissman, J.W., Walker, J.D., Armstrong, P.A., and
1420 Fryxell, J.E., 2000, Relations between hinterland and foreland shortening: Sevier orogeny
1421 central North American Cordillera: *Tectonics*, v. 19, p. 1124–1143,
1422 doi:10.1029/1999TC001141.

1423 Thatcher, W., Foulger, G.R., Julian, B.R., Svarc, J., Quilty, E., and Bawden, G.W., 1999, Present-
1424 day deformation across the Basin and Range Province, Western United States: *Science*, v.
1425 283, p. 1714–1717, doi:10.1126/science.283.5408.1714.

1426 Thorman, C.H., Ketner, K.B., Brooks, W.E., Snee, L.W., Zimmerman, R.A., and Raines, G.L.,
1427 1991, Late Mesozoic-Cenozoic tectonics in northeastern Nevada, *in* *Geology and ore*
1428 *deposits of the Great Basin: Symposium Proceedings, Geological Society of Nevada, Reno,*
1429 *Nevada*, v. 1, p. 25–45, doi:10.12681/eadd/1834.

1430 Thorman, C.H., and Peterson, F., 2003, The Middle Jurassic Elko orogeny: A major tectonic
1431 event in Nevada-Utah, *in* *Annual Meeting Expanded Abstracts*, v. 12, p. 169–174.

1432 Thorman, C.H., Sandberg, C.A., Henry, C.D., Zuza, A. V., and Ressel, M.W., 2020, Regional
1433 tectonics based on conodont CAIs and burial depths, as viewed from the Pequop Mountains,
1434 NE Nevada – An Unbiased Opinion(?), *in* *Geological Society of Nevada Symposium:*
1435 *Vision for Discovery: Geology and Ore Deposits of the Basin and Range*,.

1436 Tian, Y., and Zhao, D., 2012, P-wave tomography of the western United States: Insight into the
1437 Yellowstone hotspot and the Juan de Fuca slab: *Physics of the Earth and Planetary Interiors*,
1438 v. 200–201, p. 72–84, doi:10.1016/j.pepi.2012.04.004.

1439 Tosdal, R.M., Wooden, J.L., and Kistler, R.W., 2000, Geometry of the Neoproterozoic
1440 continental break-up, and implications for location of Nevadan mineral belts, *in* Cluer, J.K.,

1441 Price, J.G., Struhsacker, E.M., Hardyman, R.F., and Morris, C.L. eds., *Geology and Ore*
1442 *Deposits 2000: The Great Basin and Beyond Proceedings Volume I*, p. 451–466.

1443 Vandervoort, D.S., and Schmitt, J.G., 1990, Cretaceous to early Tertiary paleogeography in the
1444 hinterland of the Sevier thrust belt, east-central Nevada: *Geology*, v. 18, p. 567–570,
1445 doi:10.1130/0091-7613(1990)018<0567:CTETPI>2.3.CO;2.

1446 Wallace, A.R., Perkins, M.E., and Fleck, R.J., 2008, Late Cenozoic paleogeographic evolution of
1447 northeastern Nevada: Evidence from the sedimentary basins: *Geosphere*, v. 4, p. 36–74,
1448 doi:10.1130/GES00114.1.

1449 Wells, M.L., and Hoisch, T.D., 2012, Reply to comment by E. L. Miller et al. on “Geodynamics
1450 of synconvergent extension and tectonic mode switching: Constraints from the Sevier-
1451 Laramide orogen”: *Tectonics*, v. 31, p. n/a-n/a, doi:10.1029/2012TC003136.

1452 Wells, M.L., Hoisch, T.D., Cruz-Urbe, A.M., and Vervoort, J.D., 2012, Geodynamics of
1453 synconvergent extension and tectonic mode switching: Constraints from the Sevier-
1454 Laramide orogen: *Tectonics*, v. 31, p. 1–20, doi:10.1029/2011TC002913.

1455 Willden, R., and Kistler, R.W., 1979, Precambrian and Paleozoic stratigraphy in central Ruby
1456 Mountains, Elko County, Nevada, *in* Newman, G.W. and Goode, H.D. eds., *Basin and*
1457 *Range Symposium and Great Basin Field Conference*, Denver, CO, Rocky Mountain
1458 Association of Geologists, p. 221–243.

1459 Willden, R., and Kistler, R.W., 1979, Precambrian and Paleozoic stratigraphy in central Ruby
1460 Mountains, Elko County, Nevada, *in* Newman, G.W. and Goode, H.D. eds., *Basin and*
1461 *Range Symposium*, Denver, CO, Rocky Mountain Association of Geologists, p. 221–243.

1462 Wolfe, J.A., Forest, C.E., and Molnar, P., 1998, Paleobotanical evidence of Eocene and
1463 Oligocene paleoaltitudes in midlatitude western North America: *Bulletin of the Geological*
1464 *Society of America*, v. 110, p. 664–678, doi:10.1130/0016-
1465 7606(1998)110<0664:PEOEAO>2.3.CO;2.

1466 Wright, J.E., and Snoke, A.W., 1993, Tertiary magmatism and mylonitization in the Ruby-East
1467 Humboldt metamorphic core complex, northeastern Nevada: U-Pb geochronology and Sr,
1468 Nd, and Pb isotope geochemistry: *Geological Society of America Bulletin*, v. 105, p. 935–
1469 952, doi:10.1130/0016-7606(1993)105<0935:TMAMIT>2.3.CO;2.

1470 Yeend, W.R., 1974, Gold-bearing gravels of the ancestral Yuba River, Sierra Nevada, California:
1471 U.S. Geological Survey Professional Paper 772.

1472 Yonkee, W.A., Dehler, C.D., Link, P.K., Balgord, E.A., Keeley, J.A., Hayes, D.S., Wells, M.L.,
1473 Fanning, C.M., and Johnston, S.M., 2014, Tectono-stratigraphic framework of
1474 Neoproterozoic to Cambrian strata, west-central US: Protracted rifting, glaciation, and
1475 evolution of the North American Cordilleran margin: *Earth-Science Reviews*, v. 136, p. 59–
1476 95.

1477 Zachos, J., Pagani, M., Sloan, L., Thomas, E., and Billups, K., 2001, Trends, rhythms, and
1478 aberrations in global climate 65 Ma to present: *Science*, v. 292, p. 686–693,
1479 doi:10.1126/science.1059412.

1480 Zuza, A. V, Thorman, C.H., Henry, C.D., Levy, D.A., Dee, S., Long, S.P., Sandberg, C.A., and
1481 Soignard, E., 2020, Pulsed Mesozoic deformation in the Cordilleran hinterland and
1482 evolution of the Nevadaplano: Insights from the Pequop Mountains, NE Nevada:
1483 *Lithosphere*, v. 1, p. 1–24.
1484

GSA Data Repository

Magmatism, migrating topography, and the onset of faulting in the northern Basin and Range province, western USA

Jens-Erik Lund Snee¹ and Elizabeth L. Miller²

¹U.S. Geological Survey Geosciences and Environmental Change Science Center, P.O. Box 25046, MS 980, Denver, CO 80225

²Stanford University Department of Geological Sciences, 450 Serra Mall Bld. 320, Room 118, Stanford, CA 94305

Contents of this GSA Data Repository

1. Introduction
2. Text S1 to S4
3. Figures S1 to S3
4. References
5. Tables S1 to S3 (separate file)

INTRODUCTION

This GSA Data Repository contains appendices and figures that support the text (below) as well as supplementary data tables (separate file). The first two appendices below present the detailed methods for obtaining new U-Pb detrital zircon ages (**Text S1**) and for assigning (maximum) depositional age constraints to sedimentary rocks in the Elko area of northeast Nevada (**Text S2**). **Text S3** presents the results of U-Pb detrital zircon analysis and **Text S4** specifically details the new age constraints throughout the stratigraphic succession. **Figures S1** and **S2** respectively provide probability density plots and weighted mean age plots for each detrital zircon age sample. Finally, **Figure S3** provides references for the ages of Great Basin paleodrainages, to support Figure 2 of the main body. **References** for this Data Repository are provided at the end. Any use of trade, firm, or product names is for descriptive purposes only and does not imply endorsement by the U.S. Government.

TEXT S1. METHODS FOR U-PB DETRITAL ZIRCON GEOCHRONOLOGIC ANALYSES

We sampled fine-grained sandstones for U-Pb detrital zircon analysis. We sought fresh, unexposed samples, and we removed weathering rinds with a rock hammer or shovel. Sampling localities, rock types, and other details are given in Table S1 and the locations are shown in Fig. 4. We blew dust off sampled rocks in the field and then again using compressed air in the laboratory in order to reduce the potential for contamination. Rock crushing, mineral separation, mount-making, geochronological analysis, and data reduction techniques closely followed those outlined by Dumitru et al. (2016) in their Data Repository.

We crushed rock samples and made zircon separates at Stanford University using standard procedures that included fracturing with a steel hammer followed by dust removal with compressed air, rock crushing, rock grinding, and concentration of denser grains using a modified Gemini Table water-aided shaking apparatus. For the first of two sets of samples (15JLS002, 15JLS004, 15JLS015, 15JLS017, 15JLS027A, 15JLS029, 15JLS036B, and 15JLS037), which were separated in 2016, we employed a Frantz magnetic separator with 10° side slope and final (maximum) power setting of 2.3A to progressively remove magnetic grains. Dumitru et al. (2016) recommended a final power setting of 1.2A, so our higher setting may have removed some zircon grains containing inclusions or mantled by volcanic material, which could have resulted in lower yields of younger, primary volcanic grains (Naeser and Naeser, 1984) when these samples were analyzed at the University of California Santa Cruz. If this occurred, it would not weaken the integrity of maximum depositional ages (MDAs), but it could produce older MDAs for some samples, rendering the age constraints more conservative. Hence, for three samples initially separated in this manner in which we observed zircon in the magnetic fractions (15JLS029, 15JLS036B, and 15JLS037), we later (2018) combined all nonmagnetic fractions that were yielded from power settings of 1.2A and greater and extracted zircons again from these samples. These additional zircon separates, together with one additional sample not previously separated (15JLS041), were analyzed at the University of Arizona LaserChron Center.

Nonmagnetic mineral separates were fractionated by density using 3.32 g/cm³ methylene iodide according to methods outlined by Dumitru and Stockli (1998). The resulting heavy fraction containing zircon was rinsed multiple times using deionized water. Zircon crystals were placed on an epoxy mount, photographed with the aid of an optical microscope, and then

analyzed. For the first group of samples, separated in 2016, analyses were conducted on an Element XR high-resolution magnetic-sector inductively coupled plasma mass spectrometer (ICP–MS) outfitted with a single collector and housed at the University of California, Santa Cruz, Institute of Marine Sciences. A total of 1000 analyses were conducted on sample grains. Our analyses were conducted using the 2015 instrument configuration and workflow described by Dumitru et al. (2016), but we selected slightly different parameters for laser ablation:

- Laser fluence: 4.0 J/cm²
- Repetition rate: 8/s
- Shot count: 160 (20 s total duration)
- Spot size: 20 μm.

For these analyses, we employed Temora 2 zircon (416.78 ± 0.33 Ma isotope dilution–thermal ionization mass spectrometry weighted mean age by Black et al., 2004) as the primary age reference material (standard). A total of 210 grains of Temora 2 were analyzed, one after every fifth unknown age analysis, with additional Temora 2 analyses at the start and end of the session. We employed FC-5Z zircon (1099 ± 0.6 Ma; see Paces and Miller, 1993) as a secondary age reference material. One hundred eight analyses were made of FC-5Z. Mount Dromedary (“DROM”) zircon (98.8 ± 0.6 Ma; White and Ireland, 2012) was employed as a tertiary age reference material and analyzed 50 times during the session. The zircon concentration reference material MADDER was used to estimate U, Th, and Pb abundances. MADDER was analyzed several times at the start of the session, and then once per approximately 50 other analyses.

Data reduction was conducted with the Iolite v.2.5 add-in to IGOR Pro v.6.3 (Paton et al., 2011) using the “U_Pb_Geochronology3” data reduction scheme. Baseline subtraction was applied using the “StepForward” spline. Baseline integrations were trimmed manually to exclude zones where ²⁰²Hg and ²⁰⁴Pb signal diverged from the mean of the baseline by 3 standard deviations or more. A correction for downhole fractionation was applied using Temora 2 as the reference material. Integration windows for the all reference materials were trimmed at the start and end in order to maximize the quality of fit of a double exponential downhole correction curve. We removed spikes of ²⁰⁴Pb detected in Temora 2 analyses by manually trimming individual integrations away from the end. Finally, we interpolated signal between Temora 2 primary reference materials using “Spline_Smooth_Med5,” which yielded the following statistics for final, downhole-corrected ²⁰⁶Pb/²³⁸U ages of the reference materials: MSWD =

0.92 for primary reference material Temora 2, MSWD = 1.1 for secondary reference material FC-5Z, and MSWD = 1.3 for tertiary reference material Mount Dromedary (“DROM”). Integrations of unknown analyses were deleted or trimmed away from the end according to criteria established by Dumitru et al. (2016). We employ their comment codes in our Table S2 as explanation for modifications to integration windows. We also add the comment “moved” in cases where the integration window was simply shifted due to a mismatch with the signal time series.

The single-collector ICP–MS at the UCSC Marine Sciences is unable to resolve ^{204}Pb due to isobaric interferences with ^{204}Hg , preventing the use of a ^{204}Pb -based common Pb correction. Instead, we applied a ^{207}Pb -based correction to $^{206}\text{Pb}/^{238}\text{U}$ ages ≤ 800 Ma using Isoplot v.3.75 (Ludwig, 2008). Although the 207-correction can yield erroneously young ages in cases where crystals have experienced significant Pb loss (Andersen et al., 2019), this correction is viable for younger grains (those $\leq \sim 800$ Ma), and especially for those younger than ~ 100 Ma. This is because the common Pb composition is estimated by subtracting the radiogenic ^{207}Pb from the total. Since ^{238}U is much ($137\times$) more abundant than ^{235}U , ^{206}Pb (from ^{238}U) is highly radiogenic, unlike ^{207}Pb (from ^{235}U). Hence, at relatively young ages, subtracting out the radiogenic ^{207}Pb is more reliable because it represents a low proportion and will therefore result in a smaller potential correction. Because the youngest coherent group of ages for our samples (used to determine MDAs) is exclusively less than ca. 31 Ma, this method is especially viable for our study. Moreover, we applied a number of criteria, described below, to ensure reliable ages in general and to limit the potential that the correction could yield erroneously young ages.

In cases where the $^{206}\text{Pb}/^{238}\text{U}$ age exceeded 1000 Ma, we took uncorrected $^{207}\text{Pb}/^{206}\text{Pb}$ ages to represent the best age. We applied the following filtering criteria to omit analyses that exhibited discordance, reverse discordance, or potentially high common Pb:

- $^{206}\text{Pb}/^{238}\text{U}$ ages > 800 Ma and discordance $> 30\%$ relative to $^{207}\text{Pb}/^{206}\text{Pb}$ ages
- $^{206}\text{Pb}/^{238}\text{U}$ ages > 800 Ma and discordance $< -7\%$ (reverse discordance) relative to $^{207}\text{Pb}/^{206}\text{Pb}$ ages
- $^{206}\text{Pb}/^{238}\text{U}$ ages < 1000 Ma and ^{207}Pb -based common Pb correction to the $^{206}\text{Pb}/^{238}\text{U}$ ages $> 10\%$ relative to uncorrected $^{206}\text{Pb}/^{238}\text{U}$ ages
- $^{206}\text{Pb}/^{238}\text{U}$ ages ≥ 1000 Ma and $^{206}\text{Pb}/^{204}\text{Pb} < 250$
- Extremely high errors (2σ) that are greater than the corresponding “best age.”

There is no indication of systematic Pb loss among the grains to which the 207-correction was applied. The 207-correction was usually exceedingly small, as is documented in Table S2; the vast majority of grains were corrected by $\ll 1$ Ma ($\leq 1\%$).

For the second group of samples, separated in 2018, analyses were conducted on a Nu Plasma multi-collector LA–ICP–MS attached to a Photon Machines Analyte G2 excimer laser at the University of Arizona LaserChron Center. Reference materials were supplied by the LaserChron Center and included their Sri Lanka (SL) zircon as a primary reference material and R33 (419.26 ± 0.39 Ma; Black et al., 2004) as a secondary reference material. Analytical procedures are outlined by Gehrels et al. (2006, 2008), and they include an automatic ^{204}Pb -based common Pb correction. The same filtering criteria were applied to this second group of samples. However, because the Nu Plasma multi-collector instrument is able to resolve ^{204}Pb , we also omitted analyses with $^{204}\text{Pb} > 700$ cps.

Plots of weighted mean depositional or maximum depositional ages (Fig. S2) and age probability distributions (Fig. S1) were generated using Isoplot v.3.75. U-Pb ages by analysis and isotopic data used to calculate these ages are presented in Table S2. All weighted mean errors except for that of sample 15JLS029 are calculated according to the 95% confidence error of the weighted average. In the case of 15JLS029, only two grains are present in the youngest coherent group of ages, so we estimate the weighted mean errors using only the 2σ internal error (error propagated from only the assigned data-point errors), not multiplied by the square root of the mean square weighted deviation, MSWD). Only the young (≤ 70 Ma) analyses are shown in Fig. S2. Preferred MDAs (in green) are typically based on the weighted mean of the youngest coherent group of analyses. Fig. S2 also presents weighted mean ages (in black) with sufficient additional grains included to achieve MSWD ~ 1 , although these are not our preferred ages.

TEXT S2. METHODS FOR ASSIGNING (MAXIMUM) DEPOSITIONAL AGES

As illustrated in Fig. 5, three techniques were applied to determine depositional age constraints for the strata sampled for stable isotope values, depending on the types of rocks and available age data. The youngest isotopically dated mineral population within a detrital sample provides a maximum depositional age (MDA). Second, fossil ages (from previous studies) provide age brackets for all or part of a stratigraphic unit. Third, isotopic dating or tephra correlation conducted on volcanic minerals within air- or water-lain tuffs can, in some cases, provide absolute depositional ages. Although it is possible that such tuffs experienced some reworking by fluvial or lacustrine processes, their eruption ages are likely close to the time of deposition (probably $\ll 1$ Ma). This is supported by the large number of temporally distinct Cenozoic tuffs preserved in basins across the northern Basin and Range Province, often with short gaps between subsequent eruptions, all of which typically provide tight temporal constraints on depositional ages (Wallace et al., 2008). In particular, Neogene silicic tuffs erupted from the Snake River Plain (Fig. 1) provide excellent and high-resolution age control for basin-and-range faulting and sediment deposition throughout this region. Faulting began approximately at the onset of silicic eruptions ca. 16.5 Ma (Coble and Mahood, 2012), rapidly creating sediment accommodation in fault hanging walls. Silicic eruptions occurred frequently along the SRP from its inception ca 16.5 to the present. For these reasons, any volcanic material that spent large amounts of time being reworked at the surface would have a high probability of including material from younger eruptions.

For isotopically dated samples, maximum and absolute depositional ages from sedimentary rocks and tuffs were determined by estimating the weighted mean of the youngest coherent group of ages (Fig. S2). In several cases, the youngest coherent group was straightforwardly identified as those whose ages overlapped within 2σ uncertainty and were clearly younger than others (outside the 2σ error bounds). In less clear cases, the youngest coherent group was determined in an interpretive fashion that attempted to maximize the number of included grains while avoiding inclusion of so many grains as to significantly increase age uncertainty. All but one of such cases yielded mean square weighted deviation (MSWD) ~ 1.0 . That case (sample 15JLS002; Fig. S2b) yielded MSWD = 0.42 because of several relatively young grains, but the weighted mean age that would produce MSWD = 1 is also shown.

Data from the stratigraphic sections shown in Fig. 5 are compiled together into a generalized column (Fig. 6) based on the preferred depositional ages listed in Tables S3 and S4. The preferred ages for samples previously analyzed for stable isotope values (which do not all have isotopic ages) were assigned by assuming constant sedimentation rates between horizons with age constraints as shown in Fig. 5, although we are aware that constant deposition was unlikely. Hence, vertical error bars in Fig. 6 indicate the full range of permissible ages for individual analyses between minimum and maximum age brackets, conservatively incorporating the full 2σ uncertainties of the bounding weighted mean ages.

TEXT S3. RESULTS OF U-PB DETRITAL ZIRCON GEOCHRONOLOGY

A sandstone sample (15JLS015) collected from near the top of a thin (< 200 m) sedimentary deposit below the tuff of Hackwood Ranch (Fig. 4a) yielded an MDA of 29.9 ± 0.2 Ma on the basis of the weighted mean of 45 analyses (Figs. 5 and S2a). Lund Snee et al. (2016) obtained a U-Pb detrital zircon MDA of 33.9 ± 0.4 Ma from a sample (10JLS08) collected nearby but stratigraphically lower within the same unit. The age of these deposits is bracketed below by a U-Pb SHRIMP (zircon) age of 37.34 ± 0.33 Ma (sample 10JLS05) from the tuff of Dixie Creek and above by a $^{40}\text{Ar}/^{39}\text{Ar}$ (sanidine) age of 31.10 ± 0.47 Ma on the tuff of Hackwood Ranch (Lund Snee et al., 2016). It is unclear why the detrital zircon age of sample 15JLS015 is ≥ 0.5 Ma younger than the previously obtained $^{40}\text{Ar}/^{39}\text{Ar}$ age of the overlying tuff (including uncertainty), but we take the $^{40}\text{Ar}/^{39}\text{Ar}$ tuff age to be authoritative because multiple samples and isotopic systems have yielded consistent ages (see Lund Snee et al., 2016).

The remaining detrital zircon ages were obtained for samples collected from the latest Oligocene–Miocene Humboldt Formation. Deposition of the Humboldt Formation was previously bracketed to ca. 24.4 ± 0.1 Ma (U-Pb zircon sample ELM11-PN19) at the bottom to at least 8.2 ± 0.2 Ma (U-Pb zircon sample 12HBD09) at the top (Lund Snee et al., 2016). A tuffaceous sandstone from the western measured sections (Figs. 3 and 4b) representing the stratigraphically lowest Humboldt Formation sample that was analyzed as part of this study (15JLS002, 5 m above the angular unconformity with underlying Eocene and Oligocene tuffs) extends the oldest known depositional age of this unit to 25.1 ± 0.2 Ma (a weighted mean of 32 grains). Progressing stratigraphically upward in the western section, a pebble conglomerate with an ashy matrix (sample 15JLS004; 89 m) yielded a younger MDA of 21.7 ± 0.1 Ma on the basis of a 75-grain weighted mean. One younger grain (15.7 ± 0.9 Ma) was excluded from this analysis due to obvious zoning, which is why we consider this analysis of a tuffaceous bed to be an MDA rather than an absolute depositional age; it is therefore possible that this sample could be ca. 16 Ma or younger, although the sample's stratigraphic position near and below samples containing only significantly older ages discounts this possibility. Slightly above (101 m), a weighted mean of 3 analyses established an MDA of 18.4 ± 2.5 Ma for a matrix-supported pebble conglomerate (sample 15JLS029). Finally, an ashy sandstone (15JLS017) yielded a younger MDA of 16.6 ± 0.3 Ma from 8 grains. Four previously published approximately

absolute depositional ages from tuffs higher in this section young progressively upward to ca. 14.6 Ma (Fig. 5) (Lund Snee et al., 2016).

A second Humboldt Formation section was sampled farther east (Figs. 3 and 4c), across a normal fault with > 700 m throw that exposes the base of the Humboldt Formation in its footwall (Wallace et al., 2008; Lund Snee and Miller, 2015; Lund Snee et al., 2016). The currently available ages within this redundant basal section are not as well constrained as to the west. However, it is quite unlikely that samples from this eastern section were deposited after 9.91 Ma, which is the youngest depositional age obtained by Wallace et al. (2008) using isotopic dating methods and tephra correlations on tuffs collected farther up-section, east of Huntington Creek (Fig. 3). Stratigraphically higher in this same area, Lund Snee et al. (2016) reported a U-Pb detrital zircon age of 8.2 ± 0.2 Ma (sample 12HBD09), representing the youngest known MDA for the Humboldt Formation (Fig. 3).

A third Humboldt Formation section was sampled to the northeast, west of the Lee township (Figs. 3 and 4d), and roughly along strike of a section along Huntington Creek from which Wallace et al., (2008) reported tuff (absolute depositional) ages that decrease upward from 15.31–9.91 Ma. An approximately absolute depositional age of 14.9 ± 0.2 Ma was established based on a 3-grain weighted mean for a tephra sample (15JLS041) collected from the base of the section (0 m). Near the top of this section (325 m), a silty sandstone (sample 15JLS037) yielded an MDA of 12.4 ± 1.0 Ma based on a 3-grain weighted mean.

TEXT S4. REVISED STRATIGRAPHIC THICKNESS AND DEPOSITIONAL AGE CONSTRAINTS FOR ELKO BASIN SEDIMENTARY ROCKS, NORTHEAST NEVADA

This section provides detailed information regarding how stratigraphic thicknesses were determined and how age constraints were applied throughout the stratigraphic sections presented in Figs. 5 and 6. Sample localities are shown in Figs. 3 and 4 and listed in the Supplementary Data Tables.

Pliocene–Pleistocene Hay Ranch Formation

Depositional ages are not well constrained for the Hay Ranch Formation, which is the youngest unit considered in this study. The stable isotope results for this unit that are shown in Fig. 5 were originally obtained by Horton et al. (2004), who did not report sample locations but assigned ages based on assumed sedimentation rates. We assume that these samples were collected from Pine Valley, west of the Piñon Range, in the general location indicated in Fig. 3. Regnier (1960) and Smith et al. (1976) provided a tentative depositional age range for the Hay Ranch Formation of middle Pliocene to middle Pleistocene. We therefore assume a permissible depositional age range of 3.6–1.8 Ma for Horton et al.’s samples. Lacking information about stratigraphic depths, for visualization purposes in Fig. 6 we plot all samples as being deposited at the same time, and we retain the full permissible depositional age ranges in the error bars.

Latest Oligocene–Miocene Humboldt Formation

The latest Oligocene to Miocene Humboldt Formation (Sharp, 1939) is described in detail by Wallace et al. (2008), Lund Snee (2013), Lund Snee and Miller (2015), and Lund Snee et al. (2016). Lund Snee et al. (2016) observed a clear pattern of upward-younging ages for tuffs sampled within the Humboldt Formation. For the present study, we collected additional samples for geochronology and stable isotope analysis in several measured sections shown in Fig. 5, which add to the geochronologic data presented by Lund Snee et al. (2016). The lowest exposed levels of the Humboldt Formation were sampled in two subparallel sections near the westernmost exposures of the Humboldt Formation in the studied area, as well as a third “eastern base Humboldt Formation” section northeast of Cedar Ridge (shown in Figs. 3 and 4), for redundancy across this important interval. Samples are described from older to younger in each of these sections.

Using map relationships, stratigraphic thicknesses and depositional age constraints, the two western sections were compiled together in the “composite western base Humboldt Formation” section (Figs. 4b and 5). In our thickness measurements for this compiled section, we accounted for minor observed offset and duplication of Humboldt Formation strata across an east-striking fault in the northern of the two sections (~48 m stratigraphic thickness duplicated). An absolute maximum age constraint for this section (and for the Humboldt Formation across the area) is 31.08 ± 0.47 Ma ($^{40}\text{Ar}/^{39}\text{Ar}$ sanidine), our preferred age obtained for the tuff of Hackwood Ranch, which the Humboldt Formation overlies across a poorly exposed angular unconformity (Lund Snee et al., 2016). Above this, only a few meters above the base of this unit in the composite western section, we obtained a U-Pb detrital zircon depositional age of 25.1 ± 0.2 Ma (Fig. S2b) from a sample of air-fall tuff deposited within the Humboldt Formation (sample 15JLS002; Fig. 4b). Lund Snee et al. (2016) obtained a U-Pb detrital zircon MDA of 24.4 ± 0.1 Ma from their sample ELM11-PN19, collected from about 60 m stratigraphically above 15JLS002, also from a probable air-fall tuff deposited within the Humboldt Formation, which provides another approximate absolute depositional age for that low stratigraphic level (Fig. 5). Together, these progressively younger ages within the Humboldt Formation reveal minor but sustained lacustrine deposition well before major surface-breaking extension initiated ca. 17–16 Ma (Colgan and Henry, 2009; Colgan et al., 2010; Lund Snee et al., 2016).

Overlying sample 15JLS004 yielded an MDA of 21.7 ± 0.1 Ma based on a weighted mean of 75 grains (Fig. S2c). A single grain in sample 15JLS004 that displayed obvious zoning was omitted, but the earlier part of this grain’s analytical time series yielded a young age of 15.7 ± 0.9 Ma. Hence, we note that it is possible that sample 15JLS004 (and those above it) may be ca. 15.7 Ma or younger, but the tenuous nature of this zoned single grain age and the sample’s stratigraphic position (near and below samples containing only older ages) makes that possibility less likely. Although the large population of grains ca. 22 Ma (Fig. S2c) in this sample ($n = 91$) suggests that it may represent a reworked air-fall tuff, we conservatively do not treat this sample as a bound on minimum depositional ages for underlying strata due to the uncertainty related to the possible younger grain. Sample 15JLS027A yielded a poorly constrained MDA of 25.3 ± 1.2 Ma based on a single zircon grain (older than age constraints beneath it). Stratigraphically overlying sample 15JLS029 (from the northern section) yielded an MDA of 18.4 ± 2.5 Ma, based on a weighted mean of 3 ages (Fig. S2f).

A weighted mean age of 16.6 ± 0.3 (Fig. S2d), from 8 grains, is established for a higher sample from the southern section, 15JLS017. This sample provides an MDA for the stratigraphically overlying stable isotope analyses by Mulch et al. (2015) and sources therein. Consequently, an outcome of this work is that > 400 m of Humboldt Formation section are present below the lowest samples for which published stable isotope values are available. A minimum depositional age of 15.53 Ma is assigned to these older stable isotope samples (and to stratigraphically underlying rocks), based on a U-Pb detrital zircon age of 15.6 ± 0.1 Ma obtained by Lund Snee et al. (2016) for air-fall tuff sample Tiws-J4 (Fig. 5). Higher in this composite section, approximate absolute depositional ages reported by Lund Snee et al. (2016) on upward-younging, intercalated air-fall tuffs provide maximum and minimum depositional age constraints on overlying and underlying strata, respectively (Fig. 5). These ages enable us to assign depositional age bounds on the stable isotope samples reported by Mulch et al. (2015) and sources therein for the upper (northern) portions of their “Indian Well Formation” section as well (see Figs. 3, 4b, and 5). (Note that Lund Snee et al., 2016, recommended that the Indian Well Formation name be discontinued after they found that essentially all sedimentary strata previously included within it are latest Oligocene to Miocene in age and belong to the Humboldt Formation based on detailed re-mapping of the section by Lund Snee and Miller, 2015).

The eastern section, which also contains the base of the Humboldt Formation, is exposed ~ 8 km away from the western section described above, on the northeast side of Cedar Ridge (Figs. 3 and 4c), across a normal fault system that duplicates the Cenozoic succession (Wallace et al., 2008; Lund Snee and Miller, 2015; Lund Snee et al., 2016). In the eastern section, strata of the Humboldt Formation were deposited unconformably above rocks resembling the Eocene Elko Formation and Late Cretaceous(?)–Eocene(?) limestone (TKI) and conglomerate, sandstone, siltstone, and limestone (TKcs) units (Lund Snee and Miller, 2015; Lund Snee et al., 2016). Unlike the composite basal section exposed farther west, detrital U-Pb zircon analyses carried out in this succession (sample 12HBD06 of Lund Snee et al., 2016, and sample 15JLS036B of this study) record no grains in the age range between the end of local volcanic activity ca. 37 Ma and the onset of rapid extension ca. 17–16 Ma (Colgan et al., 2010; Lund Snee et al., 2016). The lowest sample collected near the base of the Humboldt Formation (sample 12HBD06 of Lund Snee et al., 2016) contained a single young grain at 15.7 ± 0.5 Ma, which was not employed to constrain an MDA due to its tentative nature. The lack of Cenozoic grains older

than 15.7 Ma suggests that sedimentation did not occur in this eastern area in the time span ~26–15.7 Ma, when tuffs were being deposited in the Humboldt Formation succession sampled ~8 km to the west. Minimum depositional ages are not constrained for the eastern basal Humboldt Formation section (Figs. 3 and 4c) because sample 15JLS036B (Fig. S2g) yielded only a single U-Pb zircon age (11.5 ± 0.4 Ma). However, it is quite unlikely that samples from this eastern section were deposited after 9.91 Ma, which is the youngest depositional age obtained by Wallace et al. (2008) using isotopic dating methods and tephra correlations on tuffs collected farther up-section, east of Huntington Creek (Fig. 4d).

Finally, we sampled a fourth Humboldt Formation section to the northeast of the others, near the Lee township (Figs. 3, 4d, and 5), part of which Chamberlain et al. (2012) and Mulch et al. (2015) previously sampled for stable isotope values but did not provide age constraints. We have bracketed the MDA for this succession with a U-Pb detrital zircon age of 14.9 ± 0.2 Ma obtained on tuff sample 15JLS041, from the base of the section (Figs. S2i, 4d, and 5). We account for local duplication by open folds shown in Fig. 4d, as well as minor, outcrop-scale normal faults. At the top of the section, we obtained a U-Pb detrital zircon MDA of 12.4 ± 1.0 Ma, on sample 15JLS037 (Fig. S2h). Although this MDA does not provide an upper (minimum) age constraint, the section is approximately along strike from (and ~5 km away from) the Humboldt Formation type section on the eastern banks of Huntington Creek (Sharp, 1939) in which Wallace et al. (2008) found air-fall tuff depositional ages ranging from 15.31 Ma at the base to 9.91 Ma at the top (Fig. 3). The youngest detrital zircon MDA obtained for the Humboldt Formation in Huntington Valley is 8.2 ± 0.2 Ma (Lund Snee et al., 2016, sample 12HBD09), from a sample collected ~10 km southwest of the Lee section sampled in this study. We assign best ages to the stable isotope values previously obtained from the Lee section ranging between 14.39–13.38 Ma considering the above information and assuming constant sedimentation rates, but we allow the uncertainty bars plotted in Fig. 6 to span as young as 8.01 Ma.

Eocene–Oligocene sandstone and siltstone between the Eocene tuff of Dixie Creek and the Oligocene tuff of Hackwood Ranch

A thin (< 200 m) deposit of sandstone and siltstone is exposed near the abandoned Hackwood Ranch site (Figs. 3 and 4a). The depositional ages for these strata are bracketed by a 36.84 ± 0.34 Ma (U-Pb zircon SHRIMP) age for the unconformably underlying tuff of Dixie

Creek and multiple 31.10 Ma ($^{40}\text{Ar}/^{39}\text{Ar}$ sanidine and U-Pb zircon SHRIMP) eruptive ages for the overlying tuff of Hackwood Ranch (Lund Snee et al., 2016). Hence, deposition of this sedimentary succession occurred across the time interval 37.18 to ca. 31 Ma. In addition, Lund Snee et al. (2016) reported a U-Pb detrital zircon MDA of 33.9 ± 0.4 Ma for a sample (10JLS08) collected from the lower parts of this interval, and we (this study) obtained a U-Pb detrital zircon MDA of 29.9 ± 0.2 Ma for a sample (15JLS015) collected from near the top of the succession, based on a weighted mean of 45 grains (Figs. 4a, 5, and S2a). Two grains were omitted due to the indication of zoning in their time series. It is unclear why this upper MDA is ≥ 0.5 Ma younger than (outside of the uncertainty range of) the age of the overlying tuff of Hackwood Ranch. As noted above, we consider the previously reported ca. 31 Ma ages for the tuff of Hackwood Ranch to be definitive due to the consistency of these ages across multiple isotopic systems (Lund Snee et al., 2016), and the expectation that single collector LA-ICP-MS analysis could be less accurate than U-Pb SHRIMP or $^{40}\text{Ar}/^{39}\text{Ar}$. Stable isotope values are not available for this section, but ages for these rocks are reported here because they nevertheless document localized sediment accumulation during that time span.

Eocene Elko Formation

Across the Elko Basin, the beginning of Elko Formation deposition is approximately bracketed by a pink air-fall tuff at low stratigraphic levels in the Elko Hills (Fig. S3) that yielded a U-Pb zircon (SHRIMP) age of 46.1 ± 0.2 (sample 00-188GS of Haynes, 2003), which is probably correlative with a less precise U-Pb detrital zircon age of 45.92 ± 0.95 Ma obtained by Lund Snee et al. (2016) farther south (sample ELKO-1). Here we take the more precise 46.10 ± 0.20 Ma age obtained by Haynes (2003) to conservatively suggest an approximate start of Elko Formation deposition at 46.30 Ma (including the 2σ uncertainty). An eruptive age of 38.47 ± 0.15 Ma ($^{40}\text{Ar}/^{39}\text{Ar}$ plagioclase) obtained from a basal eruptive unit within the overlying tuff of Dixie Creek (sample H10-45 of Henry et al., 2015) provides a minimum depositional age of 38.32 Ma for the Elko Formation. A U-Pb detrital zircon weighted mean age of 37.9 ± 0.5 Ma from the eastern Piñon Range (sample ELKO-2 of Lund Snee et al., 2016) indicates that deposition of the Elko Formation continued at least to that time, bracketing the youngest Elko Formation deposition to around ca. 38.4 Ma (accounting for 2σ uncertainties). The ages of the

uppermost Elko Formation strata and the lowermost overlying tuffs suggest that Elko Formation deposition continued until the onset of volcanism in this area.

None of these bracketing ages were obtained from samples collected within the immediate area of the Elko Formation section studied for stable isotope values by Horton et al. (2004) and subsequent studies (Mix et al., 2011; Chamberlain et al., 2012; Mulch et al., 2015), which is located near Emigrant Spring (Fig. 3). However, Mulch et al. (2015) obtained $^{40}\text{Ar}/^{39}\text{Ar}$ ages from detrital biotite collected across this same section, which permit establishment of MDAs throughout the sampled section. With one exception, these MDAs young upward, which could indicate that some of them represent air- or water-lain tuffs that originated from nearby eruptions of similar ages (Ressel and Henry, 2006). Accounting for this possibility, in Fig. 6 we select a best estimate of actual depositional age for each sample according to the possibility that some of the ages provided by Mulch et al. (2015) could represent absolute depositional ages, but we conservatively plot error bars that extend upward to the true minimum depositional age bound of 38.32 Ma provided by tuff sample H10-45 of Henry et al. (2015).

Horton et al. (2004) assigned additional samples at the base of this section to underlying “Cherty Limestone” and “Limestone and Limestone clast Conglomerate” units (the same samples were assigned to units called “Cherty Limestone” and “Limestone and Conglomerate” by Mulch et al., 2015). Mulch et al. (2015) reported that these samples were collected from a section near Emigrant Spring (Fig. 4). However, Horton et al. (2004) did not report sample locations, so the exact stratigraphic assignment and age cannot be determined. Horton et al. (2004, p. 864) identified these rocks as belonging to the “non-volcanic sequence” of early Cenozoic strata that precedes the Elko Formation, which would make them older than ca. 46 Ma, although Mulch et al. (2015) placed the 46.1 Ma tuff age obtained by Haynes (2003) between the “Cherty Limestone” and “Limestone and Conglomerate” units, based on stratigraphic assignments made farther north in the Elko Hills, implying that the overlying “Cherty Limestone” is younger than 46.1 Ma and the “Limestone and Conglomerate” is older.

This confusion may be at least partly resolved by the recent observation of Cenozoic volcanic clasts in a basal conglomerate within the Elko Formation from which a U-Pb zircon MDA of 44.5 ± 0.9 Ma was also obtained (sample EmigZr7 of Hollingsworth et al., 2017). This sample was collected from 50–85 m above the unconformity with underlying Paleozoic rocks at the Emigrant mine location (Ressel et al., 2015), which is ~3.5 km north of the Emigrant Spring

section studied by Horton et al. (2004) and Mulch et al. (2015) and included in this study (Figs. 5 and 6). For this reason, the strata that were previously assigned by Horton et al. (2004) and Mulch et al. (2015) to underlying units called “Cherty Limestone” and “Limestone and Conglomerate” (and similar) most likely belong to the lower part of the Elko Formation and are probably for the most part 45.4 Ma and younger, counting the 2σ age uncertainty (Figs. 5 and 6). Because that age was not obtained from a sample from the absolute bottom of the Elko Formation, we conservatively assign these basal Elko Formation strata an older MDA constraint of 46.3 Ma, the oldest age obtained from the Elko Formation (2σ uncertainty range of sample 00-188GS of Haynes, 2003). Based on these age constraints, we assign a *preferred* depositional age of 45.0 Ma to the stratigraphically lowest “Limestone and Conglomerate” sample in Fig. 5 (TL04-02). Because locations and stratigraphic depth information are not available for this unit and the “Cherty Limestone” of Horton et al. (2004) and Mulch et al. (2015), we assign best ages that decrease upward in increments of 0.1 Ma (to 44.3 Ma). As with some of the overlying strata of the middle Elko Formation described above, we employ a minimum depositional age bound of 41.2 Ma for these units, based on the 2σ range for the 41.60 ± 0.40 Ma reworked sediments analyzed by Mulch et al. (2015).

Finally, Smith et al. (2017) argued that the $^{40}\text{Ar}/^{39}\text{Ar}$ biotite ages determined by Mulch et al. (2015) and used to constrain depositional ages within the Elko Formation prior to the negative shift in $\delta^{18}\text{O}$ values were erroneously young. On this basis, they argued that Elko Formation deposition ceased by ca. 40.4 Ma, earlier than previously reported and prior to the ca. 40 Ma Middle Eocene Climatic Optimum (MECO) event (Sluijs et al., 2013). However, as explained above, multiple mineral and isotopic systems indicate that the end of Elko Formation deposition is tightly constrained to ca. 38.4 Ma, which is at odds with this ~ 2 Myr older estimate by Smith et al. (2017). Smith et al. (2017) suggested that the $^{40}\text{Ar}/^{39}\text{Ar}$ biotite ages previously obtained by Mulch et al. (2015) were ~ 2 Myr too young, and from this they proposed discounting the use of biotite $^{40}\text{Ar}/^{39}\text{Ar}$ ages in general for precise geochronologic applications. It is not clear why Smith et al. (2017) obtained systematically (ca. 1.5–2.0 Ma) older single-crystal sanidine $^{40}\text{Ar}/^{39}\text{Ar}$ ages on some of the same strata, but it is possible that their analyses were conducted on detrital grains that were older than the true sedimentary depositional ages. Moreover, unpublished sanidine $^{40}\text{Ar}/^{39}\text{Ar}$ ages by Mulch et al. (2015), from the same Elko Formation strata, agree closely with the $^{40}\text{Ar}/^{39}\text{Ar}$ biotite ages; the unpublished sanidine ages are slightly

younger (by 0.3–0.8 Ma) than the biotite ages and indistinguishable within 2σ error (M. Cosca, 2019, pers. comm.). Hence we interpret that the detrital biotite and sanidine $^{40}\text{Ar}/^{39}\text{Ar}$ MDAs reported by Mulch et al. (2015) are closest to the true depositional ages for Elko Formation strata.

Late Cretaceous(?)–early Eocene(?) limestone (TKI) and conglomerate, sandstone, siltstone, and limestone (TKcs)

Late Cretaceous(?)–early Eocene(?) limestone (TKI) and conglomerate, sandstone, siltstone, and limestone (TKcs) units underlie the Elko Formation near Cedar Ridge (Figs. 3 and 4) and are apparently older than the oldest strata sampled for this study (Fig. 5). Hence, these units are likely older than 46.10 ± 0.20 Ma, which is the age of the oldest volcanic tuff observed at the base of the Elko Formation (sample 00-188GS of Haynes, 2003). The MDA of these underlying sediments is constrained only by the presence of fossils “younger than Jurassic” (I.G. Sohn in Smith et al., 1976), with the bulk of fossil evidence provided by Smith et al. (1976) pointing to deposition during Late Cretaceous time or later, and a youngest detrital zircon population of 240 Ma (sample ELM11-PN16 of Lund Snee et al., 2016). Based on this information, we assume that the likeliest age for units TKcs and TKI is Late Cretaceous–Eocene (100 Ma to 45.9 Ma, counting the 2σ error for sample 00-188GS). The limestone unit (TKI) is thought to be slightly younger than the clastic unit (TKcs) on the basis of its generally higher stratigraphic position, although they could be partially contemporaneous (Lund Snee et al., 2016). We note that Ketner and Alpha (1992) argued that the “cherty limestone” and “conglomerate” facies in the Emigrant Spring area and elsewhere should be included within the Eocene Elko Formation due to apparently conformable relations with the overlying Elko Formation rocks and because similar cherty limestone and conglomerate rocks are clearly part of the lower Elko Formation farther north in the Elko Hills (Fig. 3). Despite this, we consider the conspicuous lack of Cenozoic volcanic detritus in these older rocks within the study area to be diagnostic and to potentially provide important information about stratigraphic age. Hence, we follow Smith et al. (1976), Lund Snee (2013), and Lund Snee and Miller (2015) and separate the TKcs and TKI units from the younger Elko Formation where these sediments demonstrably lack Cenozoic detritus.

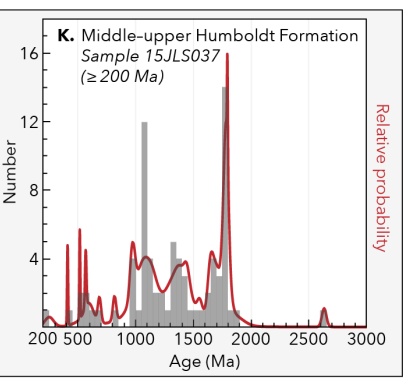
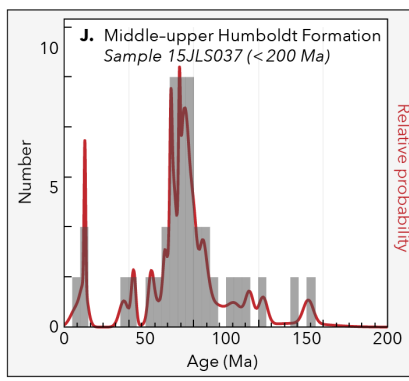
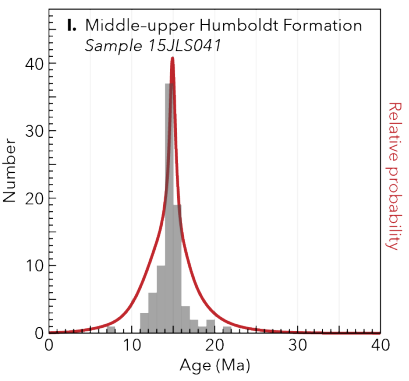
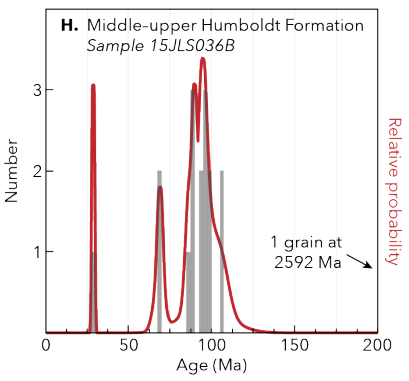
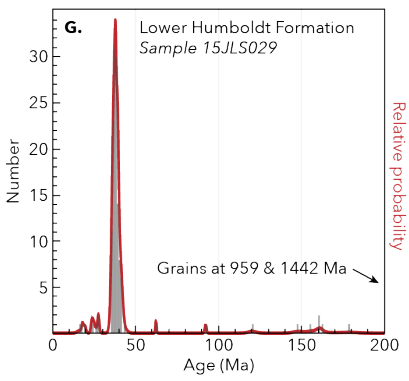
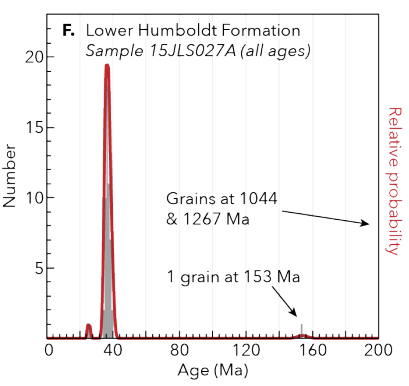
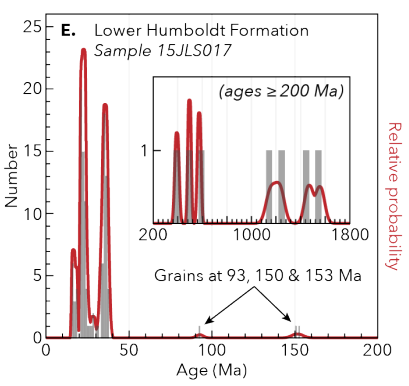
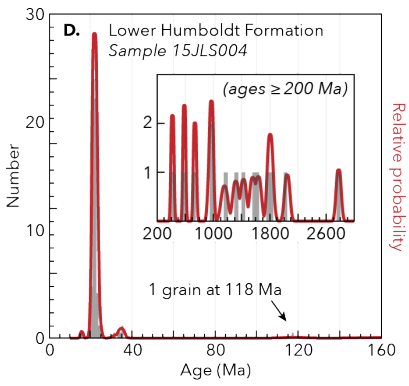
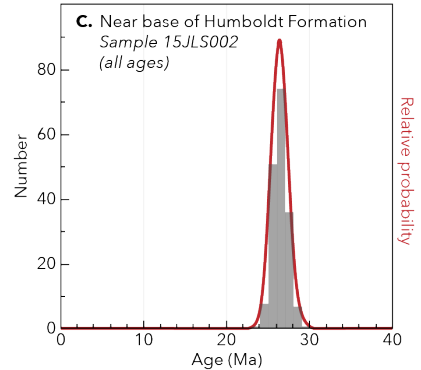
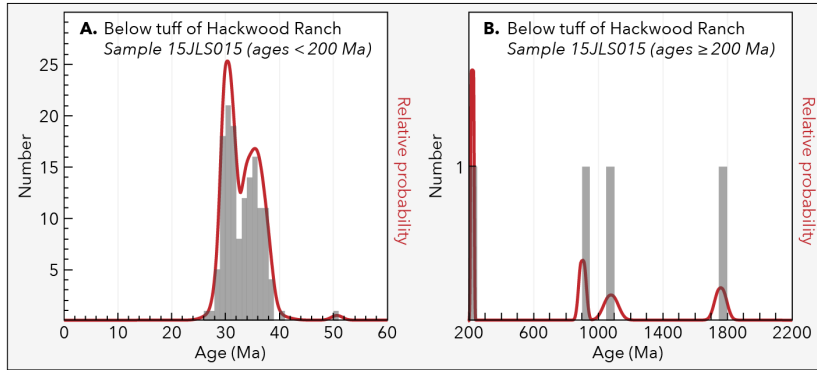


Fig. S1. Probability density plots of detrital zircon U-Pb ages.

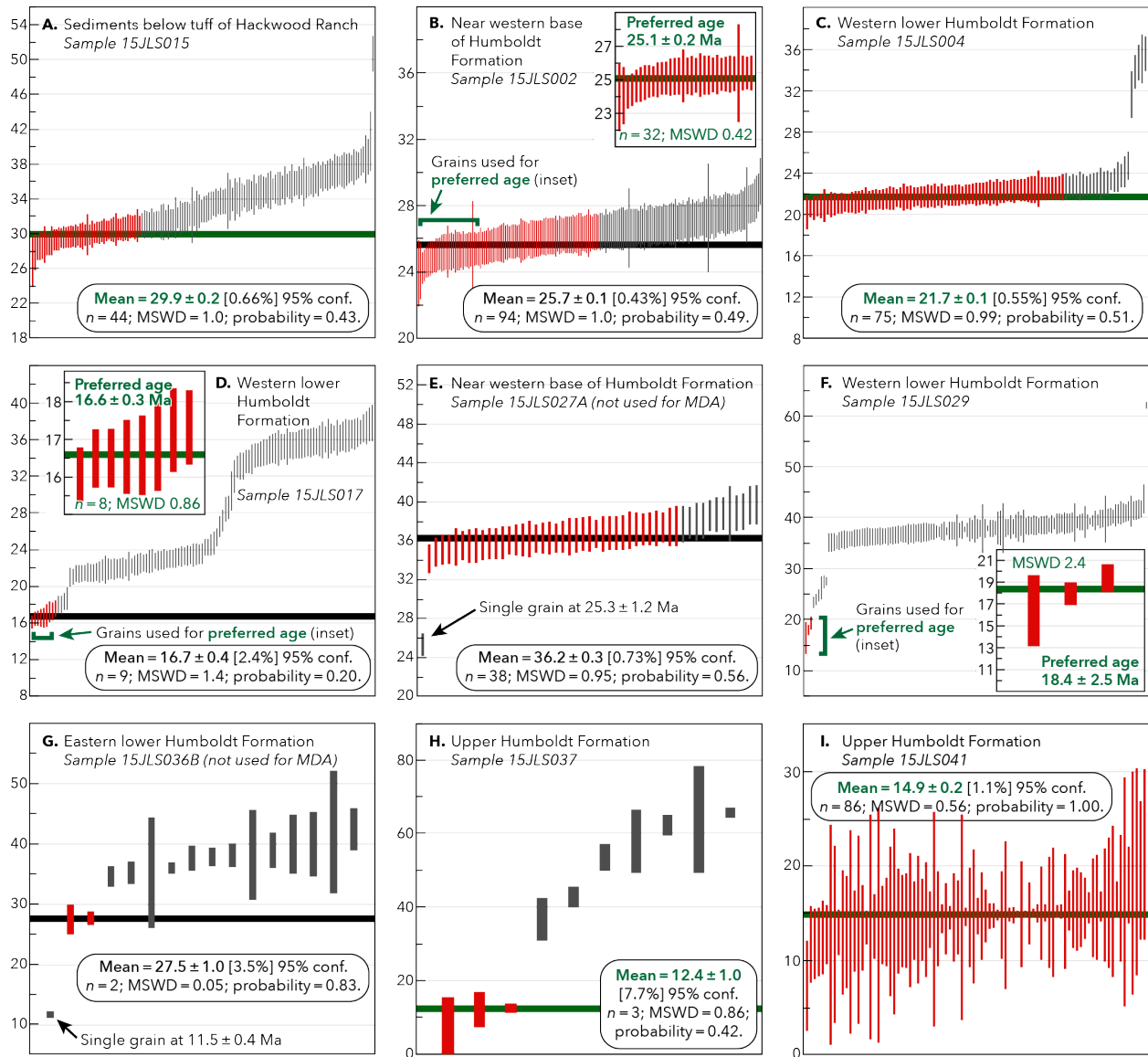


Fig. S2. Weighted mean plots for the youngest coherent groups of detrital zircon U-Pb analyses obtained from each sample, defining depositional ages or maximum depositional ages. Preferred ages are indicated in green and are also given in Table S1. Non-preferred weighted mean ages (black) are given to indicate the youngest group of ages yielding MSWD ~ 1 . Weighted by data-point errors only. Box heights represent 2σ errors. MSWD = mean square weighted deviation.

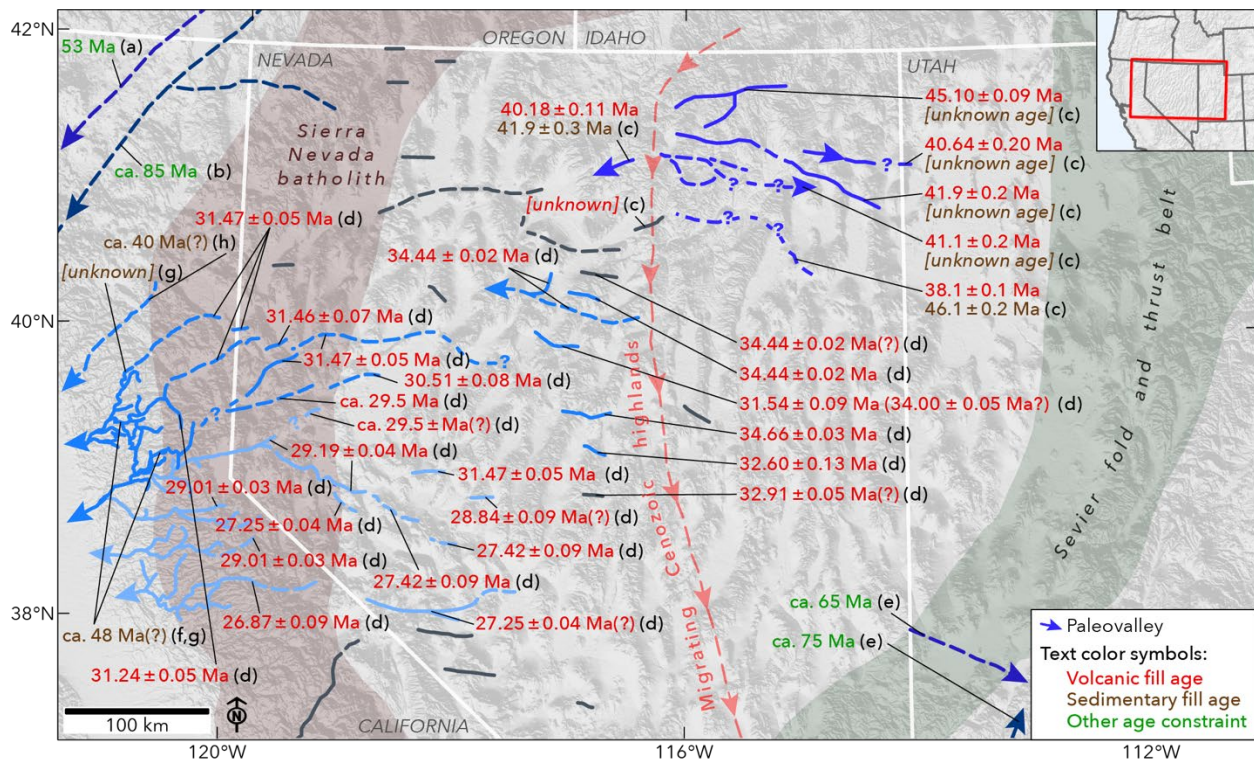


Fig. S3. Map of paleovalleys from the Great Basin and surroundings, western USA, with data sources and ages of oldest fill material or onset of drainage activity indicated. Paleovalley locations are from Henry et al. (2012), Henry and John (2013), Dumitru et al. (2015, 2016), and sources therein. Oldest sedimentary and/or volcanic fill identified in each paleovalley are indicated (orange and red type, respectively). Ages of pre-volcanic sedimentary fill are not well constrained. Grey paleovalleys indicate no relevant age constraints. The Sevier fold and thrust belt is from DeCelles (2004). The Cretaceous Sierra Nevada arc is after Van Buer and Miller (2010). This figure complements Fig. 2, providing additional age information and references. (a)—Dumitru et al. (2015); (b)—Dumitru et al. (2016); (c)—Henry (2008); (d)—Henry and John (2013); (e)—Goldstrand (1992, 1994); (f)—MacGinitie (1941); (g)—Yeend (1974); (h)—Garside et al. (2005).

REFERENCES

- Andersen, T., Elburg, M.A., and Magwaza, B.N., 2019, Sources of bias in detrital zircon geochronology: Discordance, concealed lead loss and common lead correction: *Earth-Science Reviews*, v. 197, p. 102899, doi:10.1016/j.earscirev.2019.102899.
- Black, L.P. et al., 2004, Improved $^{206}\text{Pb}/^{238}\text{U}$ microprobe geochronology by the monitoring of a trace-element-related matrix effect; SHRIMP, ID-TIMS, ELA-ICP-MS and oxygen isotope documentation for a series of zircon standards: *Chemical Geology*, v. 205, p. 115–140, doi:10.1016/j.chemgeo.2004.01.003.
- Van Buer, N.J., and Miller, E.L., 2010, Sawtooth batholith, NW Nevada: Cretaceous arc flare-up in a basinal terrane: *Lithosphere*, v. 2, p. 423–446, doi:10.1130/L105.1.
- Chamberlain, C.P., Mix, H.T., Mulch, A., Hren, M.T., Kent-Corson, M.L., Davis, S.J., Horton, T.W., and Graham, S.A., 2012, The Cenozoic climatic and topographic evolution of the western North American Cordillera: *American Journal of Science*, v. 312, p. 213–262, doi:10.2475/02.2012.05.
- Coble, M.A., and Mahood, G.A., 2012, Initial impingement of the Yellowstone plume located by widespread silicic volcanism contemporaneous with Columbia River flood basalts: *Geology*, v. 40, p. 655–658, doi:10.1130/G32692.1.
- Colgan, J.P., and Henry, C.D., 2009, Rapid middle Miocene collapse of the Mesozoic orogenic plateau in north-central Nevada: *International Geology Review*, v. 51, p. 920–961, doi:10.1080/00206810903056731.
- Colgan, J.P., Howard, K.A., Fleck, R.J., and Wooden, J.L.P., 2010, Rapid middle Miocene extension and unroofing of the southern Ruby Mountains, Nevada: *Tectonics*, v. 29, p. 417, doi:10.1029/2009TC002655.
- DeCelles, P.G., 2004, Late Jurassic to Eocene evolution of the Cordilleran thrust belt and foreland basin system, western U.S.A.: *American Journal of Science*, v. 304, p. 105–168, doi:10.2475/ajs.304.2.105.
- Dumitru, T.A., Elder, W.P., Hourigan, J.K., Chapman, A.D., Graham, S.A., and Wakabayashi, J., 2016, Four Cordilleran paleorivers that connected Sevier thrust zones in Idaho to depocenters in California, Washington, Wyoming, and, indirectly, Alaska: *Geology*, v. 44, p. 75–78, doi:10.1130/G37286.1.
- Dumitru, T.A., Ernst, W.G., Hourigan, J.K., and McLaughlin, R.J., 2015, Detrital zircon U–Pb

- reconnaissance of the Franciscan subduction complex in northwestern California: *International Geology Review*, v. 57, p. 767–800, doi:10.1080/00206814.2015.1008060.
- Dumitru, T.A., and Stockli, D.F., 1998, A better way to separate apatite from zircon using constriction tubes: *Advances in Fission-Track Geochronology*, p. 325–330.
- Garside, L.J., Henry, C.D., Faulds, J.E., and Hinz, N.H., 2005, The upper reaches of the Sierra Nevada auriferous gold channels, California and Nevada: *Geological Society of Nevada Symposium*, p. 209–235.
- Gehrels, G.E., Valencia, V.A., and Pullen, A., 2006, Detrital zircon geochronology by laser-ablation multicollector ICPMS at the Arizona Laserchron Center: *Geochronology: Emerging Opportunities*, v. 12, p. 67–76.
- Gehrels, G.E., Valencia, V.A., and Ruiz, J., 2008, Enhanced precision, accuracy, efficiency, and spatial resolution of U-Pb ages by laser ablation-multicollector-inductively coupled plasma-mass spectrometry: *Geochemistry, Geophysics, Geosystems*, v. 9, p. 1–13, doi:10.1029/2007GC001805.
- Goldstrand, P.M., 1992, Evolution of Late Cretaceous and early Tertiary basins of southwest Utah based on clastic petrology: *Journal of Sedimentary Research*, v. Vol. 62, p. 495–507, doi:10.1306/D4267933-2B26-11D7-8648000102C1865D.
- Goldstrand, P.M., 1994, Tectonic development of Upper Cretaceous to Eocene strata of southwestern Utah: *Bulletin of the Geological Society of America*, v. 106, p. 145–154, doi:10.1130/0016-7606(1994)106<0145.
- Haynes, S.R., 2003, Development of the Eocene Elko Basin, northeastern Nevada: Implications for paleogeography and regional tectonism: The University of British Columbia, https://circle.ubc.ca/bitstream/id/34598/ubc_2003-0240.pdf.
- Henry, C.D., 2008, Ash-flow tuffs and paleovalleys in northeastern Nevada: Implications for Eocene paleogeography and extension in the Sevier hinterland, northern Great Basin: *Geosphere*, v. 4, p. 1–35, doi:10.1130/GES00122.1.
- Henry, C.D., Hinz, N.H., Faulds, J.E., Colgan, J.P., John, D.A., Brooks, E.R., Cassel, E.J., Garside, L.J., Davis, D.A., and Castor, S.B., 2012, Eocene-Early Miocene paleotopography of the Sierra Nevada-Great Basin-Nevadaplano based on widespread ash-flow tuffs and paleovalleys: *Geosphere*, v. 8, p. 1–27, doi:10.1130/GES00727.1.
- Henry, C.D., Jackson, M.R., Mathewson, D.C., Koehler, S.R., and Moore, S.C., 2015, Eocene

- igneous geology and relation to mineralization: Railroad district, southern Carlin trend, Nevada, *in* Pennell, W.M. and Garside, L.J. eds., Geological Society of Nevada, New Concepts and Discoveries, p. 939–965.
- Henry, C.D., and John, D.A., 2013, Magmatism, ash-flow tuffs, and calderas of the ignimbrite flareup in the western Nevada volcanic field, Great Basin, USA: *Geosphere*, v. 9, p. 951, doi:10.1130/GES00867.1.
- Hollingsworth, E.R., Ressel, M.W., and Henry, C.D., 2017, Age and depth of Carlin-type gold deposits in the southern Carlin trend: Eocene Mountain Lakes, Big Volcanoes, and Widespread, Shallow Hydrothermal Circulation, *in* Bedell, R.L. and Ressel, M.W. eds., Geological Society of Nevada field trip guidebook: Shallow expressions of Carlin-type gold deposits: Alligator Ridge and Emigrant mines, Nevada, Reno, NV, p. 149–173.
- Horton, T.W., Sjostrom, D.J., Abruzzese, M.J., Poage, M.A., Waldbauer, J.R., Hren, M.T., Wooden, J.L.P., and Chamberlain, C.P., 2004, Spatial and temporal variation of Cenozoic surface elevation in the Great Basin and Sierra Nevada: *American Journal of Science*, v. 304, p. 862–888, doi:10.2475/ajs.304.10.862.
- Ketner, K.B., and Alpha, A.G., 1992, Mesozoic and tertiary rocks near Elko, Nevada—Evidence for Jurassic to Eocene folding and low-angle faulting: *U.S. Geological Survey Bulletin* 1988-C, 13 p.
- Ludwig, K.R., 2008, User’s manual for Isoplot 3.7: A geochronological toolkit for Microsoft Excel: Berkeley Geochronology Center Special Publication No. 4, p. 77.
- Lund Snee, J.-E., 2013, Geology and geochronology of Cenozoic units in the Piñon Range and Huntington Valley, Nevada: Stanford University, 263 p., <http://purl.stanford.edu/hx388mg6634>.
- Lund Snee, J.-E., and Miller, E.L., 2015, Preliminary geologic map of Cenozoic units of the central Robinson Mountain volcanic field and northwestern Huntington Valley: Nevada Bureau of Mines and Geology Open File, v. 15–2, p. 42, 1:24,000 scale, <http://pubs.nbmng.unr.edu/product-p/of2015-02.htm>.
- Lund Snee, J.-E., Miller, E.L., Grove, M.J., Hourigan, J.K.J.K., and Konstantinou, A., 2016, Cenozoic paleogeographic evolution of the Elko Basin and surrounding region, northeast Nevada: *Geosphere*, v. 12, p. 464–500, doi:10.1130/GES01198.1.
- MacGinitie, H.D., 1941, Contributions to Paleontology: Middle Eocene Flora from the central

- Sierra Nevada: Washington, D.C., Carnegie Institution of Washington Publication 534.
- Mix, H.T., Mulch, A., Kent-Corson, M.L., and Chamberlain, C.P., 2011, Cenozoic migration of topography in the North American Cordillera: *Geology*, v. 39, p. 87–90, doi:10.1130/G31450.1.
- Mulch, A., Chamberlain, C.P., Cosca, M.A., Teyssier, C., Methner, K., Hren, M.T., and Graham, S.A., 2015, Rapid change in high-elevation precipitation patterns of western North America during the Middle Eocene Climatic Optimum (MECO): *American Journal of Science*, v. 315, p. 317–336, doi:10.2475/04.2015.02.
- Naeser, N.D., and Naeser, C.W., 1984, Fission-track dating, *in* Mahaney, W.C. ed., *Quaternary Dating Methods*, New York, NY, Elsevier Science Publishing Company Inc., p. 87–100.
- Paces, J.B., and Miller, J.D., 1993, Precise U-Pb ages of Duluth Complex and related mafic intrusions, northeastern Minnesota: Geochronological insights to physical, petrogenetic, paleomagnetic, and tectonomagmatic processes associated with the 1.1 Ga Midcontinent Rift System: *Journal of Geophysical Research*, v. 98, p. 13997, doi:10.1029/93JB01159.
- Paton, C., Hellstrom, J., Paul, B., Woodhead, J., and Hergt, J., 2011, Iolite: Freeware for the visualisation and processing of mass spectrometric data: *Journal of Analytical Atomic Spectrometry*, v. 26, p. 2508, doi:10.1039/c1ja10172b.
- Regnier, J., 1960, Cenozoic geology in the vicinity of Carlin, Nevada: *Bulletin of the Geological Society of America*, v. 71, p. 1189–1210, doi:10.1130/0016-7606(1960)71[1189:CGITVO]2.0.CO;2.
- Ressel, M.W., Dendas, M., Lujan, R., Essman, J., and Shumway, P.J., 2015, Shallow expressions of Carlin-type hydrothermal systems: An example from the Emigrant Mine, Carlin trend, Nevada, *in* *New Concepts and Discoveries: Geological Society of Nevada 2015 Symposium*, p. 409–433.
- Ressel, M.W., and Henry, C.D., 2006, Igneous geology of the Carlin trend, Nevada: Development of the Eocene plutonic complex and significance for Carlin-type gold deposits: *Economic Geology*, v. 101, p. 347–383, doi:10.2113/gsecongeo.101.2.347.
- Sharp, R.P., 1939, The Miocene Humboldt Formation in Northeastern Nevada: *The Journal of Geology*, v. 47, p. 133–160, doi:10.1086/624749.
- Sluijs, A., Zeebe, R.E., Bijl, P.K., and Bohaty, S.M., 2013, A middle Eocene carbon cycle conundrum: *Nature Geoscience*, v. 6, p. 429–434, doi:10.1038/ngeo1807.

- Smith, M.E., Cassel, E.J., Jicha, B.R., Singer, B.S., and Canada, A.S., 2017, Hinterland drainage closure and lake formation in response to middle Eocene Farallon slab removal, Nevada, U.S.A.: *Earth and Planetary Science Letters*, v. 479, p. 156–169, doi:10.1016/j.epsl.2017.09.023.
- Smith, J.F.J., and Ketner, K.B., 1976, Stratigraphy of post-Paleozoic rocks and summary of resources in the Carlin-Pinon Range area, Nevada: U.S. Geological Survey Professional Paper 867-B, p. 1–48.
- Wallace, A.R., Perkins, M.E., and Fleck, R.J., 2008, Late Cenozoic paleogeographic evolution of northeastern Nevada: Evidence from the sedimentary basins: *Geosphere*, v. 4, p. 36–74, doi:10.1130/GES00114.1.
- White, L.T., and Ireland, T.R., 2012, High-uranium matrix effect in zircon and its implications for SHRIMP U-Pb age determinations: *Chemical Geology*, v. 306–307, p. 78–91, doi:10.1016/j.chemgeo.2012.02.025.
- Yeend, W.R., 1974, Gold-bearing gravels of the ancestral Yuba River, Sierra Nevada, California: U.S. Geological Survey Professional Paper 772.